Gut

A functional microRNA screen uncovers O-linked N-acetylglucosamine transferase as a host factor modulating hepatitis C virus morphogenesis and infectivity

Journal:	*Gut*
Manuscript ID	gutjnl-2018-317423.R1
Article Type:	Original Article
Date Submitted by the Author:	n/a
Keywords:	HEPATITIS C, HCV, HEPATOCYTE, MOLECULAR MECHANISMS

Complete List of Authors:

Herzog, Katharina; INSERM, U1110 Institute of Viral and Liver Diseases; University of Strasbourg
Bandiera, Simonetta; INSERM, U1110 Institute of Viral and Liver Diseases; University of Strasbourg
Pernot, Sophie; INSERM, U1110 Institute of Viral and Liver Diseases; University of Strasbourg
Fauvelle, Catherine; INSERM, U1110 Institute of Viral and Liver Diseases; University of Strasbourg
Jühling, Frank; INSERM, U1110 Institute of Viral and Liver Diseases; University of Strasbourg
Weiss, Amélie; Institut de Genetique et de Biologie Moleculaire et Cellulaire
Bull, Anne; INSERM, U1259
Durand, Sarah; INSERM, U1110 Institute of Viral and Liver Diseases; University of Strasbourg
Chane-Woon-Ming, Béatrice; CNRS, Architecture et Réactivité de l'ARN – UPR 9002, Institut de Biologie Moléculaire et Cellulaire du CNRS
Pfeffer, Sébastien; CNRS, Architecture et Réactivité de l'ARN – UPR 9002, Institut de Biologie Moléculaire et Cellulaire du CNRS; University of Strasbourg
Mercey, Marion; INSERM, U1209 Institute for Applied Biosciences
Lerat, Hervé; INSERM, U1209 Institute for Applied Biosciences
Meunier, Jean-Christophe; INSERM, U1259
Raffelsberger, Wolfgang; Institut de Genetique et de Biologie Moleculaire et Cellulaire
Brino, Laurent ; Institut de Genetique et de Biologie Moleculaire et Cellulaire
Baumert, Thomas; INSERM, U1110
Zeisel, Mirjam; INSERM, U1110 Institute of Viral and Liver Diseases; INSERM, U1052 Cancer Research Center of Lyon

A functional microRNA screen uncovers O-linked N-acetylglucosamine transferase as a host factor modulating hepatitis C virus morphogenesis and infectivity

Katharina Herzog[1,2*], Simonetta Bandiera[1,2*], Sophie Pernot[1,2], Catherine Fauvelle[1,2], Frank Jühling[1,2], Amélie Weiss[2,3,4,5], Anne Bull[6], Sarah C. Durand[1,2], Béatrice Chane-Woon-Ming[2,7], Sébastien Pfeffer[2,7], Marion Mercey[8], Hervé Lerat[8], Jean-Christophe Meunier[6], Wolfgang Raffelsberger[2,3,4,5], Laurent Brino[2,3,4,5], Thomas F. Baumert[1,2,9,#], Mirjam B. Zeisel[1,2,10,#]

[1]Inserm, U1110, Institut de Recherche sur les Maladies Virales et Hépatiques, Strasbourg, France; [2]Université de Strasbourg, Strasbourg, France; [3]Institut de Génétique et de Biologie Moléculaire et Cellulaire, Illkirch, France ; [4]CNRS, UMR7104, Illkirch, France ; [5]Inserm, U1258, Illkirch, France ; [6]Inserm U1259, Faculté de Médecine, Université François Rabelais and CHRU de Tours, Tours, France ; [7]Architecture et Réactivité de l'ARN – UPR 9002, Institut de Biologie Moléculaire et Cellulaire du CNRS, Strasbourg, France; [8]Institute for Applied Biosciences, Centre de Recherche UGA - Inserm U1209 - CNRS 5309, Grenoble, France [9]Institut Hospitalo-Universitaire, Pôle Hépato-digestif, Hôpitaux Universitaires de Strasbourg, Strasbourg, France; [10]Inserm, U1052, CNRS UMR 5286, Centre Léon Bérard (CLB), Cancer Research Center of Lyon (CRCL), Université de Lyon (UCBL), Lyon, France

*Authors contributed equally to this work

Word count. Abstract: 196 words; main manuscript: 3991 words; 55 references; 7 figures; 1 table; Supplementary information (including 1 Supplementary Table and 1 Supplementary Figure)

[#]Corresponding authors. Dr. Mirjam B. Zeisel, Inserm U1052 – CRCL, 151 cours Albert Thomas, 69424 Lyon Cedex 03, France, Phone: +33472681970, Fax: +33472681971, E-mail: mirjam.zeisel@inserm.fr and Prof. Thomas F. Baumert, Inserm U1110, Institut de

Recherche sur les Maladies Virales et Hépatiques, 3 rue Koeberlé, 67000 Strasbourg, France, Phone: +33368853703, Fax: +33368853724, Email: thomas.baumert@unistra.fr

Financial support. This work was supported by the European Union (INTERREG-IV-Rhin Supérieur-FEDER-Hepato-Regio-Net 2012 to T.F.B. and M.B.Z., ERC-AdG-2014-671231-HEPCIR, EU H2020-667273-HEPCAR to T.F.B), ANRS (2012/239 to T.F.B., M.B.Z. and L.B.), ARC, Paris and Institut Hospitalo-Universitaire, Strasbourg (TheraHCC IHUARC IHU201301187 to T.F.B.), the Impulsion Program of the IDEXLYON (to M.B.Z.), Ligue contre le cancer (to M.B.Z.), Inserm, and University of Strasbourg. This work has been published under the framework of the LABEX ANR-10-LABX-0028_HepSYS, ANR-10-LABX-36 NetRNA and Inserm Plan Cancer 2019-2023 and benefits from funding from the state managed by the French National Research Agency as part of the Investments for the future program. S.P. and K.H. were supported by PhD fellowships from the French Ministry of Research and the IdEx program of the University of Strasbourg, respectively.

Author contribution. M.B.Z. coordinated and supervised research. K.H., S.B., S.P., C.F., A.W., L.B., J-C.M. and M.B.Z. designed experiments. K.H., S.B., S.P, C. F., A.W., A.B., S.C.D., M.M., H.L. and J-C.M. performed experiments. K.H., S.B., S.P., C. F., F.J., A.W., A.B., B.C.W.M., S.P., J-C.M., W.R., L.B., T.F.B. and M.B.Z. analyzed data. K.H., S.B., and M.B.Z. wrote the paper.

Competing interests: The authors do not have competing interest.

Abstract

Objective: Infection of human hepatocytes by the hepatitis C virus (HCV) is a multistep process involving both viral and host factors. microRNAs (miRNAs) are small non-coding RNAs that post-transcriptionally regulate gene expression. Given that miRNAs were indicated to regulate between 30% and 75% of all human genes, we aimed to investigate the functional and regulatory role of miRNAs for the HCV life cycle.

Design: To systematically reveal human miRNAs affecting the HCV life cycle, we performed a two-step functional high-throughput miRNA mimic screen in Huh7.5.1 cells infected with recombinant cell culture-derived HCV. miRNA targeting was then assessed using a combination of computational and functional approaches.

Results: We uncovered miR-501-3p and miR-619-3p as novel modulators of HCV assembly/release. We discovered that these miRNAs regulate O-linked N-acetylglucosamine (O-GlcNAc) transferase (OGT) protein expression and identified OGT and O-GlcNAcylation as regulators of HCV morphogenesis and infectivity. Furthermore, increased OGT expression in patient-derived liver tissue was associated with HCV-induced liver disease and cancer.

Conclusion: miR-501-3p and miR-619-3p and their target OGT are previously undiscovered regulatory host factors for HCV assembly and infectivity. In addition to its effect on HCV morphogenesis, OGT may play a role in HCV-induced liver disease and hepatocarcinogenesis.

Significance of this study

What is already known about this subject?

- To establish chronic infection, the hepatitis C virus (HCV) hijacks cellular factors including microRNAs (miRNAs), known to post-transcriptionally regulate gene expression.
- miRNAs may positively or negatively modulate HCV infection either by directly targeting the viral genome or indirectly by regulating virus-associated cellular pathways[1, 2].

What are the new findings?

- A functional miRNA mimic screen uncovered miR-501-3p and miR-619-3p to enhance late steps of HCV infection.
- miR-501-3p regulates the expression of O-linked N-acetylglucosamine transferase (OGT) at the protein level.
- Silencing of OGT expression or inhibition of O-linked N-acetylglucosaminylation (O-GlcNAcylation) leads to an increase in the infectivity and size of HCV particles.
- OGT expression increases in patient-derived liver tissue during liver disease progression and cancer.

How might it impact on clinical practice in the foreseeable future?

- As upregulation of OGT and increased O-GlcNAcylation of proteins have been associated with various forms of cancer, OGT may play a dual role in HCV morphogenesis as well as pathogenesis of HCV-induced liver disease and carcinogenesis.

Introduction

Chronic hepatitis C is a major cause of chronic liver disease and hepatocellular carcinoma (HCC). Since the approval of pan-genotypic direct-acting antivirals (DAAs), it is considered a curable disease in more than 90% of treated patients. Nonetheless, an estimated 71 million individuals are still infected by the hepatitis C virus (HCV) and several challenges remain; viral cure reduces but does not eliminate the HCC risk in patients with advanced fibrosis[3], the majority of infected patients has limited access to therapy and DAA failure/viral resistance has been reported in a subset of patients[4, 5]. To overcome these limitations, approaches to target host factors involved in HCV infection and pathogenesis are developed[6, 7]. Interestingly, defined host factors that contribute to the establishment of chronic HCV infection and represent potential antiviral targets, e.g. epidermal growth factor receptor[8], also play a role in liver disease pathogenesis and represent candidate targets for treatment of advanced liver disease and HCC prevention[9]. Thus, uncovering host factors usurped by HCV not only contributes to a better understanding of virus-host interactions underlying the HCV life cycle but also to the identification of potential targets for treatment of liver disease and prevention of HCC.

The establishment of various models to study HCV infection has shed light on the molecular mechanisms that govern the HCV life cycle, which can be subdivided into early steps, including viral entry, translation and replication as well as late steps, including assembly and release of new virions. Each step of the HCV replication cycle relies on specific virus-host interactions that involve host proteins and microRNAs (miRNAs)[7], small non-coding RNAs that regulate gene expression at the post-transcriptional level. One miRNA can target numerous messenger RNAs (mRNAs) by base-pairing with a complementary site that is typically located within the 3′ untranslated region (3′UTR) of the mRNA. Accumulating evidence indicates that miRNAs participate to HCV replication by exerting pro- or antiviral effects. The breakthrough discovery of the direct targeting of HCV by miR-122, the most abundant miRNA in the liver, revealed the crucial role of this miRNA for HCV translation/replication that contributes to progression to chronic HCV infection[1, 10]. miR-

122 antisense oligonucleotides were subsequently developed as host-targeting antivirals[11, 12]. Other miRNAs can indirectly target HCV by regulating host factors that participate in antiviral responses and immune surveillance[2, 13, 14]. Since up to 60% of all human protein-coding genes were reported to be under miRNA-mediated regulation and miRNAs are involved in basically every biological process, we hypothesized that miRNAs provide a tool for loss-of-function approaches to uncover novel HCV host factors. We performed genome-wide high-throughput modulation of the human miRNome and analyzed their impact on HCV infection by combining computational and functional approaches.

Material and methods

Cells, cell culture conditions, viruses, virus purification, infectivity assays, miRNAs, antagomiRs, siRNAs, antibodies, immunoblot, immunocapture, electron microscopy analysis of viral particles and gene expression analysis in liver tissue are described in the Supplementary information.

Functional miRNA/siRNA screens. Huh7.5.1 cells were transfected with the miRIDIAN human miRNA mimic library (mIRBase 19) comprising more than 2000 mature miRNAs or 28 ON-TARGETplus smart pool siRNAs (20 nM, Dharmacon) using Interferin HTS (Polyplus) in a 96-well format[8]. After 48h, a viability test (Presto Blue, Thermo Scientific) was performed prior to a two-step infection assay[15, 16, 17]. During part 1 of the protocol, 50 µL of HCV cell culture-derived particles (HCVcc, JcR2a) were incubated with cells during 4h. The inoculum was removed and cells were incubated with 150 µl of medium for 48h. In part 2, supernatants from part 1 cells were transferred onto naïve Huh7.5.1 cells and part 1 cells were lysed to determine luciferase activity[17, 18]. After 72h, part 2 cells were lysed to determine luciferase activity[17]. siCD81 (20 nM), antagomiR-122 (100 nM) and siApoE (20 nM) were used as positive controls[17]. A non-targeting siRNA with no sequence complementarity to any human gene or homology to any human miRNA was used as negative control.

Inhibitor treatment. Four hours following HCV RNA electroporation[8], Huh7.5.1 cells were incubated with vehicle or inhibitors of OGT (peracetylated 5-thio-N-acetylglucosamine ($Ac_4$5S-GlcNAc)[19]) or OGA (Thiamet G (Sigma))[20]. After 96h, supernatants were transferred onto naïve Huh7.5.1 cells for 72h prior to determination of luciferase activity while electroporated cells were lysed to determine luciferase activity.

Gene expression analyses. Total RNA was purified[17] and transcribed into cDNA using Maxima reverse transcriptase (Thermo Scientific). *GAPDH* and *OGT* mRNA was detected by real time qPCR using iTaq™ Universal Probes Supermix (Bio-Rad) and TaqMan Gene Expression Assay (Thermo Scientific). Relative *OGT/GAPDH* gene expression was calculated by the ΔΔCt method[21].

Dual luciferase reporter gene assay. The human *OGT* 3'UTR sequence was retrieved from NCBI (NM_181672.2) and Ensembl genome browser (ENST00000373719.3). A fragment of the *OGT* 3′UTR (positions 3380-3837, NM_181672.2) (Thermo Fisher Scientific GENEART) was cloned between the *Not*I and *Xho*I sites downstream of a *Renilla* luciferase cassette in a psiCHECK2 plasmid (Promega). A mutated version of this construct (9-bp substitution in the predicted miR-501-3p target site) was generated as described[22]. The functionality of the *OGT* 3′UTR was assessed as described[23]. The miRIDIAN mimic negative control 1 was used as control. *Renilla* and *firefly* luciferase activity was assessed 48h after transfection into HeLa cells using Dual-Luciferase Reporter assay (Promega).

Bioinformatic and statistical analysis. Data analysis and statistical treatment for the miRNA mimic screen were performed in R (www.r-project.org). Cell measurement data used in further analysis were cell viability and luciferase activity. In total 26 sets of plates (performed in triplicate) were tested. The presence of multiple wells with negative and positive controls on each plate allowed stepwise normalization intra- and inter-plate. First, intra-plate zonal bias was examined and a model of median effects across the entire screen

determined using the median-polish algorithm[24] and all plates corrected accordingly. Then the dataset was examined for outlier plates, i.e. plates where all individual measurements correlate very poorly with the other remaining replicates. Three and 9 plates were excluded for part 1 and part 2 of the screen, respectively, based on poor median correlation ($r < 0.7$) so that the remaining plates correlation improved substantially (> 40%). Next, the plates were normalized inter replicates using the particularly robust quantile-quantile approach[25]. Finally, the data were tested using a moderated t-test (empirical Bayes shrinkage, R-package limma[26]) for the null-hypothesis of no change of a given miRNA compared to the negative control. The resulting *p*-values for independent testing of each miRNA where corrected for the multiple testing situation and expressed as local false discovery rate (lfdr, R-package fdrtool[27]). The testing was performed independently for part 1 and 2 of the screen and candidate miRNAs selected for each part. For data from part 1, a lfdr threshold of 0.00027 was used. Data from part 2 were subject to increase inherent stochastic noise and for this reason the minimum acceptable relative risk of false positives was increased to 0.1226 (i.e. maximum 15% risk for each of the retained hits).

Other datasets were analyzed using the two-tailed Mann-Whitney test, Wilcoxon test, Spearman correlation or the two-tailed unpaired t-test for data with normal distribution as assessed by D'Agostino and Pearson omnibus and Shapiro-Wilk normality tests (GraphPad Prism v.6 package).

Results

Genome-wide identification of human miRNAs affecting the HCV life cycle. We performed a genome-wide screen in human hepatoma Huh7.5.1 cells using a genomic miRNA mimics library and a two-step infection assay[17] with a luciferase reporter virus (JcR2a), which allowed us to functionally assess the role of miRNAs during the early steps (part 1 - viral entry/translation/replication) and the late steps (part 2 - viral assembly/release/infectivity) of the HCV life cycle (Fig. 1A). Silencing of *CD81* and *ApoE*,

two essential host factors required for HCV entry or assembly, respectively, was performed in parallel using small interfering RNA (siRNA) as controls. Silencing of *CD81* resulted in a reduction of HCV infection in part 1 and consequently in part 2 of the screen since reduced viral entry in the first part of the assay leads to a reduced production of viral particles (Fig. 1B)[17]. Silencing of *ApoE* resulted in a marked inhibition of HCV infection only in part 2 of the assay, consistent with the role of ApoE in HCV assembly (Fig. 1B)[17]. The screen identified 427 miRNAs (corresponding to about 16% of the library) that significantly modulated HCV infection (lfdr < threshold, Supplementary Table 1 and Fig. 1C): 186 miRNAs affected HCV infection in part 1, 309 miRNAs affected HCV infection in part 2, including 68 hits in part 1 and part 2. The limited number of part 1 and 2 hits may be due to the fact that a single miRNA may modulate the expression of several proteins, which may have different roles in the viral life cycle. Most hits were observed to dampen HCV infection independently of any significant alteration of cell viability (data not shown). The 186 miRNAs modulating the early steps of HCV infection all decreased viral infection. Among the 309 miRNAs that had an impact in part 2, 11 miRNAs increased HCV infection by at least 3-fold while 298 miRNAs inhibited HCV infection by at least 2.7-fold. Hits from the screen included the let-7 family[2, 28], miR-27a[29] and miR-29 family[30] that were already shown to inhibit HCV infection, as well as miR-21[31] and miR-146a-5p[17] that were shown to stimulate HCV infection thus supporting the relevance of our findings. Collectively, our screen identified a set of miRNAs whose overexpression overall impairs HCV infection by affecting viral entry/translation/replication and/or virion assembly/egress/infectivity.

miR-619-3p, miR-501-3p and OGT play a role in late steps of the HCV life cycle. We focused our analysis on miRNAs that modulate late steps of the HCV life cycle, as the molecular mechanisms of HCV assembly/release remain only partially understood. Our screen identified 241 miRNAs that modulated late steps without affecting early steps of infection: 11 miRNAs increased HCV infection while 230 miRNAs decreased HCV infection. Among the miRNAs that increased HCV infection, miR-140-3p, miR-501-3p, miR-619-3p and

miR-4778-5p have not yet been associated with HCV. Since they enhanced HCV infection in part 2 without affecting part 1, these miRNAs may target host genes that control virus assembly/egress/infectivity. We first confirmed the effect of these miRNAs in independent experiments using the same protocol as for the screen. Overexpression of miR-619-3p or miR-501-3p consistently led to an increase in the infection of progeny virions (Fig. 1D) while infection was decreased with progeny virions from antagomiR-transfected cells (Supplementary Figure S1A). miR-619-3p or miR-501-3p were thus selected for further investigation. To study the molecular mechanisms by which these miRNAs affect HCV infection, we generated a list of predicted miRNA targets using DIANA, TargetScan Human v6.2 and miRDB databases, and selected candidate targets based on their expression in our Huh7.5.1 cells as assessed by microarray (data not shown). Ingenuity Pathway Analysis enabled us to refine the gene list by selecting 28 genes involved in the following functional networks or pathways that contribute to the HCV life cycle[32, 33, 34]: lipid metabolism and cholesterol biosynthesis, protein maturation and processing at the endoplasmic reticulum (ER), components of the endosomal sorting complex, adipocyte biogenesis, cellular morphology and cell inflammation (Table 1).

To assess whether knock-down of these 28 candidate targets affects virus production, we performed a siRNA-based screen using siRNA pools exhibiting strong silencing without cytotoxicity (Fig. 2). Silencing of *CD81* and antagomiR-122 served as controls for part 1; knock-down of *ApoE* served as control for part 2 (Fig. 2). Hits were defined as genes whose knock-down modulated HCV infection in at least one part of the screen with high significance (Fig. 2, *p*-value < 0.0001, Mann-Whitney U-test). HCV entry/translation/replication was significantly modulated by silencing of *PPP3CA, CEBPA, MID1, WDFY3, DCX* and *SLC35D1*. HCV assembly/egress/infectivity was significantly modulated by knock-down of *PPP3CA, CSDE1, GAN, USP37, CEBPA, MID1, WDFY3, DCX, MAPK9, SLC35D1, DCC, RNF144A, PPP2R2C* and *OGT*. Strikingly, only the silencing of *OGT* was associated with an enhancement of HCV assembly/release/infectivity (*p*-value = 0.0002), while that of the other hits was associated with reduced HCV infection (Fig. 2).

These results indicate that the down-regulation of *OGT* phenocopies the effect of miR-501-3p and miR-619-3p on HCV infection (Fig. 2) and suggest OGT as a novel player in the HCV life cycle.

miR-501-3p post-transcriptionally regulates OGT expression. To study whether miR-501-3p and miR-619-3p target OGT, we analyzed OGT RNA and protein levels in Huh7.5.1 cells following overexpression of miR-501-3p or miR-619-3p. While neither miRNA had an impact on OGT RNA levels (Fig. 3A), up-regulation of miR-501-3p significantly decreased OGT protein expression by ~65% (Fig. 3B, *p*-value < 0.05, t-test). miR-619-3p also decreased OGT expression but less robustly than miR-501-3p (Fig. 3B), prompting us to focus our investigation on miR-501-3p. To assess whether OGT is a functional target of miR-501-3p, we subcloned a fragment of the *OGT* mRNA 3′UTR that harbors the predicted miR-501-3p target site in the *Renilla* luciferase expression cassette (RLuc) of a dual luciferase reporter construct. Co-transfection of miR-501-3p mimic with the wild-type 3'UTR reporter (RLuc wt *OGT* 3'UTR) significantly decreased luciferase activity as compared to the empty vector (Fig. 3C, p-value < 0.05, t-test). In contrast, the repression of luciferase expression was lost when the reporter with mutated miR-501-3p binding site (RLuc mt *OGT* 3'UTR) was used (Fig. 3C). These data are consistent in indicating that miR-501-3p mediates post-transcriptional regulation of OGT.

O-GlcNAcylation modulates HCVcc infectivity. To investigate whether OGT modulates HCV assembly and/or infectivity, we determined infectious virus titer (TCID50) and HCV RNA levels to calculate the specific infectivity of HCVcc particles generated in OGT-silenced Huh7.5.1 cells. Interestingly, OGT-silencing led to a significant increase in the TCID50 and the specific infectivity of HCVcc (Fig. 4A, *p*-value < 0.05, Mann-Whitney test). Noteworthy, the effect of OGT on HCVcc infectivity was genotype-independent as demonstrated by increased infectivity of HCVcc bearing the envelope glycoproteins of genotypes 1a, 1b and 2a upon OGT-silencing (Fig. 4B). We next sought to investigate how OGT could modulate

HCVcc infectivity. OGT is the only enzyme that catalyzes the addition of N-acetylglucosamine (O-GlcNAc) to serine and threonine residues of proteins. Moreover, OGT has a scaffold function and promotes binding of proteins in multiprotein complexes[35]. To assess whether the enzymatic activity of OGT modulates HCVcc infectivity, we used pharmacological inhibitors of OGT ($Ac_4$5S-GlcNAc) or O-GlcNAcase (OGA) (Thiamet G), the OGT counterpart that removes O-GlcNAc (Fig. 4C). $Ac_4$5S-GlcNAc led to a significant enhancement of HCVcc infectivity in a dose-dependent manner, while the opposite effect was observed with Thiamet G (Fig. 4D, *p*-value < 0.05, Mann-Whitney test). Collectively, these results demonstrate that O-GlcNAcylation modulates HCVcc infectivity.

OGT-silencing affects HCVcc biophysical properties and size distribution. To further assess how OGT may impact HCVcc morphogenesis, we analyzed the structural and biophysical properties of HCVcc produced in siCtrl- and siOGT-transfected Huh7.5.1 cells following iodixanol gradient ultracentrifugation. Silencing of OGT led to the production of more infectious HCVcc with higher density (Fig. 5A-B) as well as higher ApoE concentrations (Fig. 5C) suggesting that OGT/O-GlcNAcylation affects the biophysical properties of HCVcc. No change in apoB concentrations were observed between HCVcc produced from siCtrl- or siOGT-transfected cells (Fig. 5D), in line with the model that HCV lipoviroparticles contain several exchangeable ApoE molecules and one non-exchangeable apoB[36]. We also visualized HCVcc by electron microscopy (EM) following anti-E2 antibody immunocapture[36] to assess whether OGT-silencing had an impact on HCVcc size. Particle size distribution was assessed from a series of randomly acquired electron micrographs. A shift towards bigger sizes was observed for sucrose-cushion purified HCVcc generated in OGT-silenced Huh7.5.1 cells as compared to control HCVcc (Fig. 6A-B). This shift was also observed in different fractions of iodixanol gradient-separated HCVcc (Fig. 6C-F) in line with the higher infectivity and ApoE concentrations of HCVcc generated in OGT-silenced Huh7.5.1 cells (Fig. 5A-C). These data suggest that OGT-silencing affects the lipidation of HCVcc.

OGT expression increases in liver disease. Since silencing of OGT promotes HCV infectivity, we assessed whether HCV infection in turn had an effect on miR-501-3p and OGT expression. In Huh7.5.1 cells, HCV infection lead to small but significant increase of miR-501-3p and decrease of OGT levels (Fig. 7A-B and Supplementary Fig. 1B; *p*-value < 0.05, Mann-Whitney test), which may promote viral infection given the pro- and antiviral roles of miR-501-3p and O-GlcNAcylation, respectively (Fig. 1C-D and 4D). In contrast, no significant difference of OGT expression was observed between the livers of HCV transgenic and wild-type mice[37] (data not shown) suggesting that HCV proteins do not directly modulate OGT expression. In liver tissue from HCV-infected patients, HCV RNA levels were not correlated with OGT expression (Fig. 7C, Spearman correlation: 0.06004019, p-value = 0.7661) suggesting that in patients there is likely no direct effect of HCV on OGT expression.

O-GlcNAcylation has been associated with a variety of cancers, including HCC recurrence linked to increased O-GlcNAcylation after liver transplantation[38]. We therefore investigated OGT expression in chronic liver disease and HCC. While there was a trend for increased OGT expression in liver tissue from HCV-infected patients with fibrosis and inflammation (Fig. 7D-E), OGT levels were markedly and significantly elevated in the tumor liver tissue of patients chronically infected with HCV or hepatitis B virus and patients with alcoholic liver disease or non-alcoholic fatty liver disease as compared to non-tumor tissue (Fig. 7F, *p*-value < 0.05, Wilcoxon test). These data suggest that OGT expression increases in HCC in an etiology-independent manner. Collectively, these results suggest that OGT expression is likely increased in HCV-induced liver disease and cancer through inflammation and fibrosis rather than by HCV itself.

Discussion

By focusing on miRNAs affecting late steps of the viral life cycle, we uncovered that i) miR-501-3p regulates the expression of OGT; ii) silencing of OGT expression or inhibition of its enzymatic activity increases the infectivity of HCV particles; and iii) OGT knock-down leads

to the release of bigger HCV particles. Our data suggest that O-GlcNAcylation affects HCV morphogenesis and infectivity.

While we were characterizing the role of OGT/O-GlcNAcylation for HCV morphogenesis, Li and colleagues published their functional genomics study of HCV-miRNA interactions[2]. By conducting genome wide miRNA mimic and hairpin inhibitor screens, they identified a set of miRNAs exhibiting a pro- or antiviral effect on HCV. Characterization of the underlying molecular processes showed that miR-25, let-7 and miR-130 families restrict viral infection by decreasing the expression of cellular HCV co-factors[2]. Despite similarities in the cell type and HCV infection models used here and by Li and colleagues, our screen only displays a small overlap with their study (9% common miRNA hits). This is not surprising given the small overlap between previous siRNA screens to uncover HCV host factors[8, 15] and is likely due i) to the different sizes of miRNA mimic libraries as the library used here was more than 2-times larger than the one used by Li and co-workers, and ii) to the markedly distinct pipelines for hit selection that were used in the two studies. Nonetheless, both screens were consistent in confirming the proviral role of miR-146a-5p in promoting HCV assembly/egress that we previously reported[17] and the global multistep inhibitory effects of the let-7 family on HCV infection[28], further corroborating the involvement of these miRNAs in fine-tuning the HCV life cycle. Both studies also consistently indicated that miR-518a-5p, miR-517-3p, miR-185 and members of the miR-302 family inhibit early steps of HCV infection, while miR-586, miR-620 and members of the miR-200 family inhibit late steps of viral infection. Since none of these miRNAs except miR-185 has been previously associated with HCV infection[39], it might be interesting to further characterize the involvement of these miRNAs in HCV-host interactions. Interestingly, an overall proviral effect of miR-501-3p was also observed by Li and colleagues[2], however the mechanism of action was not studied. By characterizing the role of miR-501-3p in the HCV life cycle, we uncovered OGT as a miR-501-3p target in liver-derived cells and showed for the first time a link between O-GlcNAcylation and HCV infection. These results indicate that genome-wide miRNA functional

screens represent a powerful strategy to dissect the role of miRNAs in pathogen-host interactions.

While N-glycosylation of HCV envelope glycoproteins plays an important role for escape from virus-neutralizing antibodies[40], so far no functional association between HCV and O-glycosylation has been reported. In contrast to N-linked glycosylation that consists of the attachment of a glycan to a nitrogen of an asparagine residue of proteins in the ER/Golgi prior to their trafficking to the plasma membrane and/or their secretion, the glycosylation of serine and threonine residues with O-GlcNAc is a post-translational modification (PTM) of intracellular proteins that are localized in the nucleus, cytoplasm or mitochondria. The O-glycosylation/deglycosylation of proteins is catalyzed by a single pair of nucleo-cytoplasmic enzymes, OGT/OGA. O-GlcNAcylation is complementary to protein phosphorylation/dephosphorylation, another more broadly known abundant protein PTM that involves numerous kinases/phosphatases. OGT/OGA are often found in protein complexes that also include kinases/phosphatases and a protein can be either O-GlcNAcylated or phosphorylated on a same residue to fine-tune cellular signaling[41]. O-GlcNAcylation and phosphorylation on the same or neighboring serine or threonine residue is known as yin yang site[42].

O-GlcNAcylation plays a major role in the regulation of metabolic pathways in the liver, including insulin signaling, bile acid metabolism and lipogenesis[35]. The large number of OGT/OGA substrates and cellular pathways regulated by O-GlcNAcylation hampers a detailed characterization of the role of these proteins in HCV infection. Since i) HCV assembly takes place at ER-derived membranes, ii) OGT/OGA are not known to localize in the ER lumen, and iii) O-GlcNAcylation of extracellular proteins containing EGF-like domains is catalyzed by EGF domain-specific OGT (EOGT) in the ER lumen in an OGT-independent manner[43]), OGT/OGA most likely modulate HCV infection by post-translationally modifying one or several cellular factors required for HCV morphogenesis rather than by affecting viral proteins, although HCV glycoproteins contain putative O-GlcNAcylation sites as determined using OGlcNAcScan, OGTsite and YingOYang1.2 bioinformatics tools (data not shown).

Regarding HCV host factors that may be regulated by OGT/OGA, O-GlcNAcylation sites have been predicted in human CLDN1[44] and OCLN at serine sites that can also be phosphorylated and this has been suggested to potentially play a role for HCV entry[45]. However, in our experimental setting we did not observe a significant effect of OGT-silencing on the early steps of HCV infection, suggesting that O-GlcNAcylation of CLDN1 and/or OCLN likely does not play a major role in HCV infection. Other host factors important for the HCV life cycle are well-known O-GlcNAcylated proteins, as for example various nuclear pore complex proteins (Nups) including Nup98, Nup153 and Nup155 that are involved in HCV replication and assembly and/or may be associated with viral particles[46, 47, 48]. However, since depletion of Nups was reported to alter HCV replication and/or assembly but to have no impact on the specific infectivity of HCV particles[46] in contrast to the depletion of OGT as shown here, it is unlikely that a modulation of Nup O-GlcNAcylation accounts for the effects of OGT-silencing and/or OGT/OGA inhibitors on HCVcc infectivity observed in our study. This is in line with our observation that OGT knock-down had no effect on Dengue virus (DENV) replication and infectivity (unpublished observations KH, MZ and Evelyne Schaffer, IBMC, Strasbourg), although Nup98 had been suggested to potentially play a role for DENV infection[46]. These data suggest that OGT does not broadly modulate the infectivity of viruses of the *Flaviviridae* family.

However, OGT and/or O-GlcNAcylation have been reported to play a role in the infection with other viruses[49, 50, 51]. Interestingly, while OGT expression modulates the levels of human papillomavirus 16 (HPV16) oncoproteins E6 and E7[52], E6 in turn can up-regulate OGT to increase O-GlcNAcylation and the oncogene activities of HPV[53], suggesting that OGT/O-GlcNAcylation could play a role in virus-induced cancer. In cell culture, HCV infection appeared to be associated with a minor decrease in OGT expression in line with an antiviral role of O-GlcNAcylation. In contrast, an increased OGT expression was observed in HCC tissues of HCV-infected patients. Since OGT has been suggested to activate oncogenic signaling pathways in non-alcoholic steatohepatitis-related HCC[54] and O-GlcNAcylation has been associated with HCC recurrence linked to increased O-

GlcNAcylation after liver transplantation[38], these data suggest that in addition to their effect on the HCV life cycle, OGT/O-GlcNAcylation may also play a role in HCV-induced hepatocarcinogenesis.

Acknowledgments

We wish to thank Gerald W. Hart and Stéphan Hardivillé, the CardioPEG CoreC4 (NHLBI P01 HL107153) for providing AL24 and for useful technical discussions. We are grateful to David Vocadlo (Simon Fraser University, Burnaby, Canada) for the gift of $Ac_4$5S-GlcNAc. We also thank Ralf Bartenschlager (University of Heidelberg, Germany) for providing the plasmids for production of HCVcc and Frank Chisari (The Scripps Research Institute, La Jolla, CA) for the gift of Huh7.5.1 cells. We acknowledge Evelyne Schaeffer (CNRS UPR3572, IBMC, Strasbourg) for the DENV experiment, Charlotte Bach and Christine Thumann (Inserm, U1110, Strasbourg) for excellent technical work during the functional miRNA mimic screen, as well as Armando A. Roca-Suarez (Inserm, U1110, Strasbourg), Hussein El Saghire (Inserm, U1110, Strasbourg), Arnaud Kopp (IGBMC, Department of Functional Genomics and Cancer) and Erika Girardi (UPR 9002, IBMC, Strasbourg) for helpful discussions. We thank the INGESTEM infrastructure for access to the IGBMC high-throughput screening workstation.

References

1 Jopling CL, Yi M, Lancaster AM*, et al.* Modulation of hepatitis C virus RNA abundance by a liver-specific MicroRNA. Science 2005;**309**:1577-81.

2 Li Q, Lowey B, Sodroski C*, et al.* Cellular microRNA networks regulate host dependency of hepatitis C virus infection. Nat Commun 2017;**8**:1789.

3 Baumert TF, Juhling F, Ono A*, et al.* Hepatitis C-related hepatocellular carcinoma in the era of new generation antivirals. BMC Med 2017;**15**:52.

4 Pawlotsky JM. Hepatitis C Virus Resistance to Direct-Acting Antiviral Drugs in Interferon-Free Regimens. Gastroenterology 2016;**151**:70-86.

5 Dietz J, Susser S, Vermehren J, *et al.* Patterns of Resistance-Associated Substitutions in Patients With Chronic HCV Infection Following Treatment With Direct-Acting Antivirals. Gastroenterology 2018;**154**:976-88 e4.

6 Zeisel MB, Baumert TF. Clinical development of hepatitis C virus host-targeting agents. Lancet 2017;**389**:674-5.

7 Zeisel MB, Crouchet E, Baumert TF, *et al.* Host-Targeting Agents to Prevent and Cure Hepatitis C Virus Infection. Viruses 2015;**7**:5659-85.

8 Lupberger J, Zeisel MB, Xiao F, *et al.* EGFR and EphA2 are host factors for hepatitis C virus entry and possible targets for antiviral therapy. Nature Medicine 2011;**17**:589-95.

9 Fuchs BC, Hoshida Y, Fujii T, *et al.* Epidermal growth factor receptor inhibition attenuates liver fibrosis and development of hepatocellular carcinoma. Hepatology 2014;**59**:1577-90.

10 Masaki T, Arend KC, Li Y, *et al.* miR-122 stimulates hepatitis C virus RNA synthesis by altering the balance of viral RNAs engaged in replication versus translation. Cell Host Microbe 2015;**17**:217-28.

11 Janssen HL, Reesink HW, Lawitz EJ, *et al.* Treatment of HCV infection by targeting microRNA. N Engl J Med 2013;**368**:1685-94.

12 van der Ree MH, de Vree JM, Stelma F, *et al.* Safety, tolerability, and antiviral effect of RG-101 in patients with chronic hepatitis C: a phase 1B, double-blind, randomised controlled trial. Lancet 2017;**389**:709-17.

13 Bandiera S, Pfeffer S, Baumert TF, *et al.* miR-122--a key factor and therapeutic target in liver disease. J Hepatol 2015;**62**:448-57.

14 Li H, Jiang JD, Peng ZG. MicroRNA-mediated interactions between host and hepatitis C virus. World J Gastroenterol 2016;**22**:1487-96.

15 Li Q, Brass AL, Ng A, *et al.* A genome-wide genetic screen for host factors required for hepatitis C virus propagation. Proc Natl Acad Sci U S A 2009;**106**:16410-5.

16 Poenisch M, Metz P, Blankenburg H*, et al.* Identification of HNRNPK as regulator of hepatitis C virus particle production. PLoS Pathog 2015;**11**:e1004573.

17 Bandiera S, Pernot S, El Saghire H*, et al.* Hepatitis C Virus-Induced Upregulation of MicroRNA miR-146a-5p in Hepatocytes Promotes Viral Infection and Deregulates Metabolic Pathways Associated with Liver Disease Pathogenesis. J Virol 2016;**90**:6387-400.

18 Da Costa D, Turek M, Felmlee DJ*, et al.* Reconstitution of the entire hepatitis C virus life cycle in non-hepatic cells. J Virol 2012;**86**:11919-25.

19 Gloster TM, Zandberg WF, Heinonen JE*, et al.* Hijacking a biosynthetic pathway yields a glycosyltransferase inhibitor within cells. Nat Chem Biol 2011;**7**:174-81.

20 Yuzwa SA, Macauley MS, Heinonen JE*, et al.* A potent mechanism-inspired O-GlcNAcase inhibitor that blocks phosphorylation of tau in vivo. Nat Chem Biol 2008;**4**:483-90.

21 Schmittgen TD, Livak KJ. Analyzing real-time PCR data by the comparative C(T) method. Nat Protoc 2008;**3**:1101-8.

22 Jin Y, Chen Z, Liu X*, et al.* Evaluating the microRNA targeting sites by luciferase reporter gene assay. Methods Mol Biol 2013;**936**:117-27.

23 Van Renne N, Roca Suarez AA, Duong FHT*, et al.* miR-135a-5p-mediated downregulation of protein tyrosine phosphatase receptor delta is a candidate driver of HCV-associated hepatocarcinogenesis. Gut 2018;**67**:953-62.

24 Mosteller F, Tukey J. Data Analysis and Regression. Reading, MA: Addison-Wesley, 1977.

25 Amaratunga D, Cabrera J. Analysis of Data from Viral DNA Microchips. Journal of the American Statistical Association 2001;**96**:1161.

26 Smyth GK. Linear models and empirical Bayes methods for assessing differential expression in microarray experiments. Statistical Applications in Genetics and Molecular Biology 2004;**3**:Article 3.

27 Strimmer K. fdrtool: a versatile R package for estimating local and tail area-based false discovery rates. Bioinformatics 2008;**24**:1461-2.

28 Cheng M, Si Y, Niu Y, *et al.* High-throughput profiling of alpha interferon- and interleukin-28B-regulated microRNAs and identification of let-7s with anti-hepatitis C virus activity by targeting IGF2BP1. J Virol 2013;**87**:9707-18.

29 Shirasaki T, Honda M, Shimakami T, *et al.* MicroRNA-27a regulates lipid metabolism and inhibits hepatitis C virus replication in human hepatoma cells. J Virol 2013;**87**:5270-86.

30 Bandyopadhyay S, Friedman RC, Marquez RT, *et al.* Hepatitis C virus infection and hepatic stellate cell activation downregulate miR-29: miR-29 overexpression reduces hepatitis C viral abundance in culture. J Infect Dis 2011;**203**:1753-62.

31 Chen Y, Chen J, Wang H, *et al.* HCV-induced miR-21 contributes to evasion of host immune system by targeting MyD88 and IRAK1. PLoS Pathog 2013;**9**:e1003248.

32 Ariumi Y, Kuroki M, Maki M, *et al.* The ESCRT system is required for hepatitis C virus production. PLoS One 2011;**6**:e14517.

33 Paul D, Madan V, Bartenschlager R. Hepatitis C virus RNA replication and assembly: living on the fat of the land. Cell Host Microbe 2014;**16**:569-79.

34 Meyers NL, Fontaine KA, Kumar GR, *et al.* Entangled in a membranous web: ER and lipid droplet reorganization during hepatitis C virus infection. Curr Opin Cell Biol 2016;**41**:117-24.

35 Yang X, Qian K. Protein O-GlcNAcylation: emerging mechanisms and functions. Nat Rev Mol Cell Biol 2017;**18**:452-65.

36 Piver E, Boyer A, Gaillard J, *et al.* Ultrastructural organisation of HCV from the bloodstream of infected patients revealed by electron microscopy after specific immunocapture. Gut 2017;**66**:1487-95.

37 Lerat H, Honda M, Beard MR, *et al.* Steatosis and liver cancer in transgenic mice expressing the structural and nonstructural proteins of hepatitis C virus. Gastroenterology 2002;**122**:352-65.

38 de Queiroz RM, Carvalho E, Dias WB. O-GlcNAcylation: The Sweet Side of the Cancer. Front Oncol 2014;**4**:132.

39 Singaravelu R, O'Hara S, Jones DM, *et al.* MicroRNAs regulate the immunometabolic response to viral infection in the liver. Nat Chem Biol 2015;**11**:988-93.

40 Lavie M, Hanoulle X, Dubuisson J. Glycan Shielding and Modulation of Hepatitis C Virus Neutralizing Antibodies. Front Immunol 2018;**9**:910.

41 Hart GW, Slawson C, Ramirez-Correa G, *et al.* Cross talk between O-GlcNAcylation and phosphorylation: roles in signaling, transcription, and chronic disease. Annu Rev Biochem 2011;**80**:825-58.

42 Hart GW, Greis KD, Dong LY, *et al.* O-linked N-acetylglucosamine: the "yin-yang" of Ser/Thr phosphorylation? Nuclear and cytoplasmic glycosylation. Adv Exp Med Biol 1995;**376**:115-23.

43 Sakaidani Y, Nomura T, Matsuura A, *et al.* O-linked-N-acetylglucosamine on extracellular protein domains mediates epithelial cell-matrix interactions. Nat Commun 2011;**2**:583.

44 Butt AM, Khan IB, Hussain M, *et al.* Role of post translational modifications and novel crosstalk between phosphorylation and O-beta-GlcNAc modifications in human claudin-1, -3 and -4. Mol Biol Rep 2012;**39**:1359-69.

45 Butt AM, Feng D, Nasrullah I, *et al.* Computational identification of interplay between phosphorylation and O-beta-glycosylation of human occludin as potential mechanism to impair hepatitis C virus entry. Infect Genet Evol 2012;**12**:1235-45.

46 Neufeldt CJ, Joyce MA, Levin A, *et al.* Hepatitis C virus-induced cytoplasmic organelles use the nuclear transport machinery to establish an environment conducive to virus replication. PLoS Pathog 2013;**9**:e1003744.

47 Lussignol M, Kopp M, Molloy K, *et al.* Proteomics of HCV virions reveals an essential role for the nucleoporin Nup98 in virus morphogenesis. Proc Natl Acad Sci U S A 2016;**113**:2484-9.

48 Zhu Y, Liu TW, Madden Z, *et al.* Post-translational O-GlcNAcylation is essential for nuclear pore integrity and maintenance of the pore selectivity filter. J Mol Cell Biol 2016;**8**:2-16.

49 Jochmann R, Thurau M, Jung S, *et al.* O-linked N-acetylglucosaminylation of Sp1 inhibits the human immunodeficiency virus type 1 promoter. J Virol 2009;**83**:3704-18.

50 Groussaud D, Khair M, Tollenaere AI, *et al.* Hijacking of the O-GlcNAcZYME complex by the HTLV-1 Tax oncoprotein facilitates viral transcription. PLoS Pathog 2017;**13**:e1006518.

51 Angelova M, Ortiz-Meoz RF, Walker S, *et al.* Inhibition of O-Linked N-Acetylglucosamine Transferase Reduces Replication of Herpes Simplex Virus and Human Cytomegalovirus. J Virol 2015;**89**:8474-83.

52 Kim M, Kim YS, Kim H, *et al.* O-linked N-acetylglucosamine transferase promotes cervical cancer tumorigenesis through human papillomaviruses E6 and E7 oncogenes. Oncotarget 2016;**7**:44596-607.

53 Zeng Q, Zhao RX, Chen J, *et al.* O-linked GlcNAcylation elevated by HPV E6 mediates viral oncogenesis. Proc Natl Acad Sci U S A 2016;**113**:9333-8.

54 Xu W, Zhang X, Wu JL, *et al.* O-GlcNAc transferase promotes fatty liver-associated liver cancer through inducing palmitic acid and activating endoplasmic reticulum stress. J Hepatol 2017;**67**:310-20.

55 Boldanova T, Suslov A, Heim MH, *et al.* Transcriptional response to hepatitis C virus infection and interferon-alpha treatment in the human liver. EMBO Mol Med 2017;**9**:816-34.

Figure legends

Figure 1. High-throughput screen identifies human miRNAs that regulate the HCV life cycle. (A) Schematic outline of the miRNA mimic screen strategy. Huh7.5.1 cells were transfected with miRNA mimics or controls prior to infection with *Renilla* luciferase HCVcc (JcR2a) two days later (part 1). Cell supernatants of part 1 were used to inoculate naïve Huh7.5.1 cells (part 2). Cells from part 1 and part 2 were lysed at the end of each infection step (2 and 3 days post infection, respectively) to determine luciferase activity. (B) Modulation of HCV entry and replication (part 1) and/or assembly and infectivity (part 2) upon transfection of control non-targeting siRNA (siCtrl, negative control), siCD81 (inhibiting viral entry) or siApoE (inhibiting viral assembly). By inhibiting HCV entry, siCD81 impacts part 1 as well as part 2. In contrast, by specifically impairing late steps of HCV replication cycle, siApoE inhibits HCV infection only in part 2. The box plots show the sample lower quartile (25th percentile; bottom of the box), the median (50th percentile; horizontal line in box) and the upper quartile (75th percentile; top of the box) of relative light units (RLU) in each lysate. The whiskers indicate s.d. Data are from three independent experiments. (C) Effects of miRNA overexpression on each part of the HCV life cycle. Data were tested using a moderated t-test (empirical Bayes shrinkage, R-package limma[26]) for the null-hypothesis of no change of a given miRNA compared to the negative control. The resulting p-values for independent testing of each miRNA where corrected for the multiple testing situation and expressed as local false discovery rate (lfdr, R-package fdrtool[27]). miRNAs having a significant effect on either part 1 or 2 of the screen are below the thresholds indicated by dashed lines (lfdr < 0.00027 or 0.1226, respectively). miRNAs that were previously reported to impact on HCV infection as well as miR-140-3p, miR-501-3p, miR-619-3p and miR-4778-5p are highlighted in blue (Log2(FC) < 0) or red (Log2(FC) > 0). Data are from three independent experiments. (D) Effect of miR-140-3p, miR-501-3p, miR-619-3p and miR-4778-5p on the HCV life cycle. Huh7.5.1 cells were transfected with siCtrl (Ctrl), miR-140-3p, miR-501-3p, miR-619-3p or miR-4778-5p and infection experiments were carried out as described in A. HCV infection was determined as luciferase activity. Results represent mean

percentage ± s.d. from three independent experiments in triplicate. The dashed line indicates values from control-transfected cells set at 100%. Statistics**:** *, *p*-value < 0.05, Mann-Whitney test.

Figure 2. OGT is a novel host cell factor involved in the late steps of the HCV life cycle. Huh7.5.1 cells were transfected with a set of siRNAs against 28 predicted targets of miR-501-3p and/or miR-619-3p, and infected with HCVcc JcR2A according to the two-step protocol depicted in Fig. 1A. siCD81, antagomiR-122 and siApoE were used as loss-of-function controls to perturb HCV entry, translation/replication and assembly, respectively. miR-501-3p and miR-619-3p, which were ineffective in part 1 of the screen but enhanced HCV infection in part 2, were transfected in parallel. HCV infection was quantified as fold change of luciferase activity with respect to negative control (siCtrl). Results for different replicates are shown as individual points. For each gene, median fold change of luciferase activity ± s.d. is shown as black horizontal lines. The dashed line indicates a fold change of 1. Data are from three independent experiments in triplicate. Results for miR-501-3p, miR-619-3p and siOGT that increase HCV infection in part 2 are depicted in red. Results for siRNA targeting *PPP3CA, CEBPA, MID1, WDFY3, DCX, SLC35D1, CSDE1, GAN, USP37, MAPK9, DCC, RNF144A,* or *PPP2R2C* that significantly modulated HCV infection in part 1 and/or part 2 but did not phenocopy the effect of miR-501-3p and miR-619-3p are depicted in blue.

Figure 3. miR-501-3p mediates post-transcriptional regulation of OGT by decreasing its expression at the protein level. Huh7.5.1 cells were transfected with siCtrl (Ctrl), a pool of siRNA against *OGT*, miR-501-3p or miR-619-3p. After 96h, RNA and proteins were purified, and OGT expression analyzed by RT-qPCR and Western blot. (A) Percentage of *OGT* mRNA expression in miRNA-transfected cells as compared to negative control. Results are presented as mean ± s.d. and are from three independent experiments in triplicate. The dashed line indicates values from control-transfected cells set at 100%. Statistics: *, *p*-value

< 0.05, t-test (B) OGT protein expression. Left: percentage of OGT protein expression in siRNA- or miRNA-transfected cells as assessed by quantification of Western blots. OGT levels were normalized to actin levels using ImageLab™ 5.2.1 software (BioRad). Results are presented as mean ± s.d. and are from three independent experiments. The dashed line indicates values from control-transfected cells set at 100%. Statistics: *, *p*-value < 0.05, t-test. Right: representative Western blot analysis. (C) Analysis of miRNA targeting of *OGT* expression by dual luciferase reporter assay. Left: HeLa cells were co-transfected with a miR-501-3p mimic and a dual luciferase reporter plasmid containing either wild type miR-501-3p (RLuc wt *OGT* 3'UTR) or mutated miR-501-3p binding site (RLuc mt *OGT* 3'UTR) to modulate RLuc expression. Co-transfection of the miR-501-3p mimic and empty RLuc vector was used as control. Data are expressed as mean percentage of *Renilla* luciferase activity ± s.d. normalized to *firefly* luciferase, and relative to co-transfection of the vectors with non-targeting miRNA (miR-Ctrl). Results are from three independent experiments in triplicate. The dashed line indicates values from control-transfected cells set at 100%. Statistics: *, *p*-value < 0.05, t-test. Right: Schematic representation of the used constructs.

Figure 4. Silencing of *OGT* affects HCV morphogenesis and infectivity. (A) Analysis of HCV infectivity. Huh7.5.1 cells were transfected with siCtrl, a pool of siRNA against *OGT* or ApoE as a loss-of-function control to perturb HCV assembly, prior to infection with HCVcc (Jc1) two days later (entry and replication). Mock-transfected cells were used as control (Ctrl). After another 48h, intra- and extracellular HCVcc particles were used to infect naïve Huh7.5.1 cells (assembly and infectivity). Virus supernatants of Huh7.5.1 cells were assayed by (left) endpoint dilution assay (TCID50). Intra- and extracellular HCV RNA was purified and analyzed by RT-qPCR to calculate (right) the specific infectivity (TCID50/RNA). Data are expressed as mean percentage as compared to control ± s.d. Results are from four independent experiments in triplicate. The dashed line indicates values from control-transfected cells set at 100%. Statistics**:** *, *p*-value < 0.05, Mann-Whitney test. (B) Genotype-independent effect of OGT on HCV infection. Huh7.5.1 cells were transfected with siCtrl or

siOGT prior to infection with HCVcc JcR2a (genotype 2a), H77R2a (genotype 1a) or Con1R2a (genotype 1b). Experiments were carried out and analyzed as described in A. Data are expressed as mean percentage of Renilla luciferase activity as compared to control ± s.d. Results are from three independent experiments in quadruplicate. The dashed line indicates values from control-transfected cells set at 100%. Statistics**:** *, *p*-value < 0.05, Mann-Whitney test. (C) Activity of OGT/OGA inhibitors on O-GlcNAcylation. The activity of $Ac_4$5S-GlcNAc (OGT inhibitor) or Thiamet G (OGA inhibitor) on O-GlcNAcylation of proteins in Huh7.5.1 cells was demonstrated by Western blot as described in Supplementary Methods. (D) Effect of O-GlcNAcylation on HCV infectivity. Huh7.5.1 cells were electroporated with HCVcc (JcR2a), prior to treatment with increasing concentrations of $Ac_4$5S-GlcNAc (OGT inhibitor, left) or Thiamet G (OGA inhibitor, right) 4h later. After 96h, supernatants were transferred onto naïve Huh7.5.1 cells and electroporated cells were lysed to determine luciferase activity. Luciferase activity in infected Huh7.5.1 cells was assessed 72h later. Data are expressed as mean percentage as compared to control ± s.d. Results are from three independent experiments in quadruplicate. The dashed line indicates values from vehicle-treated cells set at 100%. Statistics**:** *, *p*-value < 0.05, Mann-Whitney test.

Figure 5. Silencing of *OGT* modulates HCVcc biophysical properties. (A) Separation of HCVcc by iodixanol density gradient ultracentrifugation. HCVcc were produced in non-targeting siRNA control- or siOGT-transfected Huh7.5.1 cells. After overlaying HCVcc (JcR2A) on a 4%-40% iodixanol step gradient and ultracentrifugation for 16h, fractions of HCV particles were used to infect naïve Huh7.5.1 cells in order to determine TCID50. HCV RNA of each fraction was purified and analyzed by RT-qPCR. Data are expressed as mean ± s.d. from three independent experiments. (B) Specific infectivity (TCID50/RNA) was calculated and the density was determined by weighting each fraction. Specific infectivity of each fraction is expressed as fold change as compared to the total infectivity of the control. Data are expressed as mean ± s.d. from three independent experiments. (C-D) ApoE and ApoB concentrations in the individual fractions were determined by ELISA. The dashed lines

indicate limits of quantification of the assays. Data are expressed as mean ± s.d. from three independent experiments.

Figure 6. Silencing of *OGT* increases the size of HCVcc. (A) Representative pictures of HCV particles generated in Huh7.5.1 cells transfected with non-targeting siRNA (siCtrl) or siOGT. (B-F) Comparative analysis of particle size distribution for immunocapture (IC) from HCV particles produced in Huh7.5.1 cells transfected with siCtrl or siOGT prior to infection with HCVcc (JcR2a) following sucrose-cushion purification (B) or iodixanol gradient fractionation (C-F) of HCVcc. HCVcc were transferred via anti-E2 antibody AR3A on electron microscopy (EM) grids through IC. Particle size distribution was assessed from a series of randomly acquired electron micrographs with Image-J software (NIH). Results from one of three (A-B) or two (C-F) independent experiments are shown. Black lines: size distribution of immunocaptured HCVcc produced in siCtrl-transfected cells. Grey lines: size distribution of immunocaptured HCVcc produced in siOGT-transfected cells.

Figure 7. *OGT* expression increases in HCC. (A-B) Huh7.5.1 cells were infected with HCV (JcR2a). After 72h, RNA and proteins were purified, and *OGT* expression analyzed by RT-qPCR and Western blot. (A) Percentage of *OGT* mRNA expression relative to uninfected Huh7.5.1 cells (Ctrl). Results are presented as mean ± s.d. from three independent experiments in duplicate. The dashed line indicates values from uninfected Huh7.5.1 cells set at 100%. Statistics: *, *p*-value < 0.05, Mann-Whitney test. (B) OGT protein expression. Left: percentage of OGT protein expression relative to uninfected Huh7.5.1 cells (Ctrl) following quantification of Western blots as described in Supplementary Methods. Results are presented as mean ± s.d. from three independent experiments. The dashed line indicates values from uninfected Huh7.5.1 cells set at 100%. Statistics: *, *p*-value < 0.05, Mann-Whitney test. Right: representative Western blot analysis of OGT and actin. (C) *OGT* expression and viral load in liver tissue from 22 HCV-infected patients and 6 patients not infected with HCV described in[55]. Spearman correlation: rho = 0.06004019, p-value = 0.77.

(D-E) OGT expression in liver tissue from 22 HCV-infected patients and 6 patients not infected with HCV according to fibrosis (D) or activity (E) scores described in[55]. Wilcoxon test: F1 vs F0 p-value = 0,38; F2 vs F0 p-value = 0,18; F3 vs F0 p-value = 0,43; F4 vs F0 p-value = 0,17; A1 vs A0 p-value = 0,28; A2 vs A0 p-value = 0,23; A3 vs A0 p-value = 0,09. (F) *OGT* expression in tumor (HCC) and non-tumor (Ctrl) liver tissue from 39 HCV-infected patients, 83 HBV-infected, 80 patients with alcoholic liver disease (ALD) and 13 patients with non-alcoholic liver disease (NAFLD) as described in Supplementary Methods. *, *p*-value < 0.05, Wilcoxon test.

Table 1. Computational analysis of miR-501-3p and miR-619-3p targets and pathway enrichment.

miRNA ID	Target gene symbol	*Pathway* or network
miR-501-3p	*MEF2A*; *PPP3CA*; *PPP3CC*	*Calcium signaling*
	HMGCS1	*Cholesterol biosynthesis*
	AFF4; *CHMP1B*; *CUX1*; *DCLK1*; *LMX1A*; *PTBP2*; *RBMS1*; *RC3H1*; *SCN2A*; *SEC63*; *ZFHX4*	Inflammatory response, dermatological diseases and conditions, inflammatory disease
	CDK6; *CSDE1*; *GLI2*; *HOXD10*; *LSM5*; *MEF2A*; *MYCN*; *OGT*; *PPP2R2C*; *PPP2R5E*; *SEMA3C*; *TFDP2*	Cellular development, nervous system development and function; organ morphology
	CIT; *COL10A1*; *FNBP1L*; *GAN*; *HERC1*; *KPNA4*; *NONO*; *SHPRH*; *STRN*; *TARDBP*; *UBE2H*; *USP37*	Cell death and survival; cellular compromise; free radical scavenging
	ATXN1; *CBLL1*; *CEBPA*; *DCC*; *PEX5L*; *RCC2*; *RNF144A*; *ZC3H12C*	Cell morphology, cellular assembly and organization; cellular function and maintenance
miR-619-3p	*RUNX1T1*; *SMAD3*	*Adipocyte biogenesis*
	FOXG1; *GPBP1*; *MID1*; *MKL2*; *MSI1*; *PCBP2*; *WDFY3*	Cell cycle; organismal injury and abnormalities; cancer
	ACVR2B; *DCX*; *ESRRG*; *MAPK9*; *OGT*; *PCBP1*; *PDE3B*; *SMAD3*; *SMARCC1*; *TGFB3*; *PAPOLA*	Carbohydrate metabolism, energy production; small molecule biochemistry
	RUNX1T1; *SHANK2*; *SLC35D1*	Gene expression, lipid metabolism, small molecule biochemistry

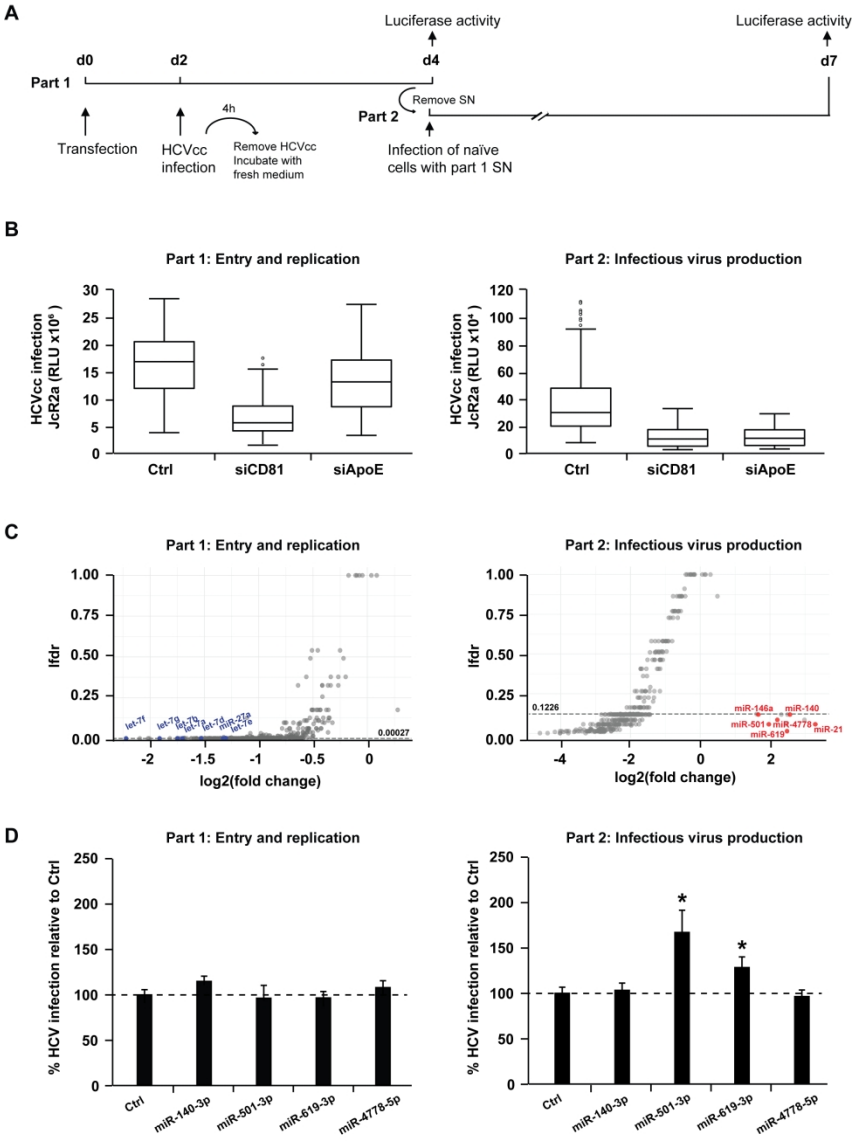
A
Luciferase activity
Luciferase activity
d0
d2
d4
d7
Part 1
Part 2
Remove SN
4h
Transfection
HCVcc infection
Remove HCVcc Incubate with fresh medium
Infection of naïve cells with part 1 SN
B
Part 1: Entry and replication
Part 2: Infectious virus production
HCVcc infection JcR2a (RLU x10⁶)
HCVcc infection JcR2a (RLU x10⁴)
Ctrl
siCD81
siApoE
C
Part 1: Entry and replication
Part 2: Infectious virus production
lfdr
log2(fold change)
0.00027
0.1226
let-7f
let-7g
let-7i
let-7d
miR-23a
let-7e
miR-146a
miR-140
miR-501
miR-4778
miR-619
miR-21
D
Part 1: Entry and replication
Part 2: Infectious virus production
% HCV infection relative to Ctrl
Ctrl
miR-140-3p
miR-501-3p
miR-619-3p
miR-4778-5p

Figure 1

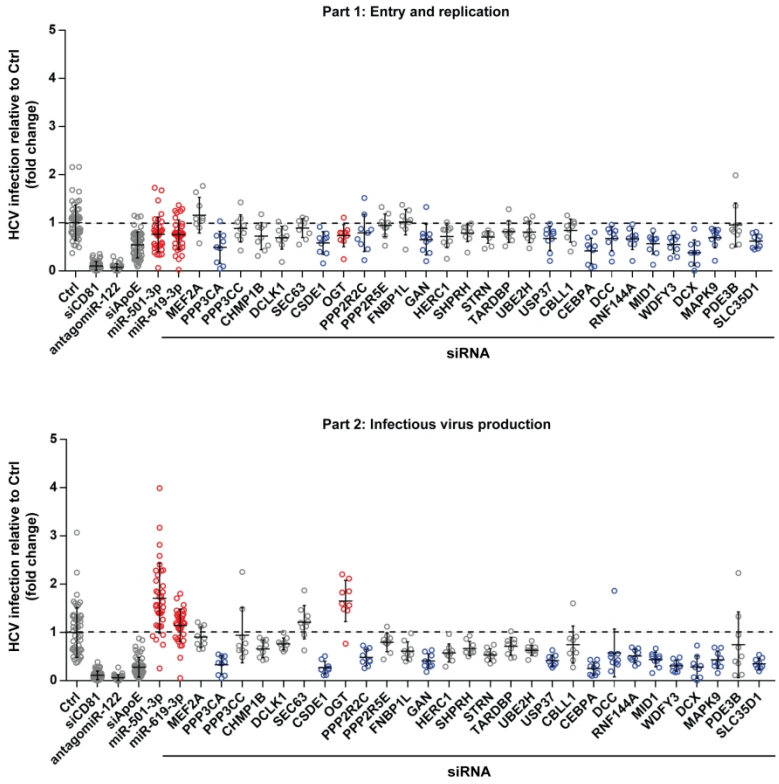
Part 1: Entry and replication
HCV infection relative to Ctrl (fold change)
0
1
2
3
4
5
Ctrl
siCD81
antagomiR-122
siApoE
miR-501-3p
miR-619-3p
MEF2A
PPP3CA
PPP3CC
CHMP1B
DCLK1
SEC63
CSDE1
OGT
PPP2R2C
PPP2R5E
FNBP1L
GAN
HERC1
SHPRH
STRN
TARDBP
UBE2H
USP37
CBLL1
CEBPA
DCC
RNF144A
MID1
WDFY3
DCX
MAPK9
PDE3B
SLC35D1
siRNA
Part 2: Infectious virus production
HCV infection relative to Ctrl (fold change)
0
1
2
3
4
5
Ctrl
siCD81
antagomiR-122
siApoE
miR-501-3p
miR-619-3p
MEF2A
PPP3CA
PPP3CC
CHMP1B
DCLK1
SEC63
CSDE1
OGT
PPP2R2C
PPP2R5E
FNBP1L
GAN
HERC1
SHPRH
STRN
TARDBP
UBE2H
USP37
CBLL1
CEBPA
DCC
RNF144A
MID1
WDFY3
DCX
MAPK9
PDE3B
SLC35D1
siRNA

Figure 2

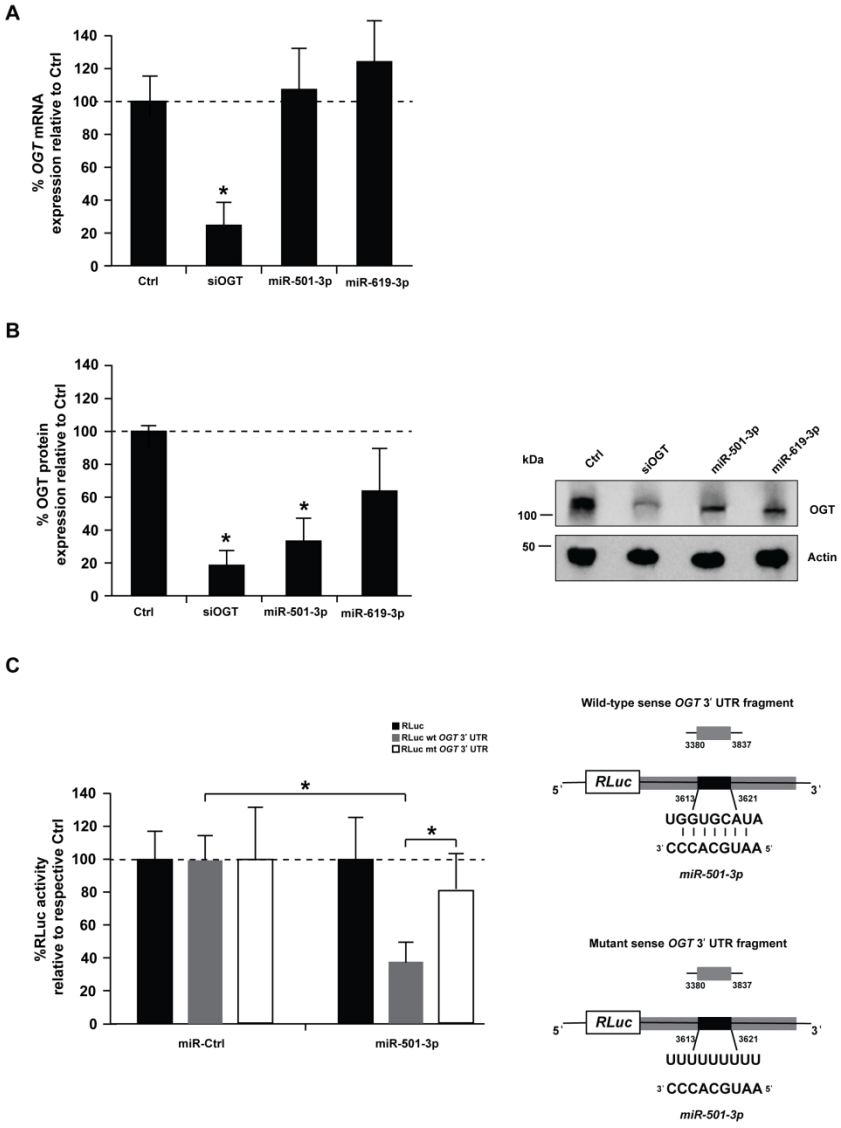
A
% OGT mRNA expression relative to Ctrl
140
120
100
80
60
40
20
0
*
Ctrl
siOGT
miR-501-3p
miR-619-3p
B
% OGT protein expression relative to Ctrl
140
120
100
80
60
40
20
0
*
*
Ctrl
siOGT
miR-501-3p
miR-619-3p
kDa
Ctrl
siOGT
miR-501-3p
miR-619-3p
100
50
OGT
Actin
C
RLuc
RLuc wt OGT 3' UTR
RLuc mt OGT 3' UTR
%RLuc activity relative to respective Ctrl
140
120
100
80
60
40
20
0
*
*
miR-Ctrl
miR-501-3p
Wild-type sense OGT 3' UTR fragment
3380
3837
5'
RLuc
3'
3613
3621
UGGUGCAUA
3' CCCACGUAA 5'
miR-501-3p
Mutant sense OGT 3' UTR fragment
3380
3837
5'
RLuc
3'
3613
3621
UUUUUUUUU
3' CCCACGUAA 5'
miR-501-3p

Figure 3

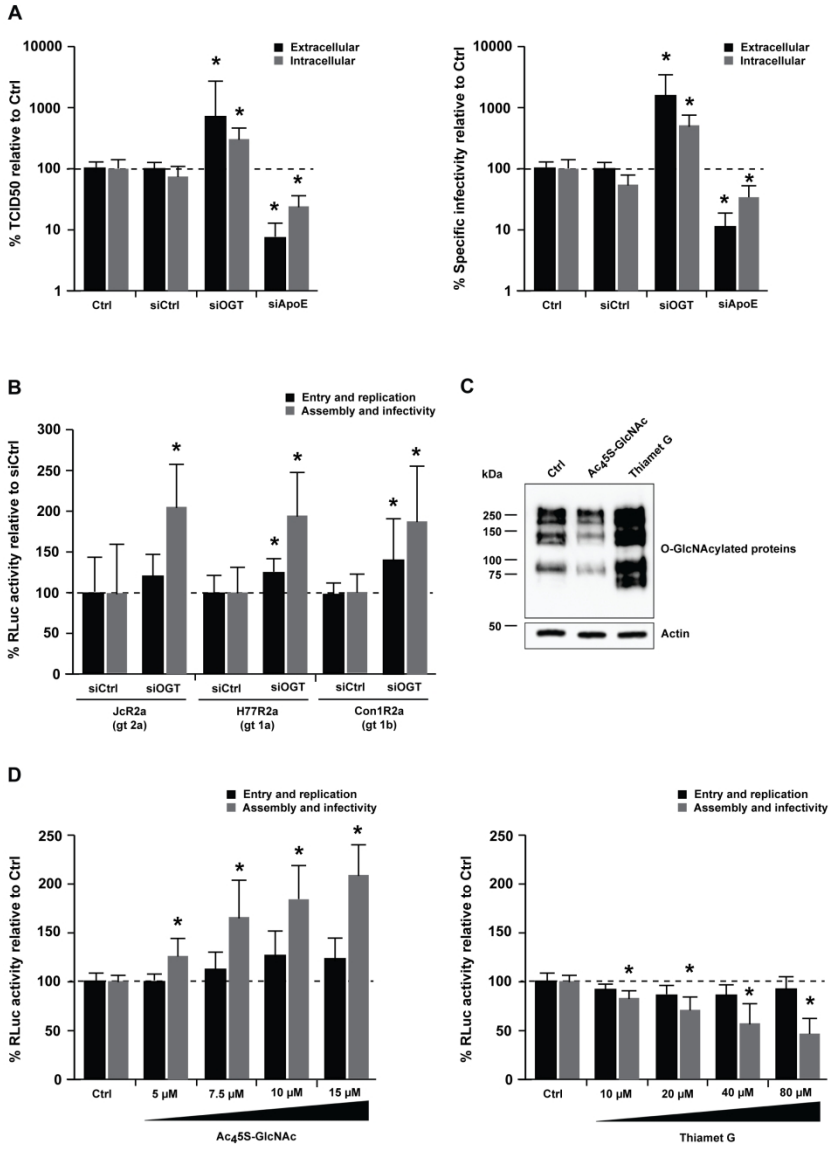
A
% TCID50 relative to Ctrl
Extracellular
Intracellular
Ctrl
siCtrl
siOGT
siApoE
% Specific infectivity relative to Ctrl
B
% RLuc activity relative to siCtrl
Entry and replication
Assembly and infectivity
JcR2a (gt 2a)
H77R2a (gt 1a)
Con1R2a (gt 1b)
C
kDa
Ctrl
Ac4 5S-GlcNAc
Thiamet G
O-GlcNAcylated proteins
Actin
D
% RLuc activity relative to Ctrl
5 µM
7.5 µM
10 µM
15 µM
Ac4 5S-GlcNAc
20 µM
40 µM
80 µM
Thiamet G

Figure 4

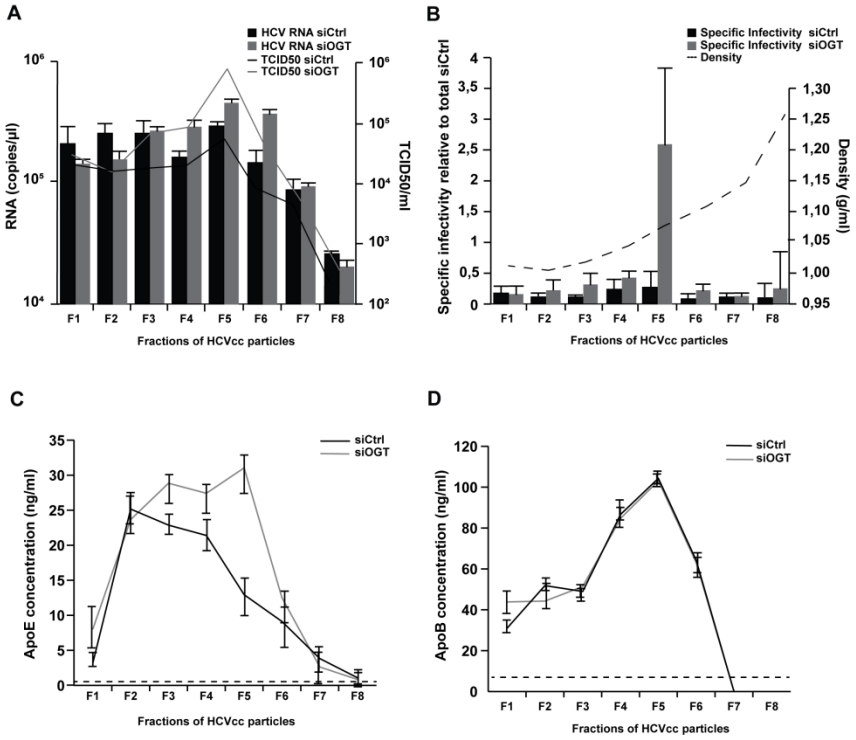
A
HCV RNA siCtrl
HCV RNA siOGT
TCID50 siCtrl
TCID50 siOGT
RNA (copies/µl)
TCID50/ml
Fractions of HCVcc particles
B
Specific Infectivity siCtrl
Specific Infectivity siOGT
Density
Specific infectivity relative to total siCtrl
Density (g/ml)
Fractions of HCVcc particles
C
siCtrl
siOGT
ApoE concentration (ng/ml)
Fractions of HCVcc particles
D
siCtrl
siOGT
ApoB concentration (ng/ml)
Fractions of HCVcc particles

Figure 5

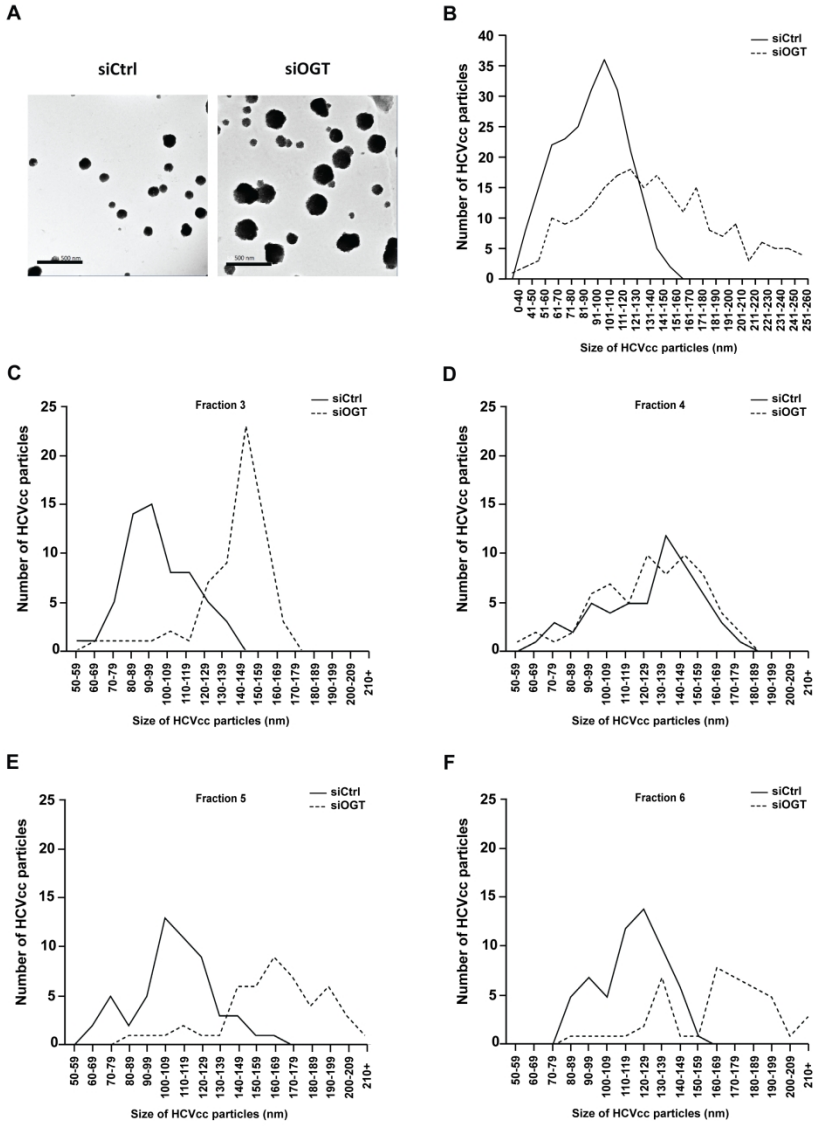
A
siCtrl
siOGT
B
siCtrl
siOGT
Number of HCVcc particles
Size of HCVcc particles (nm)
C
Fraction 3
siCtrl
siOGT
Number of HCVcc particles
Size of HCVcc particles (nm)
D
Fraction 4
siCtrl
siOGT
Number of HCVcc particles
Size of HCVcc particles (nm)
E
Fraction 5
siCtrl
siOGT
Number of HCVcc particles
Size of HCVcc particles (nm)
F
Fraction 6
siCtrl
siOGT
Number of HCVcc particles
Size of HCVcc particles (nm)

Figure 6

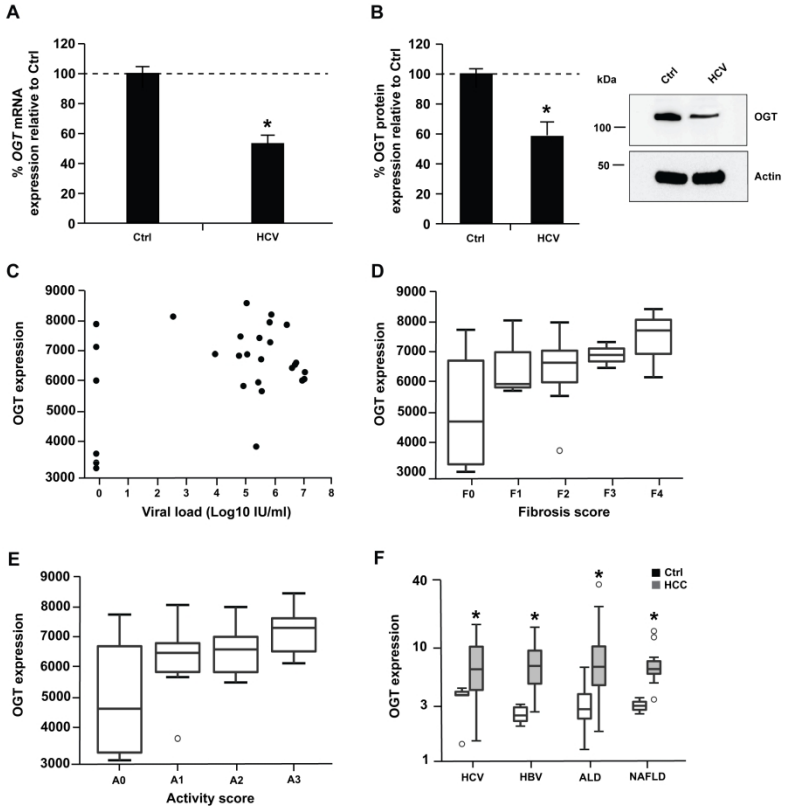
A
% OGT mRNA expression relative to Ctrl
Ctrl
HCV
B
% OGT protein expression relative to Ctrl
kDa
Ctrl
HCV
100
50
OGT
Actin
C
OGT expression
Viral load (Log10 IU/ml)
D
OGT expression
F0
F1
F2
F3
F4
Fibrosis score
E
OGT expression
A0
A1
A2
A3
Activity score
F
OGT expression
Ctrl
HCC
HCV
HBV
ALD
NAFLD

Figure 7

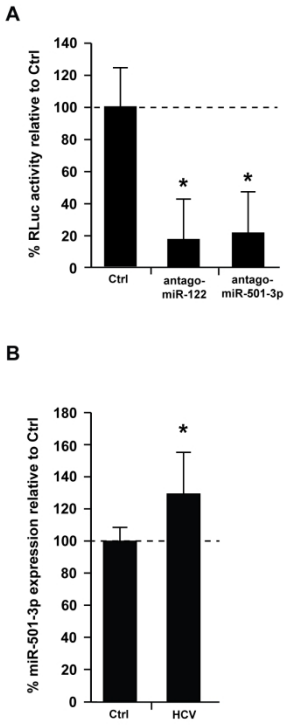
A
% RLuc activity relative to Ctrl
140
120
100
80
60
40
20
0
*
*
Ctrl
antago-miR-122
antago-miR-501-3p
B
% miR-501-3p expression relative to Ctrl
180
160
140
120
100
80
60
40
20
0
*
Ctrl
HCV

Figure S1

Supplementary Information

A functional microRNA screen uncovers O-linked N-acetylglucosamine transferase as a host factor modulating hepatitis C virus morphogenesis

Katharina Herzog[1,2*], Simonetta Bandiera[1,2*], Sophie Pernot[1,2], Catherine Fauvelle[1,2], Frank Jühling[1,2], Amélie Weiss[2,3,4,5], Anne Bull[6], Sarah C. Durand[1,2], Béatrice Chane-Woon-Ming[2,7], Sébastien Pfeffer[2,7], Marion Mercey[8], Hervé Lerat[8], Jean-Christophe Meunier[6], Wolfgang Raffelsberger[2,3,4,5], Laurent Brino[2,3,4,5], Thomas F. Baumert[1,2,9,#], Mirjam B. Zeisel[1,2,10,#]

[1]Inserm, U1110, Institut de Recherche sur les Maladies Virales et Hépatiques, Strasbourg, France; [2]Université de Strasbourg, Strasbourg, France; [3]Institut de Génétique et de Biologie Moléculaire et Cellulaire, Illkirch, France ; [4]CNRS, UMR7104, Illkirch, France ; [5]Inserm, U1258, Illkirch, France ; [6]Inserm U1259, Faculté de Médecine, Université François Rabelais and CHRU de Tours, Tours, France ; [7]Architecture et Réactivité de l'ARN – UPR 9002, Institut de Biologie Moléculaire et Cellulaire du CNRS, Strasbourg, France; [8]Institute for Advanced Biosciences, Centre de Recherche UGA - Inserm U1209 - CNRS UMR 5309, Grenoble, France, [9]Institut Hospitalo-Universitaire, Pôle Hépato-digestif, Hôpitaux Universitaires de Strasbourg, Strasbourg, France; [10]Inserm, U1052, CNRS UMR 5286, Centre Léon Bérard (CLB), Cancer Research Center of Lyon (CRCL), Université de Lyon (UCBL), Lyon, France

*Authors contributed equally to this work

Supplementary Material and methods

Cells and cell culture conditions. The source and culture conditions of Huh7.5.1 cells have been described[1]. HeLa cells were purchased from ATCC and cultured in Dulbecco´s modified Eagle medium (Gibco® DMEM GlutaMAX™, ThermoFisher Scientific) containing 1% sodium pyruvate as described for Huh7.5.1 cells[1].

Viruses and infectivity assays. Cell culture-derived recombinant cell culture-derived hepatitis C virus (HCVcc) Jc1 (genotype 2a/2a chimera), H77R2a (genotype 1a/2a chimera engineered for *Renilla* luciferase expression), Con1R2a (genotype 1b/2b chimera engineered for *Renilla* luciferase expression), and JcR2a (genotype 2a/2a chimera engineered for *Renilla* luciferase expression) were generated in Huh7.5.1 cells as described[1, 2, 3, 4]. HCVcc infectivity was determined by calculating the 50% tissue culture infectious dose (TCID50) using anti-NS5A antibody as described[5, 6] or by assessing luciferase activity. HCVcc were used at 10^5-10^6 TCID50/mL throughout the study. HCV RNA was purified using a QIAmp viral RNA minikit (Qiagen) and analyzed by one-step RT-qPCR using a Sensi Fast NO ROX kit (Bioline) according to the manufacturer's instructions. Standard curves were performed using 10-fold dilution series of HCV RNA.

Purification of HCVcc particles using sucrose cushion or iodixanol density gradient. HCVcc (JcR2a) were concentrated 10-fold using a Vivaspin column (GE Healthcare). For sucrose cushion purification, HCVcc were purified by overlaying 3.5 mL of culture media on 1.5 mL of 20% sucrose, and by ultracentrifuging samples for 4h at 40,000 rpm on a SW-55 rotor (Beckman Coulter). Purified HCVcc were resuspended in 30 µL of PBS for analysis via immunocapture and electron microscopy. Density distributions of infectious HCVcc were determined by overlaying 0.5 mL culture media on a 5 mL, 4%-40% iodixanol step gradient, and ultracentrifuging samples for 16h at 40,000 rpm on a SW-55 rotor (Beckman Coulter): 625 µl fractions were carefully harvested from the top of each tube, and density was determined by weighing. Infectivity of each fraction was quantified by TCID50 using anti-NS5A antibody as described[5, 6], while HCV RNA of fractions was purified and analyzed as described above. ApoB and ApoE concentrations of fractions were determined by enzyme-linked immunosorbent assay (Human Apolipoprotein B or E ELISA^{PRO} kit, Mabtech) undiluted or in a 1:50 dilution, respectively, according to the manufacturer's instructions (Mabtech).

miRNA mimics and siRNAs. Non-targeting control miRNA, miR-501-3p mimic, miR-619-3p mimic, antagomiR-122, antagomiR-501-3p, non-targeting control antagomiR, non-targeting control siRNA, siRNAs targeting *OGT, CD81* or *apoliporotein E* (*ApoE*) and a library of 28 custom ON-TARGETplus smart pool siRNAs were purchased from Dharmacon (GE Healthcare).

miRNA expression analysis. Total RNA (100 ng) was purified from control or HCV-infected Huh7.5.1 cells using Tri reagent® (Thermo Scientific) and Direct-zol™ RNA purification kit (Zymo Research). Total RNA was first polyadenylated and reverse transcribed using a miScript II RT system (Qiagen) according to the manufacturer's instructions. The obtained cDNA was subjected to RT-qPCR using miScript SYBR Green kit (Qiagen). Primers were the mature miRNA sequence for the forward primer (Thermo Scientific) and the universal miScript primer (Qiagen) for the reverse primer. Data were analyzed by the ΔΔCt method using small nucleolar RNA, C/D box 61 (SNORD61) as an endogenous reference and the non-infected samples as a calibrator[7].

Antibodies. Rabbit anti-OGT antibodies DM-17 and AL24 were purchased from Sigma or kindly provided by Dr. G. W. Hart and Dr. S. Hardivillé (Johns Hopkins University School of Medicine, Baltimore, MD)[8], respectively. Mouse anti-β-actin antibody was purchased from Abcam and mouse, rabbit or sheep HRP-conjugated secondary antibodies (A9044, A0545 and A3415, respectively) were purchased from Sigma. Sheep anti-NS5A serum for determination of TCID50 was a kind gift from M. Harris[9]. Human anti-E2 (AR3A) antibody[10] for electron microscopy analysis was kindly provided by Mansun Law (SCRIPPS, California, USA).

Western blotting. OGT and actin protein expression in human cells was assessed by Western blot as described[8] with some modifications. Briefly, cells were lysed in lysis buffer no. 6 (R&D Systems) according to the manufacturer's instructions. Equal amounts of protein

(40 µg) were size-separated through a Mini PROTEAN® TGX Stain-Free™ gel electrophoresis (Bio-Rad) and transferred to PVDF membranes (Bio-Rad). Immunoblots were performed using rabbit anti-OGT (1:2000) and mouse anti-β-actin (1:1000) antibodies[8, 11]. Antigen-antibody complexes were detected by incubating the membrane with the appropriate HRP-conjugated secondary antibodies (1:5000; 1:10,000) and imaged by enhanced chemiluminescence with a ChemiDoc MP imager (Bio-Rad). Quantification of protein expression was performed using ImageLab™ 5.2.1 software (BioRad). For analysis of OGT and GAPDH expression in liver tissue from HCV transgenic (FL-N/35) or wild-type mice[12], crude protein extracts were prepared by homogenization of frozen mouse livers (50–100 µg) in tissue lysis buffer from the Ambion PARIS RNA (Thermo Scientific) and protein isolation kit, supplemented with protease inhibitors (cOmpleteTM EDTA-free protease inhibitor mixture, Sigma-Aldrich) and phosphatase inhibitors (PhosSTOPTM, Sigma-Aldrich), using a tissue homogenizer (MP Fast Prep24, MP Biomedicals, Santa Ana, CA) and MP Lysing Matrix A tubes. Proteins were quantified using the BCA assay (Thermo Fisher Scientific). Western blotting was performed as described above.

Immunocapture and electron microscopy analysis of viral particles. Sucrose-cushion purified or iodixanol gradient fractionated HCVcc (JcR2a) produced in cells transfected with a non-targeting siRNA control or a pool of siRNA against OGT were transferred via anti-E2 antibody AR3A on electron microscopy (EM) grids through immunocapture (IC) as described[13]. Particles were stained with uranyl acetate dihydrate and observed in a JEOL 1230 electron microscope. Series of electron micrographs were acquired at random from IC EM grids. The images were then analyzed with Image-J software, to determine the particle size distribution.

Gene expression analysis in patient-derived liver tissue. For OGT expression analysis in patient's samples, raw data were retrieved from the Gene Expression Omnibus (GSE84346) and re-analyzed by quality-trimming (cutadapt) and mapping (HISAT2) to human genome

assembly hg19. Reads mapping to Gencode v.19 genes were counted using htseq-count and normalized applying DESeq2. Activity and fibrosis scores as well as viral load were taken from the supplemental data published in[14]. To analyze OGT expression in liver tissue of chronic hepatitis B or C patients, FPKM values and clinical data were retrieved from The Cancer Genome Atlas (TCGA, https://www.cancer.gov/about-nci/organization/ccg/research/structural-genomics/tcga). This data set includes samples from 39 HCV-infected patients, 83 hepatitis B virus (HBV)-infected, 80 patients with alcoholic liver disease (ALD) and 13 patients with non-alcoholic fatty liver disease (NAFLD).

Supplementary References

1 Zhong J, Gastaminza P, Cheng G*, et al.* Robust hepatitis C virus infection in vitro. Proc Natl Acad Sci U S A 2005;**102**:9294-9.

2 Reiss S, Rebhan I, Backes P*, et al.* Recruitment and activation of a lipid kinase by hepatitis C virus NS5A is essential for integrity of the membranous replication compartment. Cell Host Microbe 2011;**9**:32-45.

3 Da Costa D, Turek M, Felmlee DJ*, et al.* Reconstitution of the entire hepatitis C virus life cycle in non-hepatic cells. J Virol 2012;**86**:11919-25.

4 Fauvelle C, Felmlee DJ, Crouchet E*, et al.* Apolipoprotein E Mediates Evasion From Hepatitis C Virus Neutralizing Antibodies. Gastroenterology 2016;**150**:206-17 e4.

5 Lindenbach BD, Evans MJ, Syder AJ*, et al.* Complete replication of hepatitis C virus in cell culture. Science 2005;**309**:623-6.

6 Bandiera S, Pernot S, El Saghire H*, et al.* Hepatitis C Virus-Induced Upregulation of MicroRNA miR-146a-5p in Hepatocytes Promotes Viral Infection and Deregulates Metabolic Pathways Associated with Liver Disease Pathogenesis. J Virol 2016;**90**:6387-400.

7 Schmittgen TD, Livak KJ. Analyzing real-time PCR data by the comparative C(T) method. Nat Protoc 2008;**3**:1101-8.

8 Iyer SP, Akimoto Y, Hart GW. Identification and cloning of a novel family of coiled-coil domain proteins that interact with O-GlcNAc transferase. J Biol Chem 2003;**278**:5399-409.

9 Macdonald A, Crowder K, Street A*, et al.* The hepatitis C virus non-structural NS5A protein inhibits activating protein-1 function by perturbing ras-ERK pathway signaling. J Biol Chem 2003;**278**:17775-84.

10 Giang E, Dorner M, Prentoe JC*, et al.* Human broadly neutralizing antibodies to the envelope glycoprotein complex of hepatitis C virus. Proc Natl Acad Sci U S A 2012;**109**:6205-10.

11 Verrier ER, Colpitts CC, Bach C*, et al.* A targeted functional RNA interference screen uncovers glypican 5 as an entry factor for hepatitis B and D viruses. Hepatology 2016;**63**:35-48.

12 Lerat H, Honda M, Beard MR*, et al.* Steatosis and liver cancer in transgenic mice expressing the structural and nonstructural proteins of hepatitis C virus. Gastroenterology 2002;**122**:352-65.

13 Piver E, Boyer A, Gaillard J*, et al.* Ultrastructural organisation of HCV from the bloodstream of infected patients revealed by electron microscopy after specific immunocapture. Gut 2017;**66**:1487-95.

14 Boldanova T, Suslov A, Heim MH*, et al.* Transcriptional response to hepatitis C virus infection and interferon-alpha treatment in the human liver. EMBO Mol Med 2017;**9**:816-34.

Supplementary figure legends

Figure S1. (A) Effect of miR-501-3p inhibition on HCV infectivity. Huh7.5.1 cells were transfected with control antagomiR (Ctrl), antagomiR-122 as loss-of-function control to perturb HCV replication and antagomiR-501-3p, prior to infection with HCVcc (JcR2a) according to the two-step protocol depicted in Fig. 1A. After 48h, supernatants were transferred onto naive Huh7.5.1 cells. After 72h, Renilla Luciferase activity of infected Huh7.5.1 cells was determined. Data are expressed as mean percentage as compared to Ctrl ± s.d. Results are from four independent experiments in quadruplicate. The dashed line indicates values from vehicle-treated cells set at 100%. Statistics**:** *, *p*-value < 0.05, Mann-Whitney test. (B) miR-501-3p expression upon HCV infection. Huh7.5.1 cells were infected with HCVcc (JcR2a).

After 72h, RNA was purified and miR-501-3p expression analyzed by RT-qPCR. Percentage of miR-501-3p expression relative to uninfected Huh7.5.1 cells (Ctrl). Results are presented as mean ± s.d. from three independent experiments in duplicate. The dashed line indicates values from uninfected Huh7.5.1 cells set at 100%. Statistics: *, *p*-value < 0.05, Mann-Whitney test.

Supplementary Table 1. A genome-wide miRNA mimic screen identifies cellular miRNAs modulating HCV infection. Log2(FC), lfdr and effect on HCV infection in part 1 and part 2 of the screen are shown for the individual miRNAs of the miRNA mimic library. In red: proviral effect, in blue: antiviral effect. FC: fold change, lfdr: local false discovery rate

miRNA ID	Mature Sanger ID	Library ID	Mature Sequence	Part 1			Part 2		
				Log2(FC)	lfdr	Effect on HCV	Log2(FC)	lfdr	Effect on HCV
hsa-let-7a	MIMAT0000062	C-300473-05	UGAGGUAGUAGGUUGUAUAGUU	-1.70177935969617	3.9917e-05	TRUE	-3.28400225976063	0.0018396	TRUE
hsa-let-7b	MIMAT0000063	C-300476-05	UGAGGUAGUAGGUUGUGUGGUU	-1.74684091191792	8.3715e-05	TRUE	-3.61453853652595	0.009387	TRUE
hsa-let-7d	MIMAT0000065	C-300478-07	AGAGGUAGUAGGUUGCAUAGUU	-1.53075932976348	0.00023985	TRUE	-2.746321670251 62	0.057617	TRUE
hsa-let-7e	MIMAT0000066	C-300479-05	UGAGGUAGGAGGUUGUAUAGUU	-1.30271875995011	0.0014577	FALSE	-1.90993819018051	0.081661	TRUE
hsa-let-7f	MIMAT0000067	C-300480-05	UGAGGUAGUAGAUUGUAUAGUU	-2.22178435619614	6.7884e-06	TRUE	-3.76872186786763	0.014453	TRUE
hsa-let-7g	MIMAT0000414	C-300583-05	UGAGGUAGUAGUUUGUACAGUU	-1.91269526615093	6.7884e-06	TRUE	-2.71878759599202	0.057617	TRUE
hsa-miR-101	MIMAT0000099	C-300518-07	UACAGUACUGUGAUAACUGAA	-0.886376348041933	0.0030028	FALSE	-1.9796810124946	0.11887	TRUE
hsa-miR-103-as	MIMAT0007402	C-301453-00	UCAUAGCCCUGUACAAUGCUGCU	-1.11208100417218	0.0074787	FALSE	-2.91287954813545	0.057617	TRUE
hsa-miR-106a*	MIMAT0004517	C-301159-01	CUGCAAUGUAAGCACUUCUUAC	-1.32520114049511	3.9917e-05	TRUE	-2.37739666141336	0.11887	TRUE
hsa-miR-1178	MIMAT0005823	C-301319-00	UUGCUCACUGUUCUUCCCUAG	-1.22556728667978	0.00061109	FALSE	-2.3126959903038	0.08542	TRUE
hsa-miR-1178-5p	MIMAT0022940	C-301922-00	CAGGGUCAGCUGAGCAUG	-1.16672245017752	0.00026644	TRUE	-0.780775920183507	0.72813	FALSE
hsa-miR-1185	MIMAT0005798	C-301317-00	AGAGGAUACCCUUUGUAUGUU	-1.2315368528283	8.3715e-05	TRUE	-0.721316088104541	0.76975	FALSE
hsa-miR-1200	MIMAT0005863	C-301326-00	CUCCUGAGCCAUUCUGAGCCUC	-1.24866404694154	0.00054279	FALSE	-2.09711908610931	0.08542	TRUE
hsa-miR-1205	MIMAT0005869	C-301331-00	UCUGCAGGGUUUGCUUUGAG	-0.801511472736558	0.0053924	FALSE	-3.77846481724539	0.0018396	TRUE
hsa-miR-1207-3p	MIMAT0005872	C-301334-00	UCAGCUGGCCCUCAUUUC	-1.10040811819955	0.00013963	TRUE	-1.691175849016 68	0.26604	FALSE
hsa-miR-122	MIMAT0000421	C-300591-05	UGGAGUGUGACAAUGGUGUUUG	-0.70369537171691	0.040577	FALSE	-3.13425306502985	0.028781	TRUE
hsa-miR-122*	MIMAT0004590	C-301046-01	AACGCCAUUAUCACACUAAAUA	-0.557131436052541	0.037103	FALSE	-1.834045611633 16	0.11887	TRUE
hsa-miR-1226	MIMAT0005577	C-301284-01	UCACCAGCCCUGUGUUCCCUAG	-0.741744822716559	0.0099219	FALSE	-1.896881533343 56	0.11887	TRUE
hsa-miR-1228*	MIMAT0005582	C-301287-01	GUGGGCGGGGGCAGGUGUGUG	-0.947568053691086	0.0049772	FALSE	-2.29154418859234	0.11887	TRUE
hsa-miR-1237-5p	MIMAT0022946	C-302618-00	CGGGGGCGGGGCCGAAGCGCG	-0.956259568604456	0.021994	FALSE	-2.34546898601693	0.057617	TRUE
hsa-miR-1244	MIMAT0005896	C-301865-00	AAGUAGUUGGUUUGUAUGAGAUGGUU	-1.17945761818024	6.1693e-05	TRUE	-0.989861012597079	0.5811	FALSE
hsa-miR-1245b-3p	MIMAT0019951	C-302405-00	UCAGAUGAUCUAAAGGCCUAUA	-0.414846848981959	0.32544	FALSE	-2.27819747964432	0.081661	TRUE
hsa-miR-1255b-2-3p	MIMAT0022725	C-301882-00	AACCACUUUCUUUGCUCAUCCA	-0.427268737714942	0.061384	FALSE	-2.58892190360625	0.023579	TRUE
hsa-miR-1258	MIMAT0005909	C-301384-00	AGUUAGGAUUAGGUCGUGGAA	-1.57210875214914	1.5894e-05	TRUE	-1.639792766737 05	0.36109	FALSE
hsa-miR-125b-2*	MIMAT0004603	C-301061-01	UCACAAGUCAGGCUCUUGGGAC	-0.858902068537019	0.0052694	FALSE	-1.87406855538924	0.11887	TRUE
hsa-miR-1260b	MIMAT0015041	C-301716-00	AUCCCACCACUGCCACCAU	-0.476317862532308	0.10991	FALSE	2.46099391534969	0.057617	TRUE
hsa-miR-1270	MIMAT0005924	C-301867-00	CUGGAGAUAUGGAAGAGCUGUGU	-1.23553336541613	3.9917e-05	TRUE	-2.24160380684469	0.11887	TRUE
hsa-miR-1277	MIMAT0005933	C-301411-00	UACGUAGAUAUAUAUGUAUUUU	-0.745198002045239	0.0074787	FALSE	-3.58615793633136	0.014453	TRUE
hsa-miR-1278	MIMAT0005936	C-301417-00	UAGUACUGUGCAUAUCAUCUAU	-0.494528345361641	0.089234	FALSE	1.60846287059147	0.12226	TRUE
hsa-miR-1283	MIMAT0005799	C-301315-00	UCUACAAAGGAAAGCGCUUUCU	-0.538161112092319	0.061384	FALSE	-2.67520055202511	0.08542	TRUE
hsa-miR-1284	MIMAT0005941	C-301423-00	UCUAUACAGACCCUGGCUUUUC	-0.412436737654723	0.099257	FALSE	-2.28002191497783	0.11527	TRUE
hsa-miR-1287	MIMAT0005878	C-301341-00	UGCUGGAUCAGUGGUUCGAGUC	-1.20683701032783	0.00023985	TRUE	-1.98393331688063	0.08542	TRUE
hsa-miR-1288	MIMAT0005942	C-301424-00	UGGACUGCCCUGAUCUGGAGA	-0.704889827052788	0.0021076	FALSE	-2.89790974514386	0.057617	TRUE
hsa-miR-129-3p	MIMAT0004605	C-301063-01	AAGCCCUUACCCCAAAAAGCAU	-0.999602920325089	0.0021076	FALSE	-1.88681635888787	0.11887	TRUE
hsa-miR-1291	MIMAT0005881	C-301345-00	UGGCCCUGACUGAAGACCAGCAGU	-1.21284220826454	0.00061109	FALSE	-2.02374608043906	0.11887	TRUE
hsa-miR-1293	MIMAT0005883	C-301347-00	UGGGUGGUCUGGAGAUUUGUGC	-1.39687224389743	0.00026644	TRUE	-2.31295737423138	0.057617	TRUE
hsa-miR-1294	MIMAT0005884	C-301348-00	UGUGAGGUUGGCAUUGUUGUCU	-1.44051810095446	8.3715e-05	TRUE	-1.95652126826796	0.057617	TRUE
hsa-miR-1295	MIMAT0005885	C-301349-00	UUAGGCCGCAGAUCUGGGUGA	-1.2640855905457	0.00087976	FALSE	-2.34227893604624	0.11887	TRUE
hsa-miR-1295b-5p	MIMAT0022293	C-302563-00	CACCCAGAUCUGCGGCCUAAU	-0.454374224389677	0.17522	FALSE	-2.73444344828677	0.023579	TRUE
hsa-miR-1298	MIMAT0005800	C-301318-00	UUCAUUCGGCUGUCCAGAUGUA	-0.26688230187125	0.32544	FALSE	-2.44553337713544	0.11887	TRUE
hsa-miR-1302	MIMAT0005890	C-301869-00	UUGGGACAUACUUAUGCUAAA	-1.35138412635794	3.6715e-05	TRUE	-2.60359528922327	0.057617	TRUE
hsa-miR-1302	MIMAT0005890	C-301354-00	UUGGGACAUACUUAUGCUAAA	-1.11168868347783	0.00013793	TRUE	-1.29913904583381	0.51048	FALSE
hsa-miR-1307	MIMAT0005951	C-301434-00	ACUCGGCGUGGCGUCGGUCGUG	-1.12000771587297	0.00054279	FALSE	-2.10295176202445	0.057617	TRUE
hsa-miR-1307-5p	MIMAT0022727	C-301875-00	UCGACCGGACCUCGACCGGCU	-0.803481003211417	0.0030028	FALSE	-1.76491161834359	0.11887	TRUE
hsa-miR-1322	MIMAT0005953	C-301436-00	GAUGAUGCUGCUGAUGCUG	-1.23817643374983	6.1693e-05	TRUE	-1.29920754317295	0.46329	FALSE
hsa-miR-1323	MIMAT0005795	C-301311-00	UCAAAACUGAGGGGCAUUUUCU	-0.756897047236657	0.096607	FALSE	-2.43084213259459	0.11887	TRUE
hsa-miR-135b*	MIMAT0004698	C-301200-01	AUGUAGGGCUAAAAGCCAUGGG	-1.49530939618539	0.0018747	FALSE	-2.98188718020305	0.050122	TRUE
hsa-miR-139-3p	MIMAT0004552	C-301036-03	UGGAGACGCGGCCCUGUUGGAGU	-1.02065377094153	0.00079918	FALSE	-2.77458369079406	0.019699	TRUE
hsa-miR-140-3p	MIMAT0004597	C-301055-01	UACCACAGGGUAGAACCACGG	-0.172675601522775	1	FALSE	2.56894688372309	0.11887	TRUE
hsa-miR-142-3p	MIMAT0000434	C-300610-03	UGUAGUGUUUCCUACUUUAUGGA	-1.00474764620935	0.00023985	TRUE	-1.7577126946261	0.22566	FALSE
hsa-miR-146a	MIMAT0000449	C-300630-03	UGAGAACUGAAUUCCAUGGGUU	0.279820319960687	0.17522	FALSE	1.66479155066337	0.11887	TRUE
hsa-miR-150*	MIMAT0004610	C-301067-01	CUGGUACAGGCCUGGGGGACAG	-1.46501526099695	0.00023985	TRUE	-1.19620229448666	0.40677	FALSE
hsa-miR-151b	MIMAT0010214	C-301973-00	UCGAGGAGCUCACAGUCU	-1.03668648961171	3.9917e-05	TRUE	-2.8985532020104	0.057617	TRUE
hsa-miR-182	MIMAT0000259	C-300557-07	UUUGGCAAUGGUAGAACUCACACU	-0.581360116993454	0.03164	FALSE	-1.81305061189634	0.11887	TRUE
hsa-miR-184	MIMAT0000454	C-300635-03	UGGACGGAGAACUGAUAAGGGU	-1.31700777618768	3.9917e-05	TRUE	-1.52851322717993	0.36109	FALSE
hsa-miR-185	MIMAT0000455	C-300636-07	UGGAGAGAAAGGCAGUUCCUGA	-1.59673044023595	0.00013963	TRUE	-1.74454670174015	0.1633	FALSE
hsa-miR-18b*	MIMAT0004751	C-301187-01	UGCCCUAAAUGCCCCUUCUGGC	-0.825568919117559	0.0027607	FALSE	-2.30862554668178	0.023579	TRUE
hsa-miR-1909	MIMAT0007883	C-301456-00	CGCAGGGGCCGGGUGCUCACCG	-0.511863313449074	0.17522	FALSE	2.49877552994666	0.11887	TRUE
hsa-miR-1915*	MIMAT0007891	C-301466-00	ACCUUGCCUUGCUGCCCGGGCC	-1.71935071114424	8.3715e-05	TRUE	-1.13532112712663	0.46329	FALSE
hsa-miR-196b*	MIMAT0009201	C-301305-00	UCGACAGCACGACACUGCCUUC	-0.949306838412525	0.00054279	FALSE	-3.1358874675771	0.023579	TRUE
hsa-miR-19b	MIMAT0000074	C-300489-03	UGUGCAAAUCCAUGCAAAACUGA	-1.01461439258753	0.00013793	TRUE	-2.75192926226938	0.014453	TRUE
hsa-miR-19b-1*	MIMAT0004491	C-301021-01	AGUUUUGCAGGUUUGCAUCCAGC	-1.68388148726454	0.0030028	FALSE	-2.85695043305243	0.014453	TRUE
hsa-miR-19b-2*	MIMAT0004492	C-301139-01	AGUUUUGCAGGUUUGCAUUUCA	-0.594068837054281	0.037103	FALSE	-2.06967686748099	0.11887	TRUE
hsa-miR-200b*	MIMAT0004571	C-301144-01	CAUCUUACUGGGCAGCAUUGGA	-1.05721574165849	0.0074787	FALSE	-4.59657299807562	0.0018396	TRUE
hsa-miR-203b-5p	MIMAT0019813	C-302277-00	UAGUGGUCCUAAACAUUUCACA	-1.03356122225008	0.00016067	TRUE	-2.13526669981558	0.08542	TRUE
hsa-miR-208a	MIMAT0000241	C-300537-03	AUAAGACGAGCAAAAAGCUUGU	-0.823665097293502	0.0030028	FALSE	-1.54639877799123	0.11887	TRUE
hsa-miR-21	MIMAT0000076	C-300492-03	UAGCUUAUCAGACUGAUGUUGA	-0.768228630205262	0.096607	FALSE	3.29607415881261	0.057617	TRUE
hsa-miR-211-3p	MIMAT0022694	C-301905-00	GCAGGGACAGCAAAGGGUGC	-0.812107428438748	0.0027607	FALSE	-2.21028883028492	0.08542	TRUE
hsa-miR-2114	MIMAT0011156	C-301489-00	UAGUCCCUUCCUUGAAGCGGUC	-0.958796902783202	0.00016326	TRUE	-1.57682863175 63	0.26604	FALSE
hsa-miR-2114*	MIMAT0011157	C-301490-00	CGAGCCUCAAGCAAGGGACUU	-1.02419077915881	0.00013793	TRUE	-2.57866858794879	0.057617	TRUE
hsa-miR-2117	MIMAT0011162	C-301496-00	UGUUCUCUUUGCCAAGGACAG	-0.806177347742896	0.00054279	FALSE	-2.55943646917884	0.057617	TRUE
hsa-miR-216a-3p	MIMAT0022844	C-301886-00	UCACAGUGGUCUCUGGGAUUAU	-1.47806207137632	8.3715e-05	TRUE	-1.62257411616963	0.1633	FALSE
hsa-miR-22	MIMAT0000077	C-300493-03	AAGCUGCCAGUUGAAGAACUGU	-1.14812626998085	0.00054279	FALSE	-2.8254651928315	0.009387	TRUE
hsa-miR-220b	MI0005529	C-301218-01	CCACCACCGUGUCUGACACUU	-1.10856445415353	0.12653	FALSE	-2.50799687656707	0.11887	TRUE
hsa-miR-221*	MIMAT0004568	C-301163-01	ACCUGGCAUACAAUGUAGAUUU	-1.0647285020049	0.00016067	TRUE	0.493351763855846	0.86349	FALSE
hsa-miR-223*	MIMAT0004570	C-301197-01	CGUGUAUUUGACAAGCUGAGUU	-0.596047980424722	0.0074787	FALSE	-2.64001675119474	0.057617	TRUE
hsa-miR-2276	MIMAT0011775	C-301481-00	UCUGCAAGUGUCAGAGGCGAGG	-1.23563628890583	3.9917e-05	TRUE	-0.719842576977581	0.76975	FALSE
hsa-miR-2277-3p	MIMAT0011777	C-301482-00	UGACAGCGCCCUGCCUGCUC	-1.22725149342576	3.9917e-05	TRUE	-2.27801785723 73	0.11887	TRUE
hsa-miR-23a*	MIMAT0004496	C-301025-01	GGGGUUCCUGGGGAUGGGAUUU	-0.773715976814457	0.0018747	FALSE	-2.22574058493535	0.11887	TRUE
hsa-miR-25*	MIMAT0004498	C-301183-01	AGGCGGAGACUUGGGCAAUUG	-1.14410824968417	0.0018747	FALSE	-2.13159960818718	0.057617	TRUE
hsa-miR-2681-3p	MIMAT0013516	C-301978-00	UAUCAUGGAGUUGGUAAAGCAC	-0.84154241088718	0.00023985	TRUE	-0.564927523090931	0.86349	FALSE
hsa-miR-2681-5p	MIMAT0013515	C-301977-00	GUUUUACCACCCCAGGAGACU	-1.20496402288836	3.6715e-05	TRUE	-2.40988448605506	0.057617	TRUE
hsa-miR-2682-3p	MIMAT0013518	C-301980-00	CGCCUCUUCAGCGCUGUCUUCC	-0.908772237664288	0.00013793	TRUE	-1.43184476418853	0.29187	FALSE
hsa-miR-2682-5p	MIMAT0013517	C-301979-00	CAGGCAGUGACUGUUCAGACGUC	-1.24830345350196	1.5894e-05	TRUE	-2.80779774369284	0.014453	TRUE
hsa-miR-26b	MIMAT0000083	C-300501-07	UUCAAGUAAUUCAGGAUAGGU	-0.405072630482104	0.12653	FALSE	-2.50877510131769	0.081661	TRUE
hsa-miR-27a	MIMAT0000084	C-300502-03	UUCACAGUGGCUAAGUUCCGC	-1.32790971119818	3.9917e-05	TRUE	-1.95676458087438	0.1633	FALSE
hsa-miR-27a*	MIMAT0004501	C-301028-01	AGGGCUUAGCUGCUUGUGAGCA	-0.887009503478049	0.0052694	FALSE	-3.44308089121935	0.028781	TRUE
hsa-miR-27b*	MIMAT0004588	C-301154-01	AGAGCUUAGCUGAUUGGUGAAC	-1.00848877755825	0.0014577	FALSE	-2.34115081043794	0.050122	TRUE
hsa-miR-28-5p	MIMAT0000085	C-300503-05	AAGGAGCUCACAGUCUAUUGAG	-0.358344656239635	0.17522	FALSE	-1.5918060993224	0.11887	TRUE
hsa-miR-2861	MIMAT0013802	C-301642-00	GGGGCCUGGCGGUGGGCGG	-0.615484847088555	0.0046172	FALSE	-2.44784331747309	0.081661	TRUE
hsa-miR-2964a-3p	MIMAT0019748	C-302218-00	AGAAUUGCGUUUGGACAAUCAGU	-1.13977573653624	6.1693e-05	TRUE	-0.558827938583115	0.76975	FALSE
hsa-miR-298	MIMAT0004901	C-301212-01	AGCAGAAGCAGGGAGGUUCUCCCA	-0.456122353506126	0.54004	FALSE	-2.83068032162142	0.11887	TRUE
hsa-miR-299-5p	MIMAT0002890	C-300854-03	UGGUUUACCGUCCCACAUACAU	-1.25864926851518	0.00023985	TRUE	-0.317867194423722	1	FALSE
hsa-miR-29a*	MIMAT0004503	C-301178-01	ACUGAUUUCUUUUGGUGUUCAG	-1.35357089379682	0.0021076	FALSE	-2.75349311494331	0.057617	TRUE
hsa-miR-29b-1*	MIMAT0004514	C-301150-01	GCUGGUUUCAUAUGGUGGUUUAGA	-0.970652939446982	0.015067	FALSE	-2.38342736203068	0.11887	TRUE
hsa-miR-301b	MIMAT0004958	C-301252-01	CAGUGCAAUGAUAUUGUCAAAGC	-0.837318501823261	0.0014577	FALSE	-2.28547978225747	0.11887	TRUE
hsa-miR-302b*	MIMAT0000714	C-300668-07	ACUUUAACAUGGAAGUGCUUUC	-0.55091091038492 7	0.037103	FALSE	-1.76045353694163	0.12226	TRUE
hsa-miR-302f	MIMAT0005932	C-301410-00	UAAUUGCUUCCAUGUUU	-1.5960005623826	1.5894e-05	TRUE	-3.17802223827817	0.014453	TRUE
hsa-miR-30b	MIMAT0000420	C-300590-03	UGUAAACAUCCUACACUCAGCU	-0.759206041294187	0.0018747	FALSE	-2.58171571707 78	0.057617	TRUE
hsa-miR-30c-1*	MIMAT0004674	C-301199-01	CUGGGAGAGGGUUGUUUACUCC	-1.43787786865803	8.3715e-05	TRUE	0.291968781990601	1	FALSE
hsa-miR-30c-2*	MIMAT0004550	C-301034-01	CUGGGAGAAGGCUGUUUACUCU	-1.18964958597662	8.3715e-05	TRUE	-0.203715081689554	1	FALSE
hsa-miR-30d	MIMAT0000245	C-300543-03	UGUAAACAUCCCCGACUGGAAG	-0.469794284958227	0.061384	FALSE	-2.24325814749711	0.08542	TRUE
hsa-miR-3115	MIMAT0014977	C-301644-00	AUAUGGGUUUACUAGUUGGU	-0.595634685516391	0.0052694	FALSE	-2.22531374934429	0.11887	TRUE
hsa-miR-3116	MIMAT0014978	C-301645-00	UGCCUGGAACAUAGUAGGGACU	-1.61818516940984	6.7884e-06	TRUE	-1.27627977004857	0.51048	FALSE
hsa-miR-3117	MIMAT0014979	C-301647-00	AUAGGACUCAUAUAGUGCCAG	-1.07944692693698	6.1693e-05	TRUE	0.0583708702116637	1	FALSE
hsa-miR-3119	MIMAT0014981	C-301651-00	UGGCUUUUAACUUUGAUGGC	-0.77136494055742	0.00087976	FALSE	-2.20041353445194	0.11887	TRUE
hsa-miR-3121	MIMAT0014983	C-301654-00	UAAAUAGAGUAGGCAAAGGACA	-0.550473953423974	0.0074787	FALSE	-2.06892978205979	0.11887	TRUE
hsa-miR-3124	MIMAT0014986	C-301657-00	UUCGCGGGCGAAGGCAAAGUC	-1.13549064733399	3.9917e-05	TRUE	-0.910461837996433	0.5811	FALSE
hsa-miR-3126-5p	MIMAT0014989	C-301661-00	UGAGGGACAGAUGCCAGAAGCA	-1.43373948465677	1.5894e-05	TRUE	-0.744651597941774	0.76975	FALSE
hsa-miR-3127	MIMAT0014990	C-301662-00	AUCAGGGCUUGUGGAAUGGGAAG	-0.99218008649803 9	0.00013793	TRUE	-1.20167440176899	0.51048	FALSE
hsa-miR-3130-3p	MIMAT0014994	C-301665-00	GCUGCACCGGAGACUGGGUAA	-0.645251817092445	0.0021076	FALSE	-3.33421355039417	0.023579	TRUE
hsa-miR-3130-5p	MIMAT0014995	C-301666-00	UACCCAGUCUCCGGUGCAGCC	-1.12058237373742	6.1693e-05	TRUE	-2.44166606880781	0.11887	TRUE
hsa-miR-3131	MIMAT0014996	C-301669-00	UCGAGGACUGGUGGAAGGGCCUU	-1.10475333868087	6.1693e-05	TRUE	-0.776623344642163	0.76864	FALSE
hsa-miR-3132	MIMAT0014997	C-301670-00	UGGGUAGAGAAGGAGCUCAGAGGA	-1.0649683988313	8.3715e-05	TRUE	-2.09592053963675	0.11887	TRUE
hsa-miR-3136	MIMAT0015003	C-301676-00	CUGACUGAAUAGGUAGGGUCAUU	-0.837973854149906	0.00054279	FALSE	-2.76623087444917	0.057617	TRUE
hsa-miR-3137	MIMAT0015005	C-301678-00	UCUGUAGCCUGGGAGCAAUGGGGU	-1.05179643968079	8.3715e-05	TRUE	-1.1088570611196	0.51579	FALSE
hsa-miR-3138	MIMAT0015006	C-301679-00	UGUGGACAGUGAGGUAGAGGGAGU	-1.09246960431895	6.1693e-05	TRUE	-1.78790357269758	0.22566	FALSE
hsa-miR-3139	MIMAT0015007	C-301680-00	UAGGAGCUCAACAGAUGCCUGUU	-1.37716815069908	1.5894e-05	TRUE	-1.31106163706907	0.46329	FALSE
hsa-miR-3140	MIMAT0015008	C-301681-00	AGCUUUUGGGAAUUCAGGUAGU	-1.58079760272847	6.7884e-06	TRUE	-3.18144016432131	0.014453	TRUE
hsa-miR-3142	MIMAT0015011	C-301684-00	AAGGCCUUUCUGAACCUUCAGA	-0.977053358967313	0.00013963	TRUE	-1.89446739540295	0.1633	FALSE
hsa-miR-3144-5p	MIMAT0015014	C-301687-00	AGGGGACCAAAGAGAUAUAUAG	-1.13947775501217	3.9917e-05	TRUE	-0.414321660104908	1	FALSE
hsa-miR-3147	MIMAT0015019	C-301692-00	GGUUGGGCAGUGAGGAGGGUGUGA	-0.942186557775687	0.00023985	TRUE	-0.157149408887514	1	FALSE
hsa-miR-3148	MIMAT0015021	C-301694-00	UGGAAAAAACUGGUGUGUGCUU	-1.14553360648851	3.9917e-05	TRUE	-1.08300314433575	0.51579	FALSE
hsa-miR-3150	MIMAT0015023	C-301696-00	CUGGGGAGAUCCUCGAGGUUGG	-1.4167699283789	1.5894e-05	TRUE	-0.986527775853387	0.5811	FALSE
hsa-miR-3150b-5p	MIMAT0019226	C-301961-00	CAACCUCGAGGAUCUCCCCAGC	-1.04471163915449	3.9917e-05	TRUE	-2.12053729635218	0.08542	TRUE
hsa-miR-3151	MIMAT0015024	C-301697-00	GGUGGGGCAAUGGGAUCAGGU	-1.02537680303558	0.00013793	TRUE	-1.56671822128811	0.26604	FALSE
hsa-miR-3152	MIMAT0015025	C-301698-00	UGUGUUAGAAUAGGGGCAAUAA	-1.13601969432149	6.1693e-05	TRUE	-2.17593163296179	0.11887	TRUE
hsa-miR-3157	MIMAT0015031	C-301704-00	UUCAGCCAGGCUAGUGCAGUCU	-1.81838879899633	0.00023985	TRUE	-0.798984655509925	0.76975	FALSE
hsa-miR-3180	MIMAT0018178	C-301583-00	UGGGGCGGAGCUCCCGGAG	-1.37633415637047	0.00013793	TRUE	-1.97473785775 19	0.050122	TRUE
hsa-miR-3186-5p	MIMAT0015067	C-301749-00	CAGGCGUCUGUCUACGUGGCUU	-0.536494894531891	0.061384	FALSE	-2.19613374331388	0.11887	TRUE
hsa-miR-3190-5p	MIMAT0015073	C-301756-02	UCUGGCCAGCUACGUCCCCA	-1.56898213610615	3.9917e-05	TRUE	-3.02592555730969	0.014453	TRUE
hsa-miR-3191-5p	MIMAT0022732	C-302750-00	CUCUCUGGCCGUCUACCUUCCA	-0.896644736818671	0.01741	FALSE	-2.93191055011036	0.057617	TRUE
hsa-miR-32*	MIMAT0004505	C-301181-01	CAAUUUAGUGUGUGUGAUAUUU	-0.561723514860645	0.37761	FALSE	-2.47247129599692	0.11887	TRUE

hsa-miR-323-5p	MIMAT0004696	C-301085-01	AGGUGGUCCGUGGCGCGUUCGC	-0.997451491983143	0.0049772	FALSE	-2.55198466781697	0.014453	TRUE
hsa-miR-323b-5p	MIMAT0001630	C-301724-00	AGGUUGUCCGUGGUGAGUUCGCA	-0.870040751918234	0.00054279	FALSE	-3.51049237466915	0.014453	TRUE
hsa-miR-324-3p	MIMAT0000762	C-300705-05	ACUGCCCCAGGUGCUGCUGG	-0.930125097729152	0.0021076	FALSE	-2.18712046531723	0.081661	TRUE
hsa-miR-328	MIMAT0000752	C-300695-03	CUGGCCCUCUCUGCCCUUCCGU	-1.163970997555505	8.3715e-05	TRUE	-1.57395137899233	0.26604	FALSE
hsa-miR-339-3p	MIMAT0004702	C-301185-01	UGAGCGCCUCGACGACAGAGCCG	-0.424124048504717	0.061384	FALSE	-2.065151571637643	0.08542	TRUE
hsa-miR-342-5p	MIMAT0004694	C-301083-01	AGGGGUGCUAUCUGUGAUUGA	-1.66163157467999	0.0001626	TRUE	-2.01939161434937	0.12226	TRUE
hsa-miR-345-3p	MIMAT0022698	C-301887-00	GCCCUGAACGAGGGGUCUGGAG	-0.839605975652715	0.0021076	FALSE	-2.80466918793858	0.023579	TRUE
hsa-miR-346	MIMAT0000773	C-300712-03	UGUCUGCCCGCAUGCCUCCUCU	-1.22592404544756	0.00023985	TRUE	-1.35203588028221	0.20114	FALSE
hsa-miR-34a*	MIMAT0004557	C-301145-01	CAAUCAGCAAGUAUACUGCCCU	-1.27197605437233	6.1693e-05	TRUE	-0.3780518115586674	1	FALSE
hsa-miR-3529-5p	MIMAT0019828	C-302292-00	AGGUAGACUGGGAUUUGUUGUU	-0.674576387471472	0.034257	FALSE	-1.99747275957492	0.11887	TRUE
hsa-miR-3612	MIMAT0017989	C-301505-00	AGGAGGCAUCUUGAGAAAUGGA	-1.26286494709099	0.00026644	TRUE	-1.44238772362423	0.51048	FALSE
hsa-miR-3616-3p	MIMAT0017996	C-301512-00	CGAGGGCAUUUCAUGAUGCAGGC	-1.103271667150149	0.00054279	FALSE	-1.69108153949499	0.11887	TRUE
hsa-miR-3619-3p	MIMAT0019219	C-301952-00	GGGACCAUCCUGCCUGCUGUGG	-0.361591800679582	0.037103	FALSE	-2.12012061191135	0.11887	TRUE
hsa-miR-3620-5p	MIMAT0022967	C-302619-00	GUGGGCUGGGCUGGGCUGGGCC	-0.963210303847923	0.01741	FALSE	-2.95077111022971	0.014453	TRUE
hsa-miR-3622b-5p	MIMAT0018005	C-301522-00	AGGCAUGGGAGGUCAGGUGA	-1.03124833680421	0.00087976	FALSE	-1.86140566900932	0.08542	TRUE
hsa-miR-365	MIMAT0000710	C-300666-03	UAAUGCCCCUAAAAAUCCUUAU	-1.077137006038737	0.03164	FALSE	-2.565586989697	0.12226	TRUE
hsa-miR-3654	MIMAT0018074	C-301532-00	GACUGGACAAGCUGAGGAA	-0.394926641879625	0.096607	FALSE	-1.99274206927806	0.057617	TRUE
hsa-miR-365b-5p	MIMAT0022833	C-301900-00	AGGGACUUUCAGGGGCAGCUGU	-1.17934943470937	0.00026644	TRUE	-1.48034463468101	0.22566	FALSE
hsa-miR-3666	MIMAT0018088	C-301546-00	CAGUGCAAGUGUAGAUGCCGA	-0.8322031427779	0.0027607	FALSE	-2.76031104596189	0.009387	TRUE
hsa-miR-3667-3p	MIMAT0018090	C-301547-00	ACCUUCCUCUCCAUGGGUCUUU	-1.537371069212222	6.1693e-05	TRUE	-0.1898908086642778	1	FALSE
hsa-miR-3674	MIMAT0018097	C-301555-00	AUUGUAGAACCUAAGAUUGGCC	-0.686422173208126	0.0099219	FALSE	-1.66427885423157	0.08542	TRUE
hsa-miR-3675-5p	MIMAT0018098	C-301557-00	UAUGGGGCUUCUGUAGAGAUUUC	-0.704414688397948	0.0074787	FALSE	-1.47755963621301	0.11887	TRUE
hsa-miR-3676-5p	MIMAT0022734	C-301954-00	AGGAGAUCCUGGGUU	-0.876412168433536	0.00016326	TRUE	-2.81631813362903	0.028781	TRUE
hsa-miR-3680	MIMAT0018106	C-301565-00	GACUCACUCACAGGAUUGUGCA	-0.710055072199479	0.0074787	FALSE	-1.48818626629073	0.11887	TRUE
hsa-miR-3680*	MIMAT0018107	C-301564-00	UUUUGCAUGACCCUGGGAGUAGG	-0.68553099516054	0.0099219	FALSE	-1.84406688012842	0.057617	TRUE
hsa-miR-3681	MIMAT0018108	C-301566-00	UAGUGGAUGAUGCACUCUGUGC	-1.414168599113926	0.00013793	TRUE	-1.60964747472672	0.1633	FALSE
hsa-miR-3681*	MIMAT0018109	C-301567-00	ACACAGUGCUUCAUCCACUACU	-1.394728793333958	0.00013793	TRUE	-1.15667754722324	0.26604	FALSE
hsa-miR-3682	MIMAT0018110	C-301568-00	UGAUGAUACAGGUGGAGGUAG	-1.466733600047121	8.3715e-05	TRUE	-0.6431252165706606	0.72813	FALSE
hsa-miR-3682-5p	MIMAT0019222	C-301956-00	CUACUUCUACCUGUGUUAUCAU	-1.23125674549655	1.5894e-05	TRUE	-2.81908923583428	0.023579	TRUE
hsa-miR-3684	MIMAT0018112	C-301570-00	UUAGACCUAGUACACGUCCUU	-0.580463595828849	0.021994	FALSE	-1.45573759159026	0.11887	TRUE
hsa-miR-3688	MIMAT0018116	C-301574-00	UAUGGAAAGACUUUGCCACUCU	-0.832441806479729	0.0027607	FALSE	-2.02033498247755	0.057617	TRUE
hsa-miR-3688-5p	MIMAT0019223	C-301957-00	AGUGGCAAAGUCUUUCCAUAU	-0.588424467468018	0.0030028	FALSE	-2.09619814608759	0.11887	TRUE
hsa-miR-3689b*	MIMAT0018181	C-301587-00	CUGGGAGGUGUGAUAUUGUGGU	-1.45567876271802	9.6971e-05	TRUE	-1.73246672882077	0.081661	TRUE
hsa-miR-3691	MIMAT0018120	C-301578-00	AGUGGAUGAUGGAGACUCGGUAC	-1.18761474653793	0.00054279	FALSE	-1.75547134579776	0.057617	TRUE
hsa-miR-3691-3p	MIMAT0019224	C-301958-00	ACCAAGUCUGCGUCAUCCUCUC	-0.810629756562153	0.00026644	TRUE	-1.96328717500158	0.11887	TRUE
hsa-miR-374a	MIMAT0000727	C-300681-05	UUAUAAUACAACCUGAUAAGUG	-0.718874319759212	0.0021076	FALSE	-2.60836689817691	0.081661	TRUE
hsa-miR-374c	MIMAT0018443	C-301630-00	AUAAUACAACCUGCUAAGUGCU	-0.337432743025632	0.32544	FALSE	-1.98175619738517	0.11887	TRUE
hsa-miR-374c-3p	MIMAT0022735	C-301969-00	CACUUAGCAGGUUGUAUUAUAU	-0.646260597978354	0.0018747	FALSE	-2.63477891317834	0.028781	TRUE
hsa-miR-376c	MIMAT0000720	C-300674-05	AACAUAGAGGAAAUUCCACGU	-0.624380737173221	0.0053924	FALSE	-2.68639877338995	0.057617	TRUE
hsa-miR-378b	MIMAT0014999	C-301672-00	ACUGGACUUGGAGGCAGAA	-0.950272981825821	0.00016326	TRUE	-0.9014034271727 12	0.72813	FALSE
hsa-miR-378g	MIMAT0018937	C-302000-00	ACUGGGCUUGGAGUCAGAAG	-0.836483927856313	0.00023985	TRUE	-1.88595985918819	0.11887	TRUE
hsa-miR-380*	MIMAT0000734	C-300688-03	UGGUUGACCAUAGAACAUGCGC	-1.15838836623363	0.0018747	FALSE	-2.139164836318 05	0.12226	TRUE
hsa-miR-381-5p	MIMAT0022862	C-301920-00	AGCGAGGUUGCCCUUUGUAUAU	-0.569567310635211	0.021994	FALSE	-2.14982823754668	0.08542	TRUE
hsa-miR-383	MIMAT0000738	C-300692-03	AGAUCAGAAGGUGAUUGUGGCU	-0.925079491666264	0.0052694	FALSE	-2.8317437192294	0.050122	TRUE
hsa-miR-3907	MIMAT0018179	C-301585-00	AGGUGCUCCAGGCUGGCUCACA	-1.38465900005315	0.00013793	TRUE	-0.2577737606992354	1	FALSE
hsa-miR-3910	MIMAT0018184	C-301590-00	AAAGGCAUAAAACCAAGACA	-0.501095287980396	0.037103	FALSE	-1.43931285152292	0.11887	TRUE
hsa-miR-3913-3p	MIMAT0019225	C-301959-00	AGACAUCAAGAUCAGUCCCAAA	-2.00645940017379	2.9753e-06	TRUE	-3.02362886477847	0.014453	TRUE
hsa-miR-3918	MIMAT0018192	C-301600-00	ACAGGGCCGCAGAUGGAGACU	-0.975422481909615	0.015067	FALSE	-2.44273172350024	0.081661	TRUE
hsa-miR-3922-5p	MIMAT0019227	C-301962-00	UCAAGGCCAGAGGUCCCACAGCA	-1.005611078559174	6.1693e-05	TRUE	-1.71505157929257	0.1633	FALSE
hsa-miR-3935	MIMAT0018350	C-301618-00	UGUAGAUACGAGCACCAGCCAC	-0.43578505271152	0.17522	FALSE	-2.47251139472301	0.057617	TRUE
hsa-miR-3972	MIMAT0019357	C-302158-00	CUGCCAGCCCCGUUCCAGGGCA	-1.16965458786124	0.00023985	TRUE	-1.70649157359084	0.40677	FALSE
hsa-miR-3975	MIMAT0019360	C-302161-00	UGAGGCUAAUGCACUACUUCAC	-1.37543164339877	8.3715e-05	TRUE	-1.26480301471027	0.51579	FALSE
hsa-miR-425*	MIMAT0001343	C-300718-07	AUCGGGAAUGCUGUCCGCCC	-0.937175749542432	0.00054279	FALSE	-3.15498966019418	0.028781	TRUE
hsa-miR-4253	MIMAT0016882	C-301816-00	AGGGCAUGUCCAGGGGGU	-1.35070000422013	0.00016326	TRUE	-2.47892017845828	0.11887	TRUE
hsa-miR-4290	MIMAT0016921	C-301856-00	UGCCCUCCUUUCUUCCCUC	-1.2579851622971	0.00026644	TRUE	-0.7804281413369 04	0.86349	FALSE
hsa-miR-4306	MIMAT0016858	C-301792-00	UGGAGAGAAAGGCAGUA	-1.10160128889539	0.0046172	FALSE	-2.08580333486915	0.11887	TRUE
hsa-miR-4312	MIMAT0016864	C-301798-00	GGCCUUGUUCCUGUCCCCA	-0.866321092589685	0.0030028	FALSE	-2.71345507691741	0.11887	TRUE
hsa-miR-4314	MIMAT0016868	C-301802-00	CUCUGGGAAAUGGGACAG	-1.5364651282067	8.3715e-05	TRUE	-1.29173007577176	0.5811	FALSE
hsa-miR-4417	MIMAT0018929	C-301991-00	GGUGGGCUUCCCGGAGGG	-0.611560680456615	0.0021076	FALSE	-2.09593331520836	0.11887	TRUE
hsa-miR-4418	MIMAT0018930	C-301992-00	CACUGCAGGACUCAGCAG	-0.946166316606651	0.00013793	TRUE	-1.12537501301133	0.46329	FALSE
hsa-miR-4419a	MIMAT0018931	C-301993-00	UGAGGGAGGAGACUGCA	-1.57297371821019	6.7884e-06	TRUE	-1.73343971226014	0.1633	FALSE
hsa-miR-4420	MIMAT0018933	C-301995-00	GUCACUGAUGUCUGUAGCUGAG	-0.924563865566564	0.00013963	TRUE	-0.5339190745847 04	0.86349	FALSE
hsa-miR-4422	MIMAT0018935	C-301997-00	AAAAGCAUCAGGAAGUACCCA	-0.890570506779186	0.00023985	TRUE	-0.6092444833333412	0.86349	FALSE
hsa-miR-4423-3p	MIMAT0018936	C-301999-00	AUAGGCACCAAAAAGCAACAA	-0.908201173118296	0.00013793	TRUE	-0.9229838578088 18	0.5811	FALSE
hsa-miR-4423-5p	MIMAT0019232	C-301998-00	AGUUGCCUUUUUGUUCCCAUGC	-0.973577427508824	8.3715e-05	TRUE	-1.75215013385816	0.1633	FALSE
hsa-miR-4425	MIMAT0018940	C-302003-00	UGUUGGGAUUCAGCAGGACCAU	-2.09487999782656	6.0932e-07	TRUE	-4.02209575968718	0.0018396	TRUE
hsa-miR-4426	MIMAT0018941	C-302004-00	GAAGAUGGACGUACUUU	-1.519371009532 74	6.7884e-06	TRUE	-1.79705743821345	0.12226	TRUE
hsa-miR-4427	MIMAT0018942	C-302005-00	UCUGAAUAGAGUCUGAAGAGU	-0.853522749406319	0.00023985	TRUE	-1.87772807758284	0.1633	FALSE
hsa-miR-4428	MIMAT0018943	C-302006-00	CAAGGAGACGGGAACAUGGAGC	-1.008693862915 56	6.1693e-05	TRUE	-2.00933698314586	0.12226	TRUE
hsa-miR-4430	MIMAT0018945	C-302008-00	AGGCUGGAGUGAGCGGAG	-0.738546756609574	0.00054279	FALSE	-2.96189732903016	0.014453	TRUE
hsa-miR-4431	MIMAT0018947	C-302010-00	GCGACUCCUGAAAACUAGAAGGU	-0.605956299781477	0.0021076	FALSE	-1.84934532554394	0.11887	TRUE
hsa-miR-4432	MIMAT0018948	C-302011-00	AAAGACUCUGCAAGAUGCCU	-1.01744360848873	6.1693e-05	TRUE	-3.10500591742549	0.023579	TRUE
hsa-miR-4433-3p	MIMAT0018949	C-302012-00	ACAGGAGUGGGGUGGGACAU	-0.842019427210466	0.00023985	TRUE	-1.23537194391469	0.40677	FALSE
hsa-miR-4433-5p	MIMAT0020956	C-302013-00	CGUCCCACCCCCACUCCUGU	-1.143370353396948	3.6715e-05	TRUE	-1.97664293733303	0.11887	TRUE
hsa-miR-4434	MIMAT0018950	C-302014-00	AGGAGAAGUAAAGUAGAA	-0.883254828802553	0.00013963	TRUE	-1.16571755196267	0.46329	FALSE
hsa-miR-4435	MIMAT0018951	C-302015-00	AUGGCCAGAGCUCACACAGAGG	-0.883497505941514	0.00023985	TRUE	-0.6151527001123 39	0.76975	FALSE
hsa-miR-4436a	MIMAT0018952	C-302016-00	GCAGGACAGGCAGAAGUGGAU	-1.04036408328386	3.9917e-05	TRUE	-1.59208296058719	0.22566	FALSE
hsa-miR-4437	MIMAT0018953	C-302018-00	UGGGCUCAGGGUACAAAGGUU	-1.08972765547642	3.9917e-05	TRUE	-1.15841014023857	0.51048	FALSE
hsa-miR-4438	MIMAT0018956	C-302021-00	CACAGGCUUAGAAAAGACAGU	-1.17220321847248	3.6715e-05	TRUE	-1.92817351938145	0.11887	TRUE
hsa-miR-4440	MIMAT0018958	C-302023-00	UGUCGUGGGGCUUGCUGGCUUG	-1.11752167173499	3.9917e-05	TRUE	-2.33357733512522	0.08542	TRUE
hsa-miR-4441	MIMAT0018959	C-302024-00	ACAGGGAGGAGAUUGUA	-1.2984552451679	1.5894e-05	TRUE	-0.4312689619492 08	0.86349	FALSE
hsa-miR-4442	MIMAT0018960	C-302025-00	GCCGGACAAGAGGGAGG	-0.97262245143818	8.3715e-05	TRUE	-1.15721358729306	0.46329	FALSE
hsa-miR-4443	MIMAT0018961	C-302026-00	UUGGAGGCGUGGGUUUU	-1.75283027769511	3.4785e-06	TRUE	-2.08359341608655	0.11887	TRUE
hsa-miR-4445-5p	MIMAT0018963	C-301976-00	AGAUUGUUUCUUUUGCCGUGCA	-1.26374145331415	1.5894e-05	TRUE	-4.01626597303824	0.0018396	TRUE
hsa-miR-4447	MIMAT0018966	C-302029-00	GGUGGGGGCUGUUGUUU	-0.841752979683909	0.00023985	TRUE	-2.88111133299715	0.028781	TRUE
hsa-miR-4449	MIMAT0018968	C-302031-00	CGUCCCGGGGCUGCGCGAGGCA	-0.853462598263724	0.00023985	TRUE	-1.80522351536343	0.1633	FALSE
hsa-miR-4450	MIMAT0018971	C-302034-00	UGGGGAUUUGGAGAAGUGGUGA	-1.06492940641686	4.5608e-05	TRUE	-2.95948317827462	0.014453	TRUE
hsa-miR-4451	MIMAT0018973	C-302037-00	UGGUAGAGCUGAGGACA	-1.13976267989773	3.6715e-05	TRUE	-0.5264654485121 74	0.86349	FALSE
hsa-miR-4452	MIMAT0018974	C-302038-00	UUGAAUUCUUGGCCUUAAGUGAU	-0.813274313439393	0.00026644	TRUE	-0.1666366659928165	1	FALSE
hsa-miR-4453	MIMAT0018975	C-302039-00	GAGCUUGGUCUGUAGCGGUU	-1.18208500406966	3.9917e-05	TRUE	-2.62562177516204	0.050122	TRUE
hsa-miR-448	MIMAT0001532	C-300721-05	UUGCAUAUGUAGGAUGUCCCAU	-1.39737830033137	0.00054279	FALSE	-2.29949072457764	0.11887	TRUE
hsa-miR-449c	MIMAT0010251	C-301488-00	UAGGCAGUGAUUUGCUAGCGGCUGU	-0.977360548104279	0.00013963	TRUE	-1.65073035658006	0.26604	FALSE
hsa-miR-4507	MIMAT0019044	C-302113-00	CUGGGUUGGGCUGGGCUGGG	-1.08254852754089	0.015067	FALSE	-2.63018823024416	0.11887	TRUE
hsa-miR-450a-3p	MIMAT0022700	C-301907-00	AUUGGGGACAUUUUUGCAUUCAU	-1.3171609377358	0.00013793	TRUE	-1.14626230328136	0.46329	FALSE
hsa-miR-451	MIMAT0001631	C-300734-05	AAACCGUUACCAUUACUGAGUU	-1.43368456108961	8.3715e-05	TRUE	-0.268670734386333	1	FALSE
hsa-miR-452	MIMAT0001635	C-300735-07	AACUGUUUGCAGAGGAAACUGA	-0.355271404072044	0.12653	FALSE	-2.45598627080639	0.050122	TRUE
hsa-miR-4525	MIMAT0019064	C-302136-00	GGGGGGAUGUGCAUGCUGGUU	-1.29162472134399	0.00013793	TRUE	-1.82359755370572	0.26604	FALSE
hsa-miR-4526	MIMAT0019065	C-302137-00	GCUGACAGCAGGGCUGGCCGCU	-0.819545705994525	0.0021076	FALSE	-3.08101976925394	0.057617	TRUE
hsa-miR-4527	MIMAT0019066	C-302138-00	UGGUCUGCAAAGAGAUGACUGU	-1.48851753125946	3.9917e-05	TRUE	-1.1928606551261	0.5811	FALSE
hsa-miR-4533	MIMAT0019072	C-302145-00	UGGAAGGAGGUUGCCGGACGCU	-1.18624537355721	0.00016326	TRUE	-0.5931580845147 42	0.86349	FALSE
hsa-miR-4536-3p	MIMAT0020959	C-301930-00	UCGUGCAUAUAUCUACCACAU	-1.07232143191926	0.00054279	FALSE	-3.00264840143944	0.014453	TRUE
hsa-miR-4536-5p	MIMAT0019078	C-301929-00	UGUGGUAGAUAUAUGCACGAU	-1.31712298567513	0.00013963	TRUE	-1.61271864964865	0.20114	FALSE
hsa-miR-4538	MIMAT0019081	C-302154-00	GAGCUUGGAUGAGCUGGGCUGA	-1.22689177781842	0.00013963	TRUE	-1.39982249594569	0.5811	FALSE
hsa-miR-4539	MIMAT0019082	C-302155-00	GCUGAACUGGGCUGAGCUGGGC	-0.662063245722664	0.0074787	FALSE	-2.55330760069272	0.11887	TRUE
hsa-miR-4632-5p	MIMAT0022977	C-302499-00	GAGGGCAGCGUGGGUGUGGCGGA	-0.597712246032446	0.015067	FALSE	-2.79546040686595	0.057617	TRUE
hsa-miR-4642	MIMAT0019702	C-302175-00	AUGGCAUCGUCCCCUGGUGGCU	-1.24506307785847	0.00013963	TRUE	-1.87231348016783	0.26604	FALSE
hsa-miR-4645-3p	MIMAT0019706	C-302179-00	AGACAGUAGUUCUUGCCUGGUU	-1.12025038846698	0.00026644	TRUE	-1.08522858184346	0.5811	FALSE
hsa-miR-4650-3p	MIMAT0019714	C-302184-00	AGGUAGAAUGAGGCCUGACAU	-1.52761158686618	3.9917e-05	TRUE	-2.47248261479947	0.11887	TRUE
hsa-miR-4651	MIMAT0019715	C-302187-00	CGGGGUGGGUGAGGUCGGGC	-1.12142324138952	0.00023985	TRUE	-1.06587157649805	0.5811	FALSE
hsa-miR-4652-5p	MIMAT0019716	C-302188-00	AGGGGACUGGUUAAUAGAACUA	-1.12850660881293	0.00023985	TRUE	-0.6685919757163071	0.86349	FALSE
hsa-miR-4655-5p	MIMAT0019721	C-302194-00	CACCGGGGAUGGCAGAGGGUCG	-1.21402640640325	0.00016326	TRUE	-1.71020871463468	0.40677	FALSE
hsa-miR-466	MIMAT0015002	C-301675-00	AUACACAUACACGCAACACACAU	-1.57268812194273	1.5894e-05	TRUE	-1.36589716672211	0.46329	FALSE
hsa-miR-4664-3p	MIMAT0019738	C-302210-00	CUUCCGGCUCUGUGAGCCCGUC	-1.12808833805518	8.3715e-05	TRUE	-1.3144620182497	0.26604	FALSE
hsa-miR-4664-5p	MIMAT0019737	C-302209-00	UGGGGUGCCCACUCCGCAAGUU	-1.35541980608348	3.6715e-05	TRUE	-0.6238874047333 994	0.76864	FALSE
hsa-miR-4665-5p	MIMAT0019739	C-302211-00	CUGGGGGACGCGUGAGCGCGAGC	-1.14650290801351	6.1693e-05	TRUE	-2.55003959556736	0.014453	TRUE
hsa-miR-4666b	MIMAT0022485	C-302595-00	UUGCAUGUCAGAUUGUAAUUCCC	-1.25134263280118	0.0053924	FALSE	-1.96334534104703	0.11887	TRUE
hsa-miR-4668-5p	MIMAT0019745	C-302216-00	AGGGAAAAAAAAAAGGAUUUGUC	-1.06833102929774	0.00013793	TRUE	-1.46510395349218	0.1633	FALSE
hsa-miR-4672	MIMAT0019754	C-302224-00	UUACACAGCUGGACAGAGGCA	-1.69132941190395	1.5655e-05	TRUE	-1.82970618393803	0.11887	TRUE
hsa-miR-4674	MIMAT0019756	C-302226-00	CUGGGCUCGGGACGCGCGGCU	-1.30671632029371	3.9917e-05	TRUE	-1.87257075861882	0.08542	TRUE
hsa-miR-4675	MIMAT0019757	C-302227-00	GGGGCUGUGAUUGACCAGCAGG	-0.4975040082299 8	0.015067	FALSE	-1.65778479186002	0.11887	TRUE
hsa-miR-4677-5p	MIMAT0019760	C-302231-00	UUGUUCUUUGGUCUUUCAGCCA	-1.01207284849144	0.00013963	TRUE	-2.02433296093174	0.1633	FALSE
hsa-miR-4678	MIMAT0019762	C-302232-00	AAGGUAUUGUUCAGACUUAUGA	-0.678062145099685	0.0021076	FALSE	-1.8265679594388	0.11887	TRUE
hsa-miR-4682	MIMAT0019767	C-302236-00	UCUGAGUUCCUGGAGCCUGGUCU	-0.95136903371 90	0.00023985	TRUE	-0.2791563771022 57	1	FALSE
hsa-miR-4683	MIMAT0019768	C-302237-00	UGGAGAUCCAGUGCUCGCCCGAU	-1.03845589118353	0.00013793	TRUE	-2.39905380190628	0.023579	TRUE
hsa-miR-4684-3p	MIMAT0019770	C-302239-00	UGUUGCAAGUCGGUGGAGACGU	-0.997924294092217	0.00016326	TRUE	-1.70225287410888	0.1633	FALSE
hsa-miR-4687-3p	MIMAT0019775	C-302242-00	UGGCUGUUGGAGGGGCAGGC	-1.08006757648135	9.6971e-05	TRUE	-2.49518358442824	0.023579	TRUE
hsa-miR-4688	MIMAT0019777	C-302244-00	UAGGGGCAGCAGAGGACCUGGG	-0.933026739975212	0.00023985	TRUE	-2.48777268680185	0.023579	TRUE
hsa-miR-4689	MIMAT0019778	C-302245-00	UUGAGGAGACAUGGUGGGGGCC	-1.02151466268037	0.00023985	TRUE	-1.54092925086873	0.1633	FALSE
hsa-miR-4692	MIMAT0019783	C-302250-00	UCAGGCAGUGUGGGUAUCAGAU	-0.988783938058944	0.00016326	TRUE	-1.14868084000672	0.40677	FALSE
hsa-miR-4693-3p	MIMAT0019785	C-302252-00	UGAGAGUGGAAUUCACAGUAUUU	-1.44962435716591	3.6715e-05	TRUE	-1.73885084830262	0.11887	TRUE
hsa-miR-4694-3p	MIMAT0019787	C-302253-00	CAAAUGGACAGGAUAACACCU	-0.938557148222 29	0.00023985	TRUE	-1.50626462839686	0.1633	FALSE
hsa-miR-4694-5p	MIMAT0019786	C-302254-00	AGGUGUUAUCCUAUCCAUUUGC	-0.952993076462483	0.00023985	TRUE	-2.88415743782109	0.014453	TRUE
hsa-miR-4695-3p	MIMAT0019789	C-302458-00	UGAUCUCACCGCUGCCUCCUUC	-1.73712530730441	3.6715e-05	TRUE	-2.61115419781241	0.11887	TRUE
hsa-miR-4696	MIMAT0019790	C-302255-00	UGCAAGACGGAUACUGCUACU	-1.05967205505661	0.00013793	TRUE	-3.02679657831 08	0.009387	TRUE
hsa-miR-4697-5p	MIMAT0019791	C-302257-00	AGGGGGCGCAGUCACUGACGUG	-1.49838261147195	1.5894e-05	TRUE	-1.93121149945073	0.08542	TRUE

hsa-miR-4699-5p	MIMAT0019794	C-302259-00	AGAAGAUUGCAGAGUAAGUUCC	-0.321333385517737	0.096607	FALSE	-1.70896571432969	0.11887	TRUE
hsa-miR-4700-5p	MIMAT0019796	C-302262-00	UCUGGGGAUGAGGACAGUGUGU	-0.638781297378828	0.0046172	FALSE	-2.49301512707352	0.023579	TRUE
hsa-miR-4701-5p	MIMAT0019798	C-302460-00	UUGGCCACCACACCUACCCCUU	-1.254075927155911	0.00016326	TRUE	-2.10511844533172	0.1633	FALSE
hsa-miR-4706	MIMAT0019806	C-302269-00	AGCGGGGAGGAAGUGGGCGCUGCUU	-0.640574202002897	0.0030028	FALSE	-1.80378336355061	0.11887	TRUE
hsa-miR-4707-3p	MIMAT0019808	C-302270-00	AGCCCGCCCCAGCCGAGGUUCU	-0.833524657548794	0.00079918	FALSE	-2.32407172887442	0.057617	TRUE
hsa-miR-4708-3p	MIMAT0019810	C-302273-00	AGCAAGGCGGCAUCUCUCGAU	-0.969695371193823	0.00023985	TRUE	-0.525873276306624	0.86349	FALSE
hsa-miR-4708-5p	MIMAT0019809	C-302272-00	AGAGAUGCCGCCUUGCUCCUU	-0.822684020528361	0.00079918	FALSE	-2.10220660879154	0.08542	TRUE
hsa-miR-4709-3p	MIMAT0019812	C-302275-00	UUGAAGAGGAGGUGCUCUGUAGC	-0.66432740058703	0.0027607	FALSE	-1.68675985049984	0.11887	TRUE
hsa-miR-4709-5p	MIMAT0019811	C-302274-00	ACAACAGUGACUUGCUCUCCAA	-1.08969801660567	9.6971e-05	TRUE	-0.80626334250579	0.5811	FALSE
hsa-miR-4711-5p	MIMAT0019816	C-302279-00	UGCAUCAGGCCAGAAGACAUGAG	-0.502094584622719	0.015067	FALSE	-2.22945919207469	0.057617	TRUE
hsa-miR-4712-3p	MIMAT0019819	C-302282-00	AAUGAGAGACCUGUACUGUAU	-1.26003058356888	3.9917e-05	TRUE	-2.5282291027878	0.028781	TRUE
hsa-miR-4713-5p	MIMAT0019820	C-302283-00	UUCUCCCACUACCAGGCUCCCA	-1.41056492413791	3.6715e-05	TRUE	0.152837140204165	1	FALSE
hsa-miR-4714-5p	MIMAT0019822	C-302286-00	AACUCUGACCCCUUAGGUUGAU	-0.971641326370144	0.00023985	TRUE	-1.9820676345786	0.08542	TRUE
hsa-miR-4715-3p	MIMAT0019825	C-302288-00	GUGCCACCUUAACUGCAGCCAAU	-0.831711497711227	0.0014577	FALSE	-1.64639738941666	0.11887	TRUE
hsa-miR-4720-3p	MIMAT0019834	C-302297-00	UGCUUAAGUUGUACCAAGUAU	-0.267039361511682	0.37761	FALSE	-2.41942301448004	0.057617	TRUE
hsa-miR-4726-3p	MIMAT0019846	C-302309-00	ACCCAGGUCCCCUCUGGCCGCA	-1.05457626001572	0.0046172	FALSE	-1.96757030993053	0.11887	TRUE
hsa-miR-4726-5p	MIMAT0019845	C-302310-00	AGGGCCAGAGGAGCCUGGAGUGG	-0.548731137329315	0.061384	FALSE	-2.20367296738285	0.11887	TRUE
hsa-miR-4730	MIMAT0019852	C-302314-00	CUGGCGGAGCCCAUUCCAUGCCA	-1.14323623131763	0.0021076	FALSE	-3.22072847594229	0.014453	TRUE
hsa-miR-4731-3p	MIMAT0019854	C-302316-00	CACACAAGUGGCCCCCAACACU	-0.715286408900071	0.021994	FALSE	-2.11972721193743	0.11887	TRUE
hsa-miR-4733-5p	MIMAT0019857	C-302319-00	AAUCCCAAUGCUAGACCCGGUG	-0.918486094585803	0.0074787	FALSE	-2.80327741332156	0.023579	TRUE
hsa-miR-4740-3p	MIMAT0019870	C-302329-00	GCCCGAGAGGAUCCGUCCCUGC	-0.824911201381423	0.015067	FALSE	-3.46216635615516	0.014453	TRUE
hsa-miR-4743-5p	MIMAT0019874	C-302462-00	UGGCCGGAUGGGACAGGAGGCAU	-1.02760222969445	0.00061109	FALSE	-2.22597648616421	0.11887	TRUE
hsa-miR-4745-3p	MIMAT0019879	C-302464-00	UGGCCCGGCGACGUCUCACGGUC	-1.23742515486855	0.00016326	TRUE	-2.78131955234324	0.08542	TRUE
hsa-miR-4747-3p	MIMAT0019883	C-302339-00	AAGGCCCGGGCUUUCCUCCCAG	-0.465231590374108	0.12653	FALSE	-2.90430878110698	0.023579	TRUE
hsa-miR-4747-5p	MIMAT0019882	C-302340-00	AGGGAAGGAGGCUUGGUCUUAG	-0.431504547805173	0.17522	FALSE	-1.91877072137694	0.12226	TRUE
hsa-miR-4748	MIMAT0019884	C-302341-00	GAGGUUUGGGGAGGAUUUGCU	-0.555957276676544	0.061384	FALSE	-2.01827086334852	0.11887	TRUE
hsa-miR-4750-3p	MIMAT0022979	C-302491-00	CCUGACCCACCCCCUCCCGCAG	-0.714754040609532	0.0074787	FALSE	-2.39203721905178	0.11887	TRUE
hsa-miR-4755-5p	MIMAT0019895	C-302349-00	UUUCCCUUCAGAGCCUGGCUUU	-0.539113669488979	0.061384	FALSE	-2.80807175968132	0.057617	TRUE
hsa-miR-4760-5p	MIMAT0019906	C-302359-00	UUUAGAUUGAACAUGAAGUUAG	-0.823743933447296	0.015067	FALSE	-2.78675399181231	0.028781	TRUE
hsa-miR-4768-5p	MIMAT0019920	C-302372-00	AUUCUCUCUGGAUCCCAUGGAU	-0.784576616178355	0.061384	FALSE	-2.06931455868509	0.11887	TRUE
hsa-miR-4774-3p	MIMAT0019930	C-302383-00	AUUGCCUAACAUGUGCCAGAA	-0.980156502965659	0.03164	FALSE	-1.92072766628618	0.12226	TRUE
hsa-miR-4778-3p	MIMAT0019937	C-302393-00	UCUUCUUCCUUUGCAGAGUUGA	-0.468380465892249	0.17522	FALSE	-2.12161516444605	0.11887	TRUE
hsa-miR-4778-5p	MIMAT0019936	C-302392-00	AAUUCUGUAAAGGAAGAAGAGG	-0.108428651324849	1	FALSE	2.20881646867654	0.08542	TRUE
hsa-miR-4782-3p	MIMAT0019945	C-302398-00	UGAUUGUCUUCAUAUCUAGAAC	-0.415227659905038	0.32544	FALSE	-1.91949188729733	0.11887	TRUE
hsa-miR-4792	MIMAT0019964	C-302418-00	CGGUGAGCGCUCGCUGGC	-0.681007711978918	0.096607	FALSE	-2.35869521814417	0.057617	TRUE
hsa-miR-4799-5p	MIMAT0019976	C-302431-00	AUCUAAAUGCAGCAUGCCAGUC	-0.362222805879938	0.32544	FALSE	-1.88523388837028	0.11887	TRUE
hsa-miR-4800-5p	MIMAT0019978	C-302435-00	AGUGGACCGAGGAAGGAAGGA	-1.32275981315377	0.0074787	FALSE	-2.73500556024618	0.028781	TRUE
hsa-miR-4804-3p	MIMAT0019985	C-302441-00	UGCUUAACCUUGCCCUCGAAA	-0.336610566496397	0.37761	FALSE	-2.24438580605872	0.11887	TRUE
hsa-miR-486-3p	MIMAT0004762	C-301211-01	CGGGGCAGCUCAGUACAGGAU	-0.915928947716196	0.0027607	FALSE	-1.90219636227184	0.11887	TRUE
hsa-miR-487a	MIMAT0002178	C-300747-03	AAUCAUACAGGGACAUCCAGUU	-0.747164545262154	0.015067	FALSE	-2.42832566173827	0.040079	TRUE
hsa-miR-488	MIMAT0004763	C-301189-01	UUGAAAGGCUAUUUCUUGGUC	-0.908290335869122	0.01741	FALSE	-2.18110182296813	0.11887	TRUE
hsa-miR-491-3p	MIMAT0004765	C-301091-01	CUUAUGCAAGAUUCCCUUCUAC	-1.62232250510605	0.00023985	TRUE	-1.07582371390113	0.46329	FALSE
hsa-miR-492	MIMAT0002812	C-300757-05	AGGACCUGCGGGACAAGAUUCUU	-0.468584149908068	0.061384	FALSE	-2.72511166766836	0.014453	TRUE
hsa-miR-494	MIMAT0002816	C-300761-05	UGAAACAUACACGGGAAACCUC	-0.970219284972552	0.0021076	FALSE	-3.24114885056762	0.014453	TRUE
hsa-miR-499b-3p	MIMAT0019898	C-302351-00	AACAUCACUGCAAGUCUAAACA	-0.450448811655319	0.10991	FALSE	-2.12877293491975	0.11887	TRUE
hsa-miR-5001-3p	MIMAT0021022	C-302470-00	UUCUGCCUCUGUCCAGGUCCUU	-1.33428639345599	0.00013793	TRUE	-1.54637406738355	0.40677	FALSE
hsa-miR-5003-5p	MIMAT0021025	C-302474-00	UCACAACAACCUUGCAGGGUAGA	-1.32073825957867	0.00013793	TRUE	-1.18738346839705	0.51579	FALSE
hsa-miR-5004-5p	MIMAT0021027	C-302477-00	UGAGGACAGGGCAAAUUCACGA	-1.00354080968358	0.00079918	FALSE	-3.14572597959306	0.057617	TRUE
hsa-miR-5006-5p	MIMAT0021033	C-302479-00	UUGCCAGGGCAGGAGGUGGAA	-1.29090326952253	0.00013963	TRUE	-1.67173993218432	0.40677	FALSE
hsa-miR-501-3p	MIMAT0004774	C-301167-01	AAUGCACCCGGGCAAGGAUUCU	-0.0731774010060508	1	FALSE	1.96439959148781	0.057617	TRUE
hsa-miR-5087	MIMAT0021079	C-301942-00	GGGUUUGUAGCUUUGCUGGCAUG	-0.359339924285983	0.10991	FALSE	-1.78188598696404	0.11887	TRUE
hsa-miR-509-5p	MIMAT0004779	C-301166-01	UACUGCAGACAGUGGCAAUCA	-1.74945283553728	0.00013793	TRUE	-2.47315672999895	0.081661	TRUE
hsa-miR-5092	MIMAT0021084	C-302456-00	AAUCCACGCUGAGCUUGGCAUC	-1.18967239061038	0.00023985	TRUE	-1.511756387148	0.46329	FALSE
hsa-miR-513a-5p	MIMAT0002877	C-300844-07	UUCACAGGGAGGUGUCAU	-1.05997050839063	0.0074787	FALSE	-2.37670537648159	0.11887	TRUE
hsa-miR-513c-3p	MIMAT0022728	C-301908-00	UAAAUUUCACCUUUCUGAGAAGA	-0.803025559359186	0.0046172	FALSE	-2.73190794276724	0.014453	TRUE
hsa-miR-514	MIMAT0002883	C-300851-07	AUUGACACUUCUGUGAGUAGA	-0.348236527420602	0.12653	FALSE	-1.56224654603507	0.11887	TRUE
hsa-miR-516a-5p	MIMAT0004770	C-301104-01	UUCUCGAGGAAAGAAGCACUUUC	-0.681407959396855	0.0046172	FALSE	-2.18673664105892	0.11887	TRUE
hsa-miR-517a	MIMAT0002852	C-300811-05	AUCGUGCAUCCCUUUAGAGUGU	-1.09820612826732	0.0018747	FALSE	-2.32535259864992	0.08542	TRUE
hsa-miR-517b-3p	MIMAT0002857	C-300817-06	AUCGUGCAUCCCUUUAGAGUGU	-1.68014170163936	3.9917e-05	TRUE	-1.45577777456063	0.26604	FALSE
hsa-miR-517c	MIMAT0002866	C-300832-03	AUCGUGCAUCCUUUUAGAGUGU	-1.39967029576568	0.00054279	FALSE	-3.92792989935189	0.009387	TRUE
hsa-miR-518a-5p	MIMAT0005457	C-301099-01	CUGCAAAGGGAAGCCCUUUC	-1.69701165144962	0.00013963	TRUE	-3.84851299481868	0.014453	TRUE
hsa-miR-518b	MIMAT0002844	C-300798-03	CAAAGCGCUCCCCUUUAGAGGU	-1.15359484149699	0.00087976	FALSE	-2.22045683232246	0.08542	TRUE
hsa-miR-518c*	MIMAT0002847	C-300804-03	UCUCUGGAGGGAAGCACUUUCUG	-1.15870379627599	0.0014577	FALSE	-3.20841244988613	0.014453	TRUE
hsa-miR-518d-5p	MIMAT0005456	C-301100-01	CUCUAGAGGGAAGCACUUUCUG	-0.509493211764305	0.54004	FALSE	-2.82765759572384	0.081661	TRUE
hsa-miR-5192	MIMAT0021123	C-302496-00	AGGAGAGUGGAUUCCAGGUGGU	-0.929717635688366	0.0014577	FALSE	-4.01918995190962	0.014453	TRUE
hsa-miR-5196-5p	MIMAT0021128	C-301981-00	AGGGAAGGGGACGAGGGUUGGG	-1.16761124143466	3.6715e-05	TRUE	-2.56840698714633	0.040079	TRUE
hsa-miR-520a-3p	MIMAT0002834	C-300788-03	AAAGUGCUUCCUUUGGACUGU	0.0374069999290813	1	FALSE	2.98674734617433	0.08542	TRUE
hsa-miR-520c-3p	MIMAT0002846	C-300803-05	AAAGUGCUUCCUUUAGAGGGU	-0.199389168688778	0.37761	FALSE	-1.76230191681356	0.11887	TRUE
hsa-miR-520h	MIMAT0002867	C-300833-03	ACAAAGUGCUUCCCUUUAGAGU	-0.6946767953735559	0.015067	FALSE	-2.26960151079303	0.08542	TRUE
hsa-miR-532-5p	MIMAT0002888	C-300867-01	CAUGCCUUGAGUGUAGGACCGU	-0.687783861572295	0.021994	FALSE	-3.38518185188287	0.014453	TRUE
hsa-miR-539-3p	MIMAT0022705	C-301909-00	AUCAUACAAGGACAAUUCCUUU	-0.712513192949551	0.0074787	FALSE	-1.7777539713116	0.12226	TRUE
hsa-miR-544b	MIMAT0015004	C-301677-00	ACCUGAGGUUGUGCAUUUCUAA	-1.14820342901038	3.9917e-05	TRUE	-0.449549813604399	0.91039	FALSE
hsa-miR-548ab	MIMAT0018928	C-301990-00	AAAAGUAAUUGUGGAUUUUGCU	-0.602579302030159	0.0021076	FALSE	-2.46432616915756	0.057617	TRUE
hsa-miR-548ac	MIMAT0018938	C-302001-00	CAAAAACCGGCAAUUACUUUUG	-0.979633570213558	6.1693e-05	TRUE	-2.02176022235335	0.11887	TRUE
hsa-miR-548ae	MIMAT0018954	C-302019-00	CAAAAACUGCAAUUACUUUCA	-0.606375099488669	0.0030028	FALSE	-2.77725501966519	0.057617	TRUE
hsa-miR-548ah-3p	MIMAT0020957	C-302036-00	CAAAAACUGCAGUUACUUUUGC	-0.668405768437197	0.0014577	FALSE	-2.22611084098903	0.081661	TRUE
hsa-miR-548at-5p	MIMAT0022277	C-302544-00	AAAAGUUAUUGCGGUUUUGGCU	-0.0453519642557928	1	FALSE	-1.8924808826669	0.11887	TRUE
hsa-miR-548au-3p	MIMAT0022292	C-302561-00	UGGCAGUUACUUUUGCACCAG	-1.52595082150064	0.0021076	FALSE	-3.17672563043804	0.014453	TRUE
hsa-miR-548ax	MIMAT0022474	C-302582-00	AGAAGUAAUUGCGGUUUUGCCA	-0.564257743083232	0.10991	FALSE	-2.34784280477006	0.057617	TRUE
hsa-miR-548ay-5p	MIMAT0025452	C-302660-00	AAAAGUAAUUGUGGUUUUUGC	-0.653127591660778	0.021994	FALSE	-3.23819702467989	0.014453	TRUE
hsa-miR-548h-3p	MIMAT0022723	C-301888-00	CAAAAACCGCAAUUACUUUUGCA	-1.06047561824622	0.00054279	FALSE	-2.88715465104665	0.014453	TRUE
hsa-miR-548l	MIMAT0005889	C-301353-00	AAAAGUAUUUGCGGUUUUGUC	-0.59227174574884	0.061384	FALSE	-2.37472439626248	0.11887	TRUE
hsa-miR-548s	MIMAT0014987	C-301658-00	AUGGCCAAAACUGCAGUUAUUUU	-0.871664637647317	0.00054279	FALSE	-2.25194852231406	0.11887	TRUE
hsa-miR-549	MIMAT0003333	C-300991-01	UGACAACUAUGGAUGAGCUCU	-0.718517483220711	0.01741	FALSE	-2.02535291589875	0.12226	TRUE
hsa-miR-550b-2-5p	MIMAT0022737	C-301971-00	AUGUGCCUGAGGGAGUAAGACA	-0.509912734915377	0.0074787	FALSE	-1.84020688668008	0.12226	TRUE
hsa-miR-5580-5p	MIMAT0022273	C-302541-00	UGCUGGCUCAUUUCAUAAUGUG	-0.250725616752794	0.54004	FALSE	-2.09116428366529	0.08542	TRUE
hsa-miR-5583-3p	MIMAT0022282	C-302549-00	GAAUAUGGGUAUAUUAGUUUGG	-0.580364168150873	0.10991	FALSE	-2.82822091546	0.014453	TRUE
hsa-miR-5583-5p	MIMAT0022281	C-302548-00	AAACUAAUAUACCCAUAUUCUG	-0.74119839633839	0.050037	FALSE	-2.77350973293048	0.014453	TRUE
hsa-miR-568	MIMAT0003232	C-300886-01	AUGUAUAAAUGUAUACACAC	-0.546512240064326	0.050037	FALSE	-2.16900241945777	0.11887	TRUE
hsa-miR-5681a	MIMAT0022469	C-302576-00	AGAAAGGGUGGCAAUACCUCUU	-0.554451480617061	0.10991	FALSE	-2.10313927081946	0.11887	TRUE
hsa-miR-5681b	MIMAT0022480	C-302589-00	AGGUAUUGCCACCCUUUCUAGU	-0.990407574357977	0.015067	FALSE	-2.24966625727449	0.11887	TRUE
hsa-miR-5685	MIMAT0022475	C-302583-00	ACAGCCCAGCAGUUAUCACGGG	-1.10866668617995	0.0099219	FALSE	-1.81151890217456	0.11887	TRUE
hsa-miR-5686	MIMAT0022477	C-302586-00	UAUCGUAUCGUAUUGUAUUGU	-0.618603205233964	0.096607	FALSE	-3.26787707054355	0.014453	TRUE
hsa-miR-5687	MIMAT0022478	C-302587-00	UUAGAACGUUUUAGGGUCAAAU	-0.4136100982672	0.25618	FALSE	-1.96140285293105	0.11887	TRUE
hsa-miR-5688	MIMAT0022479	C-302588-00	UAACAAACACCUGUAAAACAGC	-0.496708860788786	0.17522	FALSE	-2.54610797665859	0.028781	TRUE
hsa-miR-5689	MIMAT0022481	C-302590-00	AGCAUACACCUGUAGUCCUAGA	-0.623295340978942	0.089234	FALSE	-2.01329320718309	0.11887	TRUE
hsa-miR-5692a	MIMAT0022484	C-302593-00	CAAAUAAUACCACAGUGGGUGU	-0.71714659454192	0.061384	FALSE	-2.47331051365896	0.057617	TRUE
hsa-miR-5692c	MIMAT0022476	C-302584-00	AAUAAAUACCACAGUAGGUGUAC	-0.930027776637268	0.021994	FALSE	-2.41733401849822	0.057617	TRUE
hsa-miR-5697	MIMAT0022490	C-302600-00	UCAAGUAGUUUCAUGAUAAAGG	-0.509179181511475	0.17522	FALSE	-1.87679966081257	0.11887	TRUE
hsa-miR-5701	MIMAT0022494	C-302604-00	UUAUUGUCACGUUCUGAUU	-0.713050083304961	0.061384	FALSE	-2.19998791399188	0.081661	TRUE
hsa-miR-5702	MIMAT0022495	C-302605-00	UGAGUCAGCAACAUAUCCCAUG	-0.634695457873147	0.089234	FALSE	-2.91461280705682	0.014453	TRUE
hsa-miR-571	MIMAT0003236	C-300890-01	UGAGUUGGCCAUCUGAGUGAG	-1.04012448788134	0.00016326	TRUE	-1.0680220266461	0.5811	FALSE
hsa-miR-574-3p	MIMAT0003239	C-300893-03	CACGCUCAUGCACACACCCACA	-1.45214143219312	0.0018747	FALSE	-2.74091004364483	0.057617	TRUE
hsa-miR-578	MIMAT0003243	C-300897-01	CUUCUUGUGCUCUAGGAUUGU	-0.525376007672939	0.038627	FALSE	-2.14162436977285	0.081661	TRUE
hsa-miR-579	MIMAT0003244	C-300898-03	UUCAUUUGGUAUAAACCGCGAUU	-1.2654167775587	0.0030028	FALSE	-3.8111485398612	0.014453	TRUE
hsa-miR-582-5p	MIMAT0003247	C-300901-01	UUACAGUUGUUCAACCAGUUACU	-1.2010641323251	0.00070025	FALSE	-2.60372535467359	0.040079	TRUE
hsa-miR-586	MIMAT0003252	C-300906-01	UAUGCAUUGUAUUUUUAGGUCC	-0.445099473295375	0.10991	FALSE	-3.97498411008623	0.014453	TRUE
hsa-miR-593*	MIMAT0003261	C-300917-01	AGGCACCAGCCAGGCAUUGCUCAGC	-1.46368716545378	0.00023985	TRUE	-1.69498877920483	0.1633	FALSE
hsa-miR-606	MIMAT0003274	C-300931-01	AAACUACUGAAAAUCAAAGAU	-0.637631782545375	0.32544	FALSE	-2.73649791406254	0.11887	TRUE
hsa-miR-607	MIMAT0003275	C-300932-01	GUUCAAAUCCAGAUCUAUAAC	-0.0963984694817977	1	FALSE	2.32421836737172	0.11887	TRUE
hsa-miR-6071	MIMAT0023696	C-302625-00	UUCUGCUGCCGGCCAAGGC	-0.528822533996229	0.12653	FALSE	-2.19345834630633	0.11887	TRUE
hsa-miR-6075	MIMAT0023700	C-302629-00	ACGGCCCAGGCGGCAUUGGUG	-0.592038077604373	0.037103	FALSE	-2.63925181780449	0.057617	TRUE
hsa-miR-6080	MIMAT0023276	C-300933-01	AGGGGUGGUGUUGGGACAGCUCCGU	-1.41476375494069	9.6971e-05	TRUE	-1.32647981772413	0.22566	FALSE
hsa-miR-6080	MIMAT0023705	C-302634-00	UCUAGUGCGGGCGUCCCG	-0.377302781648075	0.17522	FALSE	-3.12142545628473	0.023579	TRUE
hsa-miR-6081	MIMAT0023706	C-302635-00	AGGAGCAGUGCCGGCCAAGGCGCC	-1.07161737179969	0.0018747	FALSE	-2.06272320366808	0.11887	TRUE
hsa-miR-6086	MIMAT0023711	C-302640-00	GGAGGUUGGGAAGGGCAGAG	-0.556948350994301	0.040903	FALSE	-2.86501870739423	0.028781	TRUE
hsa-miR-6133	MIMAT0024617	C-302655-00	UGAGGGAGGAGGUUGGGUA	-1.00026187079406	0.0021076	FALSE	-3.11682515905473	0.014453	TRUE
hsa-miR-617	MIMAT0003286	C-300943-01	AGACUUCCCAUUUGAAGGUGGC	-1.41203659250412	0.00023985	TRUE	-0.966712399788375	0.51579	FALSE
hsa-miR-619	MIMAT0003288	C-300945-01	GACCUGGACAUGUUUGUGCCCAGU	0.0866202298806936	1	FALSE	2.48494644624597	0.014453	TRUE
hsa-miR-620	MIMAT0003289	C-300946-01	AUGGAGAUAGAUAUAGAAAU	-0.746644845920626	0.096607	FALSE	-3.35303260797096	0.057617	TRUE
hsa-miR-621	MIMAT0003290	C-300947-01	GGCUAGCAACAGCGCUUACCU	-0.524135944687041	0.49143	FALSE	-3.56178952288145	0.023579	TRUE
hsa-miR-624*	MIMAT0003293	C-300950-01	UAGUACCAGUACCUUGUGUUCA	-1.18323865292578	8.3715e-05	TRUE	-2.08818623024311	0.11887	TRUE
hsa-miR-627	MIMAT0003296	C-300953-01	GUGAGUCUCUAAGAAAAGAGGA	-1.05366486573687	0.00016326	TRUE	-1.71256975426944	0.22566	FALSE
hsa-miR-631	MIMAT0003300	C-300957-01	AGACCUGGCCCAGACCUCAGC	-2.01925344204044	3.9917e-05	TRUE	-1.07267199301577	0.51048	FALSE
hsa-miR-634	MIMAT0003304	C-300961-01	AACCAGCACCCCAACUUUGGAC	-1.30123850604998	0.00016067	TRUE	-0.64623077279342	0.76864	FALSE
hsa-miR-638	MIMAT0003308	C-300965-01	AGGGAUCGCGGGCGGGUGGCGGCCU	-0.639193662554625	0.03164	FALSE	-1.99612853656179	0.12226	TRUE
hsa-miR-642a-3p	MIMAT0020924	C-301902-00	AGACACAUUUGGAGAGGGAACC	-0.669360409839209	0.0099219	FALSE	-2.67786191538987	0.023579	TRUE
hsa-miR-642b-5p	MIMAT0022736	C-301970-00	GGUUCCCUCUCCAAAUGUGUCU	-0.982372985036737	6.1693e-05	TRUE	-2.91448575097456	0.023579	TRUE
hsa-miR-644	MIMAT0003314	C-300971-01	AGUGUGGCUUUCUUAGAGC	-1.1328764594198	0.0014577	FALSE	-2.28201156273226	0.12226	TRUE
hsa-miR-646	MIMAT0003316	C-300973-01	AAGCAGCUGCCUCUGAGGC	-1.37335174868112	3.9917e-05	TRUE	-1.88378259141162	0.1633	FALSE
hsa-miR-647	MIMAT0003317	C-300974-01	GUGGCUGCACUCCAUCCUUC	-0.662202123721489	0.015067	FALSE	-2.34112755480514	0.057617	TRUE
hsa-miR-6499-3p	MIMAT0025451	C-302659-00	AGCAGUGUUUGUUUUGCCCACA	-0.78931105472599	0.0099219	FALSE	-2.42776308682332	0.08542	TRUE
hsa-miR-650	MIMAT0003320	C-300977-01	AGGAGGCAGCGCUCUCAGGAC	-1.32232002772507	0.00054279	FALSE	-2.38532145199764	0.11887	TRUE
hsa-miR-6503-3p	MIMAT0025463	C-302671-00	GGGACUAGGAUGCAGACCUCC	-0.701857748301807	0.01741	FALSE	-2.26797239631951	0.08542	TRUE
hsa-miR-6503-5p	MIMAT0025462	C-302670-00	AGGUCUGCAUUCAAAUCCCCAGA	-1.28829279156107	0.00061109	FALSE	-4.16301032924927	0.009387	TRUE

hsa-miR-6504-3p	MIMAT0025465	C-302672-00	CAUUACAGCACAGCCAUUCU	-0.219268298279075	0.49143	FALSE	-2.3682663259571	0.08542	TRUE
hsa-miR-6505-3p	MIMAT0025467	C-302675-00	UGACUUCUACCUCUUCCAAAG	-1.41016990839787	0.00054279	FALSE	-2.92045878806631	0.040079	TRUE
hsa-miR-6507-5p	MIMAT0025470	C-302679-00	GAAGAAUAGGAGGGACUUUGU	-0.637513482741369	0.03164	FALSE	-2.64696299700191	0.057617	TRUE
hsa-miR-6514-3p	MIMAT0025485	C-302693-00	CUGCCUGUUCUUCCACUCCAG	-1.57253367763337	0.00023985	TRUE	-0.857463656453242	0.72813	FALSE
hsa-miR-652-5p	MIMAT0022709	C-301928-00	CAACCCUAGGAGAGGGUGCCAUUCA	-0.590578760858739	0.01741	FALSE	-2.041136016716 63	0.11887	TRUE
hsa-miR-654-5p	MIMAT0003330	C-300988-01	UGGUGGGCCGCAGAACAUGUGC	-1.24102088307823	0.00054279	FALSE	-4.37321715649902	0.0018396	TRUE
hsa-miR-659	MIMAT0003337	C-300994-01	CUUGGUUCAGGGAGGGUCCCCA	-0.865338332757254	0.0053924	FALSE	-2.29702545878 48	0.12226	TRUE
hsa-miR-660-3p	MIMAT0022711	C-301897-00	ACCUCCUGUGUGCAUGGAUUA	-0.914364872105563	0.0018747	FALSE	-2.79896766965 45	0.028781	TRUE
hsa-miR-661	MIMAT0003324	C-300981-01	UGCCUGGGUCUCUGGCCUGCGCGU	-0.966061272920722	0.0046172	FALSE	-2.04789510522588	0.11887	TRUE
hsa-miR-664b-3p	MIMAT0022272	C-302539-00	UUCAUUUGCCUCCCAGCCUACA	-0.63588937093853	0.061384	FALSE	-2.38779084523873	0.057617	TRUE
hsa-miR-671-5p	MIMAT0003880	C-301000-03	AGGAAGCCCUGGAGGGGCUGGAG	-1.01268622344544	0.00023985	TRUE	-0.995050180707598	0.5811	FALSE
hsa-miR-6721-5p	MIMAT0025852	C-302707-00	UGGGCAGGGGCUUAUUGUAGGAG	-1.0522716562067	0.0021076	FALSE	-2.86092601806193	0.028781	TRUE
hsa-miR-7	MIMAT0000252	C-300546-07	UGGAAGACUAGUGAUUUUGUUGU	-0.833080606802588	0.0014577	FALSE	-2.34382127982937	0.11887	TRUE
hsa-miR-718	MIMAT0012735	C-301486-00	CUUCCGCCCCGCCGGGCGUCG	-0.712476270533885	0.0014577	FALSE	-2.51689917044679	0.08542	TRUE
hsa-miR-744	MIMAT0004945	C-301242-01	UGCGGGGCUAGGGCUAACAGCA	-1.31292964878657	0.0027607	FALSE	-2.17130853543699	0.057617	TRUE
hsa-miR-744*	MIMAT0004946	C-301241-01	CUGUUGCCACUAACCUCAACCU	-0.909425861300587	3.9917e-05	TRUE	-2.41920375944258	0.11887	TRUE
hsa-miR-764	MIMAT0010367	C-301640-00	GCAGGUGCUCACUUGUCCUCCU	-1.1596052122796	6.1693e-05	TRUE	-0.963991799367289	0.5811	FALSE
hsa-miR-767-3p	MIMAT0003883	C-301003-01	UCUGCUCAUACCCCAUGGUUUCU	-0.875815222995269	0.0021076	FALSE	-2.87852305265755	0.009387	TRUE
hsa-miR-801	MI0005202	C-301014-01	GAUUGCUCUGCGUGCGGAAUCGAC	-1.02838938735747	0.00023985	TRUE	0.128066636696993	1	FALSE
hsa-miR-873-3p	MIMAT0022717	C-301921-00	GGAGACUGAUGAGUUCCCGGGA	-0.45500701580676	0.050037	FALSE	-2.17559760678154	0.08542	TRUE
hsa-miR-888*	MIMAT0004917	C-301227-01	GACUGACACCUCUUUGGGUGAA	-0.798719536763374	0.015067	FALSE	-1.83668949541677	0.11887	TRUE
hsa-miR-940	MIMAT0004983	C-301269-01	AAGGCAGGGCCCCCGCUCCCC	-1.31504996360232	0.00054279	FALSE	-2.52010733193133	0.11887	TRUE
hsa-miR-96	MIMAT0000095	C-300514-07	UUUGGCACUAGCACAUUUUUGCU	-0.788957233607577	0.0074787	FALSE	-2.19234338350236	0.11527	TRUE
hsa-miR-99a	MIMAT0000097	C-300516-03	AACCCGUAGAUCCGAUCUUGUG	-0.986802247020601	0.0030028	FALSE	-2.42723567464877	0.11887	TRUE

Legend
Antiviral effect
Proviral effect

Note: Hits were selected using the following Local False Discovery Rate (lfdr) thresholds: 0.00027 in screen part 1 and 0.1226 in screen part 2. Positive log2 fold change values indicate a proviral effect of the miRNA on the HCV life cycle, while negative log2 fold change values indicate an antiviral effect.

A functional microRNA screen uncovers O-linked N-acetylglucosamine transferase as a host factor modulating hepatitis C virus morphogenesis and infectivity

Katharina Herzog[1,2*], Simonetta Bandiera[1,2*], Sophie Pernot[1,2], Catherine Fauvelle[1,2], Frank Jühling[1,2], Amélie Weiss[2,3,4,5], Anne Bull[6], Sarah C. Durand[1,2], Béatrice Chane-Woon-Ming[2,7], Sébastien Pfeffer[2,7], Marion Mercey[8], Hervé Lerat[8], Jean-Christophe Meunier[6], Wolfgang Raffelsberger[2,3,4,5], Laurent Brino[2,3,4,5], Thomas F. Baumert[1,2,9,#], Mirjam B. Zeisel[1,2,10,#]

[1]Inserm, U1110, Institut de Recherche sur les Maladies Virales et Hépatiques, Strasbourg, France; [2]Université de Strasbourg, Strasbourg, France; [3]Institut de Génétique et de Biologie Moléculaire et Cellulaire, Illkirch, France ; [4]CNRS, UMR7104, Illkirch, France ; [5]Inserm, U1258, Illkirch, France ; [6]Inserm U1259, Faculté de Médecine, Université François Rabelais and CHRU de Tours, Tours, France ; [7]Architecture et Réactivité de l'ARN – UPR 9002, Institut de Biologie Moléculaire et Cellulaire du CNRS, Strasbourg, France; [8]Institute for Applied Biosciences, Centre de Recherche UGA - Inserm U1209 - CNRS 5309, Grenoble, France [9]Institut Hospitalo-Universitaire, Pôle Hépato-digestif, Hôpitaux Universitaires de Strasbourg, Strasbourg, France; [10]Inserm, U1052, CNRS UMR 5286, Centre Léon Bérard (CLB), Cancer Research Center of Lyon (CRCL), Université de Lyon (UCBL), Lyon, France

*Authors contributed equally to this work

Word count. Abstract: 196 words; main manuscript: 3991 words; 55 references; 7 figures; 1 table; Supplementary information (including 1 Supplementary Table and 1 Supplementary Figure)

#Corresponding authors. Dr. Mirjam B. Zeisel, Inserm U1052 – CRCL, 151 cours Albert Thomas, 69424 Lyon Cedex 03, France, Phone: +33472681970, Fax: +33472681971, E-mail: mirjam.zeisel@inserm.fr and Prof. Thomas F. Baumert, Inserm U1110, Institut de

Recherche sur les Maladies Virales et Hépatiques, 3 rue Koeberlé, 67000 Strasbourg, France, Phone: +33368853703, Fax: +33368853724, Email: thomas.baumert@unistra.fr

Financial support. This work was supported by the European Union (INTERREG-IV-Rhin Supérieur-FEDER-Hepato-Regio-Net 2012 to T.F.B. and M.B.Z., ERC-AdG-2014-671231-HEPCIR, EU H2020-667273-HEPCAR to T.F.B), ANRS (2012/239 to T.F.B., M.B.Z. and L.B.), ARC, Paris and Institut Hospitalo-Universitaire, Strasbourg (TheraHCC IHUARC IHU201301187 to T.F.B.), the Impulsion Program of the IDEXLYON (to M.B.Z.), Ligue contre le cancer (to M.B.Z.), Inserm, and University of Strasbourg. This work has been published under the framework of the LABEX ANR-10-LABX-0028_HepSYS, ANR-10-LABX-36 NetRNA and Inserm Plan Cancer 2019-2023 and benefits from funding from the state managed by the French National Research Agency as part of the Investments for the future program. S.P. and K.H. were supported by PhD fellowships from the French Ministry of Research and the IdEx program of the University of Strasbourg, respectively.

Author contribution. M.B.Z. coordinated and supervised research. K.H., S.B., S.P., C.F., A.W., L.B., J-C.M. and M.B.Z. designed experiments. K.H., S.B., S.P, C. F., A.W., A.B., S.C.D., M.M., H.L. and J-C.M. performed experiments. K.H., S.B., S.P., C. F., F.J., A.W., A.B., B.C.W.M., S.P., J-C.M., W.R., L.B., T.F.B. and M.B.Z. analyzed data. K.H., S.B., and M.B.Z. wrote the paper.

Competing interests: The authors do not have competing interest.

Abstract

Objective: Infection of human hepatocytes by the hepatitis C virus (HCV) is a multistep process involving both viral and host factors. microRNAs (miRNAs) are small non-coding RNAs that post-transcriptionally regulate gene expression. Given that miRNAs were indicated to regulate between 30% and 75% of all human genes, we aimed to investigate the functional and regulatory role of miRNAs for the HCV life cycle.

Design: To systematically reveal human miRNAs affecting the HCV life cycle, we performed a two-step functional high-throughput miRNA mimic screen in Huh7.5.1 cells infected with recombinant cell culture-derived HCV. miRNA targeting was then assessed using a combination of computational and functional approaches.

Results: We uncovered miR-501-3p and miR-619-3p as novel modulators of HCV assembly/release. We discovered that these miRNAs regulate O-linked N-acetylglucosamine (O-GlcNAc) transferase (OGT) protein expression and identified OGT and O-GlcNAcylation as regulators of HCV morphogenesis and infectivity. Furthermore, increased OGT expression in patient-derived liver tissue was associated with HCV-induced liver disease and cancer.

Conclusion: miR-501-3p and miR-619-3p and their target OGT are previously undiscovered regulatory host factors for HCV assembly and infectivity. In addition to its effect on HCV morphogenesis, OGT may play a role in HCV-induced liver disease and hepatocarcinogenesis.

Significance of this study

What is already known about this subject?

- To establish chronic infection, the hepatitis C virus (HCV) hijacks cellular factors including microRNAs (miRNAs), known to post-transcriptionally regulate gene expression.
- miRNAs may positively or negatively modulate HCV infection either by directly targeting the viral genome or indirectly by regulating virus-associated cellular pathways[1, 2].

What are the new findings?

- A functional miRNA mimic screen uncovered miR-501-3p and miR-619-3p to enhance late steps of HCV infection.
- miR-501-3p regulates the expression of O-linked N-acetylglucosamine transferase (OGT) at the protein level.
- Silencing of OGT expression or inhibition of O-linked N-acetylglucosaminylation (O-GlcNAcylation) leads to an increase in the infectivity and size of HCV particles.
- OGT expression increases in patient-derived liver tissue during liver disease progression and cancer.

How might it impact on clinical practice in the foreseeable future?

- As upregulation of OGT and increased O-GlcNAcylation of proteins have been associated with various forms of cancer, OGT may play a dual role in HCV morphogenesis as well as pathogenesis of HCV-induced liver disease and carcinogenesis.

Introduction

Chronic hepatitis C is a major cause of chronic liver disease and hepatocellular carcinoma (HCC). Since the approval of pan-genotypic direct-acting antivirals (DAAs), it is considered a curable disease in more than 90% of treated patients. Nonetheless, an estimated 71 million individuals are still infected by the hepatitis C virus (HCV) and several challenges remain; viral cure reduces but does not eliminate the HCC risk in patients with advanced fibrosis[3], the majority of infected patients has limited access to therapy and DAA failure/viral resistance has been reported in a subset of patients[4, 5]. To overcome these limitations, approaches to target host factors involved in HCV infection and pathogenesis are developed[6, 7]. Interestingly, defined host factors that contribute to the establishment of chronic HCV infection and represent potential antiviral targets, e.g. epidermal growth factor receptor[8], also play a role in liver disease pathogenesis and represent candidate targets for treatment of advanced liver disease and HCC prevention[9]. Thus, uncovering host factors usurped by HCV not only contributes to a better understanding of virus-host interactions underlying the HCV life cycle but also to the identification of potential targets for treatment of liver disease and prevention of HCC.

The establishment of various models to study HCV infection has shed light on the molecular mechanisms that govern the HCV life cycle, which can be subdivided into early steps, including viral entry, translation and replication as well as late steps, including assembly and release of new virions. Each step of the HCV replication cycle relies on specific virus-host interactions that involve host proteins and microRNAs (miRNAs)[7], small non-coding RNAs that regulate gene expression at the post-transcriptional level. One miRNA can target numerous messenger RNAs (mRNAs) by base-pairing with a complementary site that is typically located within the 3′ untranslated region (3′UTR) of the mRNA. Accumulating evidence indicates that miRNAs participate to HCV replication by exerting pro- or antiviral effects. The breakthrough discovery of the direct targeting of HCV by miR-122, the most abundant miRNA in the liver, revealed the crucial role of this miRNA for HCV translation/replication that contributes to progression to chronic HCV infection[1, 10]. miR-

122 antisense oligonucleotides were subsequently developed as host-targeting antivirals[11, 12]. Other miRNAs can indirectly target HCV by regulating host factors that participate in antiviral responses and immune surveillance[2, 13, 14]. Since up to 60% of all human protein-coding genes were reported to be under miRNA-mediated regulation and miRNAs are involved in basically every biological process, we hypothesized that miRNAs provide a tool for loss-of-function approaches to uncover novel HCV host factors. We performed genome-wide high-throughput modulation of the human miRNome and analyzed their impact on HCV infection by combining computational and functional approaches.

Material and methods

Cells, cell culture conditions, viruses, virus purification, infectivity assays, miRNAs, antagomiRs, siRNAs, antibodies, immunoblot, immunocapture, electron microscopy analysis of viral particles and gene expression analysis in liver tissue are described in the Supplementary information.

Functional miRNA/siRNA screens. Huh7.5.1 cells were transfected with the miRIDIAN human miRNA mimic library (mIRBase 19) comprising more than 2000 mature miRNAs or 28 ON-TARGETplus smart pool siRNAs (20 nM, Dharmacon) using Interferin HTS (Polyplus) in a 96-well format[8]. After 48h, a viability test (Presto Blue, Thermo Scientific) was performed prior to a two-step infection assay[15, 16, 17]. During part 1 of the protocol, 50 µL of HCV cell culture-derived particles (HCVcc, JcR2a) were incubated with cells during 4h. The inoculum was removed and cells were incubated with 150 µl of medium for 48h. In part 2, supernatants from part 1 cells were transferred onto naïve Huh7.5.1 cells and part 1 cells were lysed to determine luciferase activity[17, 18]. After 72h, part 2 cells were lysed to determine luciferase activity[17]. siCD81 (20 nM), antagomiR-122 (100 nM) and siApoE (20 nM) were used as positive controls[17]. A non-targeting siRNA with no sequence complementarity to any human gene or homology to any human miRNA was used as negative control.

Inhibitor treatment. Four hours following HCV RNA electroporation[8], Huh7.5.1 cells were incubated with vehicle or inhibitors of OGT (peracetylated 5-thio-N-acetylglucosamine ($Ac_4$5S-GlcNAc)[19]) or OGA (Thiamet G (Sigma))[20]. After 96h, supernatants were transferred onto naïve Huh7.5.1 cells for 72h prior to determination of luciferase activity while electroporated cells were lysed to determine luciferase activity.

Gene expression analyses. Total RNA was purified[17] and transcribed into cDNA using Maxima reverse transcriptase (Thermo Scientific). *GAPDH* and *OGT* mRNA was detected by real time qPCR using iTaq™ Universal Probes Supermix (Bio-Rad) and TaqMan Gene Expression Assay (Thermo Scientific). Relative *OGT/GAPDH* gene expression was calculated by the ΔΔCt method[21].

Dual luciferase reporter gene assay. The human *OGT* 3'UTR sequence was retrieved from NCBI (NM_181672.2) and Ensembl genome browser (ENST00000373719.3). A fragment of the *OGT* 3′UTR (positions 3380-3837, NM_181672.2) (Thermo Fisher Scientific GENEART) was cloned between the *Not*I and *Xho*I sites downstream of a *Renilla* luciferase cassette in a psiCHECK2 plasmid (Promega). A mutated version of this construct (9-bp substitution in the predicted miR-501-3p target site) was generated as described[22]. The functionality of the *OGT* 3′UTR was assessed as described[23]. The miRIDIAN mimic negative control 1 was used as control. *Renilla* and *firefly* luciferase activity was assessed 48h after transfection into HeLa cells using Dual-Luciferase Reporter assay (Promega).

Bioinformatic and statistical analysis. Data analysis and statistical treatment for the miRNA mimic screen were performed in R (www.r-project.org). Cell measurement data used in further analysis were cell viability and luciferase activity. In total 26 sets of plates (performed in triplicate) were tested. The presence of multiple wells with negative and positive controls on each plate allowed stepwise normalization intra- and inter-plate. First, intra-plate zonal bias was examined and a model of median effects across the entire screen

determined using the median-polish algorithm[24] and all plates corrected accordingly. Then the dataset was examined for outlier plates, i.e. plates where all individual measurements correlate very poorly with the other remaining replicates. Three and 9 plates were excluded for part 1 and part 2 of the screen, respectively, based on poor median correlation ($r < 0.7$) so that the remaining plates correlation improved substantially (> 40%). Next, the plates were normalized inter replicates using the particularly robust quantile-quantile approach[25]. Finally, the data were tested using a moderated t-test (empirical Bayes shrinkage, R-package limma[26]) for the null-hypothesis of no change of a given miRNA compared to the negative control. The resulting *p*-values for independent testing of each miRNA where corrected for the multiple testing situation and expressed as local false discovery rate (lfdr, R-package fdrtool[27]). The testing was performed independently for part 1 and 2 of the screen and candidate miRNAs selected for each part. For data from part 1, a lfdr threshold of 0.00027 was used. Data from part 2 were subject to increase inherent stochastic noise and for this reason the minimum acceptable relative risk of false positives was increased to 0.1226 (i.e. maximum 15% risk for each of the retained hits).

Other datasets were analyzed using the two-tailed Mann-Whitney test, Wilcoxon test, Spearman correlation or the two-tailed unpaired t-test for data with normal distribution as assessed by D'Agostino and Pearson omnibus and Shapiro-Wilk normality tests (GraphPad Prism v.6 package).

Results

Genome-wide identification of human miRNAs affecting the HCV life cycle. We performed a genome-wide screen in human hepatoma Huh7.5.1 cells using a genomic miRNA mimics library and a two-step infection assay[17] with a luciferase reporter virus (JcR2a), which allowed us to functionally assess the role of miRNAs during the early steps (part 1 - viral entry/translation/replication) and the late steps (part 2 - viral assembly/release/infectivity) of the HCV life cycle (Fig. 1A). Silencing of *CD81* and *ApoE*,

two essential host factors required for HCV entry or assembly, respectively, was performed in parallel using small interfering RNA (siRNA) as controls. Silencing of *CD81* resulted in a reduction of HCV infection in part 1 and consequently in part 2 of the screen since reduced viral entry in the first part of the assay leads to a reduced production of viral particles (Fig. 1B)[17]. Silencing of *ApoE* resulted in a marked inhibition of HCV infection only in part 2 of the assay, consistent with the role of ApoE in HCV assembly (Fig. 1B)[17]. The screen identified 427 miRNAs (corresponding to about 16% of the library) that significantly modulated HCV infection (lfdr < threshold, Supplementary Table 1 and Fig. 1C): 186 miRNAs affected HCV infection in part 1, 309 miRNAs affected HCV infection in part 2, including 68 hits in part 1 and part 2. The limited number of part 1 and 2 hits may be due to the fact that a single miRNA may modulate the expression of several proteins, which may have different roles in the viral life cycle. Most hits were observed to dampen HCV infection independently of any significant alteration of cell viability (data not shown). The 186 miRNAs modulating the early steps of HCV infection all decreased viral infection. Among the 309 miRNAs that had an impact in part 2, 11 miRNAs increased HCV infection by at least 3-fold while 298 miRNAs inhibited HCV infection by at least 2.7-fold. Hits from the screen included the let-7 family[2, 28], miR-27a[29] and miR-29 family[30] that were already shown to inhibit HCV infection, as well as miR-21[31] and miR-146a-5p[17] that were shown to stimulate HCV infection thus supporting the relevance of our findings. Collectively, our screen identified a set of miRNAs whose overexpression overall impairs HCV infection by affecting viral entry/translation/replication and/or virion assembly/egress/infectivity.

miR-619-3p, miR-501-3p and OGT play a role in late steps of the HCV life cycle. We focused our analysis on miRNAs that modulate late steps of the HCV life cycle, as the molecular mechanisms of HCV assembly/release remain only partially understood. Our screen identified 241 miRNAs that modulated late steps without affecting early steps of infection: 11 miRNAs increased HCV infection while 230 miRNAs decreased HCV infection. Among the miRNAs that increased HCV infection, miR-140-3p, miR-501-3p, miR-619-3p and

miR-4778-5p have not yet been associated with HCV. Since they enhanced HCV infection in part 2 without affecting part 1, these miRNAs may target host genes that control virus assembly/egress/infectivity. We first confirmed the effect of these miRNAs in independent experiments using the same protocol as for the screen. Overexpression of miR-619-3p or miR-501-3p consistently led to an increase in the infection of progeny virions (Fig. 1D) while infection was decreased with progeny virions from antagomiR-transfected cells (Supplementary Figure S1A). miR-619-3p or miR-501-3p were thus selected for further investigation. To study the molecular mechanisms by which these miRNAs affect HCV infection, we generated a list of predicted miRNA targets using DIANA, TargetScan Human v6.2 and miRDB databases, and selected candidate targets based on their expression in our Huh7.5.1 cells as assessed by microarray (data not shown). Ingenuity Pathway Analysis enabled us to refine the gene list by selecting 28 genes involved in the following functional networks or pathways that contribute to the HCV life cycle[32, 33, 34]: lipid metabolism and cholesterol biosynthesis, protein maturation and processing at the endoplasmic reticulum (ER), components of the endosomal sorting complex, adipocyte biogenesis, cellular morphology and cell inflammation (Table 1).

To assess whether knock-down of these 28 candidate targets affects virus production, we performed a siRNA-based screen using siRNA pools exhibiting strong silencing without cytotoxicity (Fig. 2). Silencing of *CD81* and antagomiR-122 served as controls for part 1; knock-down of *ApoE* served as control for part 2 (Fig. 2). Hits were defined as genes whose knock-down modulated HCV infection in at least one part of the screen with high significance (Fig. 2, *p*-value $\leq$ 0.0001, Mann-Whitney U-test). HCV entry/translation/replication was significantly modulated by silencing of *PPP3CA, CEBPA, MID1, WDFY3, DCX* and *SLC35D1*. HCV assembly/egress/infectivity was significantly modulated by knock-down of *PPP3CA, CSDE1, GAN, USP37, CEBPA, MID1, WDFY3, DCX, MAPK9, SLC35D1, DCC, RNF144A, PPP2R2C* and *OGT*. Strikingly, only the silencing of *OGT* was associated with an enhancement of HCV assembly/release/infectivity (*p*-value = 0.0002), while that of the other hits was associated with reduced HCV infection (Fig. 2).

These results indicate that the down-regulation of *OGT* phenocopies the effect of miR-501-3p and miR-619-3p on HCV infection (Fig. 2) and suggest OGT as a novel player in the HCV life cycle.

miR-501-3p post-transcriptionally regulates OGT expression. To study whether miR-501-3p and miR-619-3p target OGT, we analyzed OGT RNA and protein levels in Huh7.5.1 cells following overexpression of miR-501-3p or miR-619-3p. While neither miRNA had an impact on OGT RNA levels (Fig. 3A), up-regulation of miR-501-3p significantly decreased OGT protein expression by ~65% (Fig. 3B, *p*-value ≤ 0.05, t-test). miR-619-3p also decreased OGT expression but less robustly than miR-501-3p (Fig. 3B), prompting us to focus our investigation on miR-501-3p. To assess whether OGT is a functional target of miR-501-3p, we subcloned a fragment of the *OGT* mRNA 3′UTR that harbors the predicted miR-501-3p target site in the *Renilla* luciferase expression cassette (RLuc) of a dual luciferase reporter construct. Co-transfection of miR-501-3p mimic with the wild-type 3'UTR reporter (RLuc wt *OGT* 3'UTR) significantly decreased luciferase activity as compared to the empty vector (Fig. 3C, p-value < 0.05, t-test). In contrast, the repression of luciferase expression was lost when the reporter with mutated miR-501-3p binding site (RLuc mt *OGT* 3'UTR) was used (Fig. 3C). These data are consistent in indicating that miR-501-3p mediates post-transcriptional regulation of OGT.

O-GlcNAcylation modulates HCVcc infectivity. To investigate whether OGT modulates HCV assembly and/or infectivity, we determined infectious virus titer (TCID50) and HCV RNA levels to calculate the specific infectivity of HCVcc particles generated in OGT-silenced Huh7.5.1 cells. Interestingly, OGT-silencing led to a significant increase in the TCID50 and the specific infectivity of HCVcc (Fig. 4A, *p*-value ≤ 0.05, Mann-Whitney test). Noteworthy, the effect of OGT on HCVcc infectivity was genotype-independent as demonstrated by increased infectivity of HCVcc bearing the envelope glycoproteins of genotypes 1a, 1b and 2a upon OGT-silencing (Fig. 4B). We next sought to investigate how OGT could modulate

HCVcc infectivity. OGT is the only enzyme that catalyzes the addition of N-acetylglucosamine (O-GlcNAc) to serine and threonine residues of proteins. Moreover, OGT has a scaffold function and promotes binding of proteins in multiprotein complexes[35]. To assess whether the enzymatic activity of OGT modulates HCVcc infectivity, we used pharmacological inhibitors of OGT ($Ac_4$5S-GlcNAc) or O-GlcNAcase (OGA) (Thiamet G), the OGT counterpart that removes O-GlcNAc (Fig. 4C). $Ac_4$5S-GlcNAc led to a significant enhancement of HCVcc infectivity in a dose-dependent manner, while the opposite effect was observed with Thiamet G (Fig. 4D, *p*-value ≤ 0.05, Mann-Whitney test). Collectively, these results demonstrate that O-GlcNAcylation modulates HCVcc infectivity.

OGT-silencing affects HCVcc biophysical properties and size distribution. To further assess how OGT may impact HCVcc morphogenesis, we analyzed the structural and biophysical properties of HCVcc produced in siCtrl- and siOGT-transfected Huh7.5.1 cells following iodixanol gradient ultracentrifugation. Silencing of OGT led to the production of more infectious HCVcc with higher density (Fig. 5A-B) as well as higher ApoE concentrations (Fig. 5C) suggesting that OGT/O-GlcNAcylation affects the biophysical properties of HCVcc. No change in apoB concentrations were observed between HCVcc produced from siCtrl- or siOGT-transfected cells (Fig. 5D), in line with the model that HCV lipoviroparticles contain several exchangeable ApoE molecules and one non-exchangeable apoB[36]. We also visualized HCVcc by electron microscopy (EM) following anti-E2 antibody immunocapture[36] to assess whether OGT-silencing had an impact on HCVcc size. Particle size distribution was assessed from a series of randomly acquired electron micrographs. A shift towards bigger sizes was observed for sucrose-cushion purified HCVcc generated in OGT-silenced Huh7.5.1 cells as compared to control HCVcc (Fig. 6A-B). This shift was also observed in different fractions of iodixanol gradient-separated HCVcc (Fig. 6C-F) in line with the higher infectivity and ApoE concentrations of HCVcc generated in OGT-silenced Huh7.5.1 cells (Fig. 5A-C). These data suggest that OGT-silencing affects the lipidation of HCVcc.

OGT expression increases in liver disease. Since silencing of OGT promotes HCV infectivity, we assessed whether HCV infection in turn had an effect on miR-501-3p and OGT expression. In Huh7.5.1 cells, HCV infection lead to small but significant increase of miR-501-3p and decrease of OGT levels (Fig. 7A-B and Supplementary Fig. 1B; *p*-value < 0.05, Mann-Whitney test), which may promote viral infection given the pro- and antiviral roles of miR-501-3p and O-GlcNAcylation, respectively (Fig. 1C-D and 4D). In contrast, no significant difference of OGT expression was observed between the livers of HCV transgenic and wild-type mice[37] (data not shown) suggesting that HCV proteins do not directly modulate OGT expression. In liver tissue from HCV-infected patients, HCV RNA levels were not correlated with OGT expression (Fig. 7C, Spearman correlation: 0.06004019, p-value = 0.7661) suggesting that in patients there is likely no direct effect of HCV on OGT expression.

O-GlcNAcylation has been associated with a variety of cancers, including HCC recurrence linked to increased O-GlcNAcylation after liver transplantation[38]. We therefore investigated OGT expression in chronic liver disease and HCC. While there was a trend for increased OGT expression in liver tissue from HCV-infected patients with fibrosis and inflammation (Fig. 7D-E), OGT levels were markedly and significantly elevated in the tumor liver tissue of patients chronically infected with HCV or hepatitis B virus and patients with alcoholic liver disease or non-alcoholic fatty liver disease as compared to non-tumor tissue (Fig. 7F, *p*-value < 0.05, Wilcoxon test). These data suggest that OGT expression increases in HCC in an etiology-independent manner. Collectively, these results suggest that OGT expression is likely increased in HCV-induced liver disease and cancer through inflammation and fibrosis rather than by HCV itself.

Discussion

By focusing on miRNAs affecting late steps of the viral life cycle, we uncovered that i) miR-501-3p regulates the expression of OGT; ii) silencing of OGT expression or inhibition of its enzymatic activity increases the infectivity of HCV particles; and iii) OGT knock-down leads

to the release of bigger HCV particles. Our data suggest that O-GlcNAcylation affects HCV morphogenesis and infectivity.

While we were characterizing the role of OGT/O-GlcNAcylation for HCV morphogenesis, Li and colleagues published their functional genomics study of HCV-miRNA interactions[2]. By conducting genome wide miRNA mimic and hairpin inhibitor screens, they identified a set of miRNAs exhibiting a pro- or antiviral effect on HCV. Characterization of the underlying molecular processes showed that miR-25, let-7 and miR-130 families restrict viral infection by decreasing the expression of cellular HCV co-factors[2]. Despite similarities in the cell type and HCV infection models used here and by Li and colleagues, our screen only displays a small overlap with their study (9% common miRNA hits). This is not surprising given the small overlap between previous siRNA screens to uncover HCV host factors[8, 15] and is likely due i) to the different sizes of miRNA mimic libraries as the library used here was more than 2-times larger than the one used by Li and co-workers, and ii) to the markedly distinct pipelines for hit selection that were used in the two studies. Nonetheless, both screens were consistent in confirming the proviral role of miR-146a-5p in promoting HCV assembly/egress that we previously reported[17] and the global multistep inhibitory effects of the let-7 family on HCV infection[28], further corroborating the involvement of these miRNAs in fine-tuning the HCV life cycle. Both studies also consistently indicated that miR-518a-5p, miR-517-3p, miR-185 and members of the miR-302 family inhibit early steps of HCV infection, while miR-586, miR-620 and members of the miR-200 family inhibit late steps of viral infection. Since none of these miRNAs except miR-185 has been previously associated with HCV infection[39], it might be interesting to further characterize the involvement of these miRNAs in HCV-host interactions. Interestingly, an overall proviral effect of miR-501-3p was also observed by Li and colleagues[2], however the mechanism of action was not studied. By characterizing the role of miR-501-3p in the HCV life cycle, we uncovered OGT as a miR-501-3p target in liver-derived cells and showed for the first time a link between O-GlcNAcylation and HCV infection. These results indicate that genome-wide miRNA functional

screens represent a powerful strategy to dissect the role of miRNAs in pathogen-host interactions.

While N-glycosylation of HCV envelope glycoproteins plays an important role for escape from virus-neutralizing antibodies[40], so far no functional association between HCV and O-glycosylation has been reported. In contrast to N-linked glycosylation that consists of the attachment of a glycan to a nitrogen of an asparagine residue of proteins in the ER/Golgi prior to their trafficking to the plasma membrane and/or their secretion, the glycosylation of serine and threonine residues with O-GlcNAc is a post-translational modification (PTM) of intracellular proteins that are localized in the nucleus, cytoplasm or mitochondria. The O-glycosylation/deglycosylation of proteins is catalyzed by a single pair of nucleo-cytoplasmic enzymes, OGT/OGA. O-GlcNAcylation is complementary to protein phosphorylation/dephosphorylation, another more broadly known abundant protein PTM that involves numerous kinases/phosphatases. OGT/OGA are often found in protein complexes that also include kinases/phosphatases and a protein can be either O-GlcNAcylated or phosphorylated on a same residue to fine-tune cellular signaling[41]. O-GlcNAcylation and phosphorylation on the same or neighboring serine or threonine residue is known as yin yang site[42].

O-GlcNAcylation plays a major role in the regulation of metabolic pathways in the liver, including insulin signaling, bile acid metabolism and lipogenesis[35]. The large number of OGT/OGA substrates and cellular pathways regulated by O-GlcNAcylation hampers a detailed characterization of the role of these proteins in HCV infection. Since i) HCV assembly takes place at ER-derived membranes, ii) OGT/OGA are not known to localize in the ER lumen, and iii) O-GlcNAcylation of extracellular proteins containing EGF-like domains is catalyzed by EGF domain-specific OGT (EOGT) in the ER lumen in an OGT-independent manner[43]), OGT/OGA most likely modulate HCV infection by post-translationally modifying one or several cellular factors required for HCV morphogenesis rather than by affecting viral proteins, although HCV glycoproteins contain putative O-GlcNAcylation sites as determined using OGlcNAcScan, OGTsite and YingOYang1.2 bioinformatics tools (data not shown).

Regarding HCV host factors that may be regulated by OGT/OGA, O-GlcNAcylation sites have been predicted in human CLDN1[44] and OCLN at serine sites that can also be phosphorylated and this has been suggested to potentially play a role for HCV entry[45]. However, in our experimental setting we did not observe a significant effect of OGT-silencing on the early steps of HCV infection, suggesting that O-GlcNAcylation of CLDN1 and/or OCLN likely does not play a major role in HCV infection. Other host factors important for the HCV life cycle are well-known O-GlcNAcylated proteins, as for example various nuclear pore complex proteins (Nups) including Nup98, Nup153 and Nup155 that are involved in HCV replication and assembly and/or may be associated with viral particles[46, 47, 48]. However, since depletion of Nups was reported to alter HCV replication and/or assembly but to have no impact on the specific infectivity of HCV particles[46] in contrast to the depletion of OGT as shown here, it is unlikely that a modulation of Nup O-GlcNAcylation accounts for the effects of OGT-silencing and/or OGT/OGA inhibitors on HCVcc infectivity observed in our study. This is in line with our observation that OGT knock-down had no effect on Dengue virus (DENV) replication and infectivity (unpublished observations KH, MZ and Evelyne Schaffer, IBMC, Strasbourg), although Nup98 had been suggested to potentially play a role for DENV infection[46]. These data suggest that OGT does not broadly modulate the infectivity of viruses of the *Flaviviridae* family.

However, OGT and/or O-GlcNAcylation have been reported to play a role in the infection with other viruses[49, 50, 51]. Interestingly, while OGT expression modulates the levels of human papillomavirus 16 (HPV16) oncoproteins E6 and E7[52], E6 in turn can up-regulate OGT to increase O-GlcNAcylation and the oncogene activities of HPV[53], suggesting that OGT/O-GlcNAcylation could play a role in virus-induced cancer. In cell culture, HCV infection appeared to be associated with a minor decrease in OGT expression in line with an antiviral role of O-GlcNAcylation. In contrast, an increased OGT expression was observed in HCC tissues of HCV-infected patients. Since OGT has been suggested to activate oncogenic signaling pathways in non-alcoholic steatohepatitis-related HCC[54] and O-GlcNAcylation has been associated with HCC recurrence linked to increased O-

GlcNAcylation after liver transplantation[38], these data suggest that in addition to their effect on the HCV life cycle, OGT/O-GlcNAcylation may also play a role in HCV-induced hepatocarcinogenesis.

Acknowledgments

We wish to thank Gerald W. Hart and Stéphan Hardivillé, the CardioPEG CoreC4 (NHLBI P01 HL107153) for providing AL24 and for useful technical discussions. We are grateful to David Vocadlo (Simon Fraser University, Burnaby, Canada) for the gift of $Ac_4$5S-GlcNAc. We also thank Ralf Bartenschlager (University of Heidelberg, Germany) for providing the plasmids for production of HCVcc and Frank Chisari (The Scripps Research Institute, La Jolla, CA) for the gift of Huh7.5.1 cells. We acknowledge Evelyne Schaeffer (CNRS UPR3572, IBMC, Strasbourg) for the DENV experiment, Charlotte Bach and Christine Thumann (Inserm, U1110, Strasbourg) for excellent technical work during the functional miRNA mimic screen, as well as Armando A. Roca-Suarez (Inserm, U1110, Strasbourg), Hussein El Saghire (Inserm, U1110, Strasbourg), Arnaud Kopp (IGBMC, Department of Functional Genomics and Cancer) and Erika Girardi (UPR 9002, IBMC, Strasbourg) for helpful discussions. We thank the INGESTEM infrastructure for access to the IGBMC high-throughput screening workstation.

References

1 Jopling CL, Yi M, Lancaster AM*, et al.* Modulation of hepatitis C virus RNA abundance by a liver-specific MicroRNA. Science 2005;**309**:1577-81.

2 Li Q, Lowey B, Sodroski C*, et al.* Cellular microRNA networks regulate host dependency of hepatitis C virus infection. Nat Commun 2017;**8**:1789.

3 Baumert TF, Juhling F, Ono A*, et al.* Hepatitis C-related hepatocellular carcinoma in the era of new generation antivirals. BMC Med 2017;**15**:52.

4 Pawlotsky JM. Hepatitis C Virus Resistance to Direct-Acting Antiviral Drugs in Interferon-Free Regimens. Gastroenterology 2016;**151**:70-86.

5 Dietz J, Susser S, Vermehren J, *et al.* Patterns of Resistance-Associated Substitutions in Patients With Chronic HCV Infection Following Treatment With Direct-Acting Antivirals. Gastroenterology 2018;**154**:976-88 e4.

6 Zeisel MB, Baumert TF. Clinical development of hepatitis C virus host-targeting agents. Lancet 2017;**389**:674-5.

7 Zeisel MB, Crouchet E, Baumert TF, *et al.* Host-Targeting Agents to Prevent and Cure Hepatitis C Virus Infection. Viruses 2015;**7**:5659-85.

8 Lupberger J, Zeisel MB, Xiao F, *et al.* EGFR and EphA2 are host factors for hepatitis C virus entry and possible targets for antiviral therapy. Nature Medicine 2011;**17**:589-95.

9 Fuchs BC, Hoshida Y, Fujii T, *et al.* Epidermal growth factor receptor inhibition attenuates liver fibrosis and development of hepatocellular carcinoma. Hepatology 2014;**59**:1577-90.

10 Masaki T, Arend KC, Li Y, *et al.* miR-122 stimulates hepatitis C virus RNA synthesis by altering the balance of viral RNAs engaged in replication versus translation. Cell Host Microbe 2015;**17**:217-28.

11 Janssen HL, Reesink HW, Lawitz EJ, *et al.* Treatment of HCV infection by targeting microRNA. N Engl J Med 2013;**368**:1685-94.

12 van der Ree MH, de Vree JM, Stelma F, *et al.* Safety, tolerability, and antiviral effect of RG-101 in patients with chronic hepatitis C: a phase 1B, double-blind, randomised controlled trial. Lancet 2017;**389**:709-17.

13 Bandiera S, Pfeffer S, Baumert TF, *et al.* miR-122--a key factor and therapeutic target in liver disease. J Hepatol 2015;**62**:448-57.

14 Li H, Jiang JD, Peng ZG. MicroRNA-mediated interactions between host and hepatitis C virus. World J Gastroenterol 2016;**22**:1487-96.

15 Li Q, Brass AL, Ng A, *et al.* A genome-wide genetic screen for host factors required for hepatitis C virus propagation. Proc Natl Acad Sci U S A 2009;**106**:16410-5.

16 Poenisch M, Metz P, Blankenburg H*, et al.* Identification of HNRNPK as regulator of hepatitis C virus particle production. PLoS Pathog 2015;**11**:e1004573.

17 Bandiera S, Pernot S, El Saghire H*, et al.* Hepatitis C Virus-Induced Upregulation of MicroRNA miR-146a-5p in Hepatocytes Promotes Viral Infection and Deregulates Metabolic Pathways Associated with Liver Disease Pathogenesis. J Virol 2016;**90**:6387-400.

18 Da Costa D, Turek M, Felmlee DJ*, et al.* Reconstitution of the entire hepatitis C virus life cycle in non-hepatic cells. J Virol 2012;**86**:11919-25.

19 Gloster TM, Zandberg WF, Heinonen JE*, et al.* Hijacking a biosynthetic pathway yields a glycosyltransferase inhibitor within cells. Nat Chem Biol 2011;**7**:174-81.

20 Yuzwa SA, Macauley MS, Heinonen JE*, et al.* A potent mechanism-inspired O-GlcNAcase inhibitor that blocks phosphorylation of tau in vivo. Nat Chem Biol 2008;**4**:483-90.

21 Schmittgen TD, Livak KJ. Analyzing real-time PCR data by the comparative C(T) method. Nat Protoc 2008;**3**:1101-8.

22 Jin Y, Chen Z, Liu X*, et al.* Evaluating the microRNA targeting sites by luciferase reporter gene assay. Methods Mol Biol 2013;**936**:117-27.

23 Van Renne N, Roca Suarez AA, Duong FHT*, et al.* miR-135a-5p-mediated downregulation of protein tyrosine phosphatase receptor delta is a candidate driver of HCV-associated hepatocarcinogenesis. Gut 2018;**67**:953-62.

24 Mosteller F, Tukey J. Data Analysis and Regression. Reading, MA: Addison-Wesley, 1977.

25 Amaratunga D, Cabrera J. Analysis of Data from Viral DNA Microchips. Journal of the American Statistical Association 2001;**96**:1161.

26 Smyth GK. Linear models and empirical Bayes methods for assessing differential expression in microarray experiments. Statistical Applications in Genetics and Molecular Biology 2004;**3**:Article 3.

27 Strimmer K. fdrtool: a versatile R package for estimating local and tail area-based false discovery rates. Bioinformatics 2008;**24**:1461-2.

28 Cheng M, Si Y, Niu Y, *et al.* High-throughput profiling of alpha interferon- and interleukin-28B-regulated microRNAs and identification of let-7s with anti-hepatitis C virus activity by targeting IGF2BP1. J Virol 2013;**87**:9707-18.

29 Shirasaki T, Honda M, Shimakami T, *et al.* MicroRNA-27a regulates lipid metabolism and inhibits hepatitis C virus replication in human hepatoma cells. J Virol 2013;**87**:5270-86.

30 Bandyopadhyay S, Friedman RC, Marquez RT, *et al.* Hepatitis C virus infection and hepatic stellate cell activation downregulate miR-29: miR-29 overexpression reduces hepatitis C viral abundance in culture. J Infect Dis 2011;**203**:1753-62.

31 Chen Y, Chen J, Wang H, *et al.* HCV-induced miR-21 contributes to evasion of host immune system by targeting MyD88 and IRAK1. PLoS Pathog 2013;**9**:e1003248.

32 Ariumi Y, Kuroki M, Maki M, *et al.* The ESCRT system is required for hepatitis C virus production. PLoS One 2011;**6**:e14517.

33 Paul D, Madan V, Bartenschlager R. Hepatitis C virus RNA replication and assembly: living on the fat of the land. Cell Host Microbe 2014;**16**:569-79.

34 Meyers NL, Fontaine KA, Kumar GR, *et al.* Entangled in a membranous web: ER and lipid droplet reorganization during hepatitis C virus infection. Curr Opin Cell Biol 2016;**41**:117-24.

35 Yang X, Qian K. Protein O-GlcNAcylation: emerging mechanisms and functions. Nat Rev Mol Cell Biol 2017;**18**:452-65.

36 Piver E, Boyer A, Gaillard J, *et al.* Ultrastructural organisation of HCV from the bloodstream of infected patients revealed by electron microscopy after specific immunocapture. Gut 2017;**66**:1487-95.

37 Lerat H, Honda M, Beard MR, *et al.* Steatosis and liver cancer in transgenic mice expressing the structural and nonstructural proteins of hepatitis C virus. Gastroenterology 2002;**122**:352-65.

38 de Queiroz RM, Carvalho E, Dias WB. O-GlcNAcylation: The Sweet Side of the Cancer. Front Oncol 2014;**4**:132.

39 Singaravelu R, O'Hara S, Jones DM, *et al.* MicroRNAs regulate the immunometabolic response to viral infection in the liver. Nat Chem Biol 2015;**11**:988-93.

40 Lavie M, Hanoulle X, Dubuisson J. Glycan Shielding and Modulation of Hepatitis C Virus Neutralizing Antibodies. Front Immunol 2018;**9**:910.

41 Hart GW, Slawson C, Ramirez-Correa G, *et al.* Cross talk between O-GlcNAcylation and phosphorylation: roles in signaling, transcription, and chronic disease. Annu Rev Biochem 2011;**80**:825-58.

42 Hart GW, Greis KD, Dong LY, *et al.* O-linked N-acetylglucosamine: the "yin-yang" of Ser/Thr phosphorylation? Nuclear and cytoplasmic glycosylation. Adv Exp Med Biol 1995;**376**:115-23.

43 Sakaidani Y, Nomura T, Matsuura A, *et al.* O-linked-N-acetylglucosamine on extracellular protein domains mediates epithelial cell-matrix interactions. Nat Commun 2011;**2**:583.

44 Butt AM, Khan IB, Hussain M, *et al.* Role of post translational modifications and novel crosstalk between phosphorylation and O-beta-GlcNAc modifications in human claudin-1, -3 and -4. Mol Biol Rep 2012;**39**:1359-69.

45 Butt AM, Feng D, Nasrullah I, *et al.* Computational identification of interplay between phosphorylation and O-beta-glycosylation of human occludin as potential mechanism to impair hepatitis C virus entry. Infect Genet Evol 2012;**12**:1235-45.

46 Neufeldt CJ, Joyce MA, Levin A, *et al.* Hepatitis C virus-induced cytoplasmic organelles use the nuclear transport machinery to establish an environment conducive to virus replication. PLoS Pathog 2013;**9**:e1003744.

47 Lussignol M, Kopp M, Molloy K, *et al.* Proteomics of HCV virions reveals an essential role for the nucleoporin Nup98 in virus morphogenesis. Proc Natl Acad Sci U S A 2016;**113**:2484-9.

48 Zhu Y, Liu TW, Madden Z, *et al.* Post-translational O-GlcNAcylation is essential for nuclear pore integrity and maintenance of the pore selectivity filter. J Mol Cell Biol 2016;**8**:2-16.

49 Jochmann R, Thurau M, Jung S, *et al.* O-linked N-acetylglucosaminylation of Sp1 inhibits the human immunodeficiency virus type 1 promoter. J Virol 2009;**83**:3704-18.

50 Groussaud D, Khair M, Tollenaere AI, *et al.* Hijacking of the O-GlcNAcZYME complex by the HTLV-1 Tax oncoprotein facilitates viral transcription. PLoS Pathog 2017;**13**:e1006518.

51 Angelova M, Ortiz-Meoz RF, Walker S, *et al.* Inhibition of O-Linked N-Acetylglucosamine Transferase Reduces Replication of Herpes Simplex Virus and Human Cytomegalovirus. J Virol 2015;**89**:8474-83.

52 Kim M, Kim YS, Kim H, *et al.* O-linked N-acetylglucosamine transferase promotes cervical cancer tumorigenesis through human papillomaviruses E6 and E7 oncogenes. Oncotarget 2016;**7**:44596-607.

53 Zeng Q, Zhao RX, Chen J, *et al.* O-linked GlcNAcylation elevated by HPV E6 mediates viral oncogenesis. Proc Natl Acad Sci U S A 2016;**113**:9333-8.

54 Xu W, Zhang X, Wu JL, *et al.* O-GlcNAc transferase promotes fatty liver-associated liver cancer through inducing palmitic acid and activating endoplasmic reticulum stress. J Hepatol 2017;**67**:310-20.

55 Boldanova T, Suslov A, Heim MH, *et al.* Transcriptional response to hepatitis C virus infection and interferon-alpha treatment in the human liver. EMBO Mol Med 2017;**9**:816-34.

Figure legends

Figure 1. High-throughput screen identifies human miRNAs that regulate the HCV life cycle. (A) Schematic outline of the miRNA mimic screen strategy. Huh7.5.1 cells were transfected with miRNA mimics or controls prior to infection with *Renilla* luciferase HCVcc (JcR2a) two days later (part 1). Cell supernatants of part 1 were used to inoculate naïve Huh7.5.1 cells (part 2). Cells from part 1 and part 2 were lysed at the end of each infection step (2 and 3 days post infection, respectively) to determine luciferase activity. (B) Modulation of HCV entry and replication (part 1) and/or assembly and infectivity (part 2) upon transfection of control non-targeting siRNA (siCtrl, negative control), siCD81 (inhibiting viral entry) or siApoE (inhibiting viral assembly). By inhibiting HCV entry, siCD81 impacts part 1 as well as part 2. In contrast, by specifically impairing late steps of HCV replication cycle, siApoE inhibits HCV infection only in part 2. The box plots show the sample lower quartile (25th percentile; bottom of the box), the median (50th percentile; horizontal line in box) and the upper quartile (75th percentile; top of the box) of relative light units (RLU) in each lysate. The whiskers indicate s.d. Data are from three independent experiments. (C) Effects of miRNA overexpression on each part of the HCV life cycle. Data were tested using a moderated t-test (empirical Bayes shrinkage, R-package limma[26]) for the null-hypothesis of no change of a given miRNA compared to the negative control. The resulting p-values for independent testing of each miRNA where corrected for the multiple testing situation and expressed as local false discovery rate (lfdr, R-package fdrtool[27]). miRNAs having a significant effect on either part 1 or 2 of the screen are below the thresholds indicated by dashed lines (lfdr < 0.00027 or 0.1226, respectively). miRNAs that were previously reported to impact on HCV infection as well as miR-140-3p, miR-501-3p, miR-619-3p and miR-4778-5p are highlighted in blue (Log2(FC) < 0) or red (Log2(FC) > 0). Data are from three independent experiments. (D) Effect of miR-140-3p, miR-501-3p, miR-619-3p and miR-4778-5p on the HCV life cycle. Huh7.5.1 cells were transfected with siCtrl (Ctrl), miR-140-3p, miR-501-3p, miR-619-3p or miR-4778-5p and infection experiments were carried out as described in A. HCV infection was determined as luciferase activity. Results represent mean

percentage ± s.d. from three independent experiments in triplicate. The dashed line indicates values from control-transfected cells set at 100%. Statistics: *, *p*-value ≤ 0.05, Mann-Whitney test.

Figure 2. OGT is a novel host cell factor involved in the late steps of the HCV life cycle. Huh7.5.1 cells were transfected with a set of siRNAs against 28 predicted targets of miR-501-3p and/or miR-619-3p, and infected with HCVcc JcR2A according to the two-step protocol depicted in Fig. 1A. siCD81, antagomiR-122 and siApoE were used as loss-of-function controls to perturb HCV entry, translation/replication and assembly, respectively. miR-501-3p and miR-619-3p, which were ineffective in part 1 of the screen but enhanced HCV infection in part 2, were transfected in parallel. HCV infection was quantified as fold change of luciferase activity with respect to negative control (siCtrl). Results for different replicates are shown as individual points. For each gene, median fold change of luciferase activity ± s.d. is shown as black horizontal lines. The dashed line indicates a fold change of 1. Data are from three independent experiments in triplicate. Results for miR-501-3p, miR-619-3p and siOGT that increase HCV infection in part 2 are depicted in red. Results for siRNA targeting *PPP3CA, CEBPA, MID1, WDFY3, DCX, SLC35D1, CSDE1, GAN, USP37, MAPK9, DCC, RNF144A,* or *PPP2R2C* that significantly modulated HCV infection in part 1 and/or part 2 but did not phenocopy the effect of miR-501-3p and miR-619-3p are depicted in blue.

Figure 3. miR-501-3p mediates post-transcriptional regulation of OGT by decreasing its expression at the protein level. Huh7.5.1 cells were transfected with siCtrl (Ctrl), a pool of siRNA against *OGT*, miR-501-3p or miR-619-3p. After 96h, RNA and proteins were purified, and OGT expression analyzed by RT-qPCR and Western blot. (A) Percentage of *OGT* mRNA expression in miRNA-transfected cells as compared to negative control. Results are presented as mean ± s.d. and are from three independent experiments in triplicate. The dashed line indicates values from control-transfected cells set at 100%. Statistics: *, *p*-value

≤ 0.05, t-test (B) OGT protein expression. Left: percentage of OGT protein expression in siRNA- or miRNA-transfected cells as assessed by quantification of Western blots. OGT levels were normalized to actin levels using ImageLab™ 5.2.1 software (BioRad). Results are presented as mean ± s.d. and are from three independent experiments. The dashed line indicates values from control-transfected cells set at 100%. Statistics: *, *p*-value ≤ 0.05, t-test. Right: representative Western blot analysis. (C) Analysis of miRNA targeting of *OGT* expression by dual luciferase reporter assay. Left: HeLa cells were co-transfected with a miR-501-3p mimic and a dual luciferase reporter plasmid containing either wild type miR-501-3p (RLuc wt *OGT* 3'UTR) or mutated miR-501-3p binding site (RLuc mt *OGT* 3'UTR) to modulate RLuc expression. Co-transfection of the miR-501-3p mimic and empty RLuc vector was used as control. Data are expressed as mean percentage of *Renilla* luciferase activity ± s.d. normalized to *firefly* luciferase, and relative to co-transfection of the vectors with non-targeting miRNA (miR-Ctrl). Results are from three independent experiments in triplicate. The dashed line indicates values from control-transfected cells set at 100%. Statistics: *, *p*-value ≤ 0.05, t-test. Right: Schematic representation of the used constructs.

Figure 4. Silencing of *OGT* affects HCV morphogenesis and infectivity. (A) Analysis of HCV infectivity. Huh7.5.1 cells were transfected with siCtrl, a pool of siRNA against *OGT* or ApoE as a loss-of-function control to perturb HCV assembly, prior to infection with HCVcc (Jc1) two days later (entry and replication). Mock-transfected cells were used as control (Ctrl). After another 48h, intra- and extracellular HCVcc particles were used to infect naïve Huh7.5.1 cells (assembly and infectivity). Virus supernatants of Huh7.5.1 cells were assayed by (left) endpoint dilution assay (TCID50). Intra- and extracellular HCV RNA was purified and analyzed by RT-qPCR to calculate (right) the specific infectivity (TCID50/RNA). Data are expressed as mean percentage as compared to control ± s.d. Results are from four independent experiments in triplicate. The dashed line indicates values from control-transfected cells set at 100%. Statistics**:** *, *p*-value ≤ 0.05, Mann-Whitney test. (B) Genotype-independent effect of OGT on HCV infection. Huh7.5.1 cells were transfected with siCtrl or

siOGT prior to infection with HCVcc JcR2a (genotype 2a), H77R2a (genotype 1a) or Con1R2a (genotype 1b). Experiments were carried out and analyzed as described in A. Data are expressed as mean percentage of Renilla luciferase activity as compared to control ± s.d. Results are from three independent experiments in quadruplicate. The dashed line indicates values from control-transfected cells set at 100%. Statistics: *, *p*-value < 0.05, Mann-Whitney test. (C) Activity of OGT/OGA inhibitors on O-GlcNAcylation. The activity of $Ac_4$5S-GlcNAc (OGT inhibitor) or Thiamet G (OGA inhibitor) on O-GlcNAcylation of proteins in Huh7.5.1 cells was demonstrated by Western blot as described in Supplementary Methods. (D) Effect of O-GlcNAcylation on HCV infectivity. Huh7.5.1 cells were electroporated with HCVcc (JcR2a), prior to treatment with increasing concentrations of $Ac_4$5S-GlcNAc (OGT inhibitor, left) or Thiamet G (OGA inhibitor, right) 4h later. After 96h, supernatants were transferred onto naïve Huh7.5.1 cells and electroporated cells were lysed to determine luciferase activity. Luciferase activity in infected Huh7.5.1 cells was assessed 72h later. Data are expressed as mean percentage as compared to control ± s.d. Results are from three independent experiments in quadruplicate. The dashed line indicates values from vehicle-treated cells set at 100%. Statistics: *, *p*-value < 0.05, Mann-Whitney test.

Figure 5. Silencing of *OGT* modulates HCVcc biophysical properties. (A) Separation of HCVcc by iodixanol density gradient ultracentrifugation. HCVcc were produced in non-targeting siRNA control- or siOGT-transfected Huh7.5.1 cells. After overlaying HCVcc (JcR2A) on a 4%-40% iodixanol step gradient and ultracentrifugation for 16h, fractions of HCV particles were used to infect naïve Huh7.5.1 cells in order to determine TCID50. HCV RNA of each fraction was purified and analyzed by RT-qPCR. Data are expressed as mean ± s.d. from three independent experiments. (B) Specific infectivity (TCID50/RNA) was calculated and the density was determined by weighting each fraction. Specific infectivity of each fraction is expressed as fold change as compared to the total infectivity of the control. Data are expressed as mean ± s.d. from three independent experiments. (C-D) ApoE and ApoB concentrations in the individual fractions were determined by ELISA. The dashed lines

indicate limits of quantification of the assays. Data are expressed as mean ± s.d. from three independent experiments.

Figure 6. Silencing of *OGT* increases the size of HCVcc. (A) Representative pictures of HCV particles generated in Huh7.5.1 cells transfected with non-targeting siRNA (siCtrl) or siOGT. (B-F) Comparative analysis of particle size distribution for immunocapture (IC) from HCV particles produced in Huh7.5.1 cells transfected with siCtrl or siOGT prior to infection with HCVcc (JcR2a) following sucrose-cushion purification (B) or iodixanol gradient fractionation (C-F) of HCVcc. HCVcc were transferred via anti-E2 antibody AR3A on electron microscopy (EM) grids through IC. Particle size distribution was assessed from a series of randomly acquired electron micrographs with Image-J software (NIH). Results from one of three (A-B) or two (C-F) independent experiments are shown. Black lines: size distribution of immunocaptured HCVcc produced in siCtrl-transfected cells. Grey lines: size distribution of immunocaptured HCVcc produced in siOGT-transfected cells.

Figure 7. *OGT* expression increases in HCC. (A-B) Huh7.5.1 cells were infected with HCV (JcR2a). After 72h, RNA and proteins were purified, and *OGT* expression analyzed by RT-qPCR and Western blot. (A) Percentage of *OGT* mRNA expression relative to uninfected Huh7.5.1 cells (Ctrl). Results are presented as mean ± s.d. from three independent experiments in duplicate. The dashed line indicates values from uninfected Huh7.5.1 cells set at 100%. Statistics: *, *p*-value < 0.05, Mann-Whitney test. (B) OGT protein expression. Left: percentage of OGT protein expression relative to uninfected Huh7.5.1 cells (Ctrl) following quantification of Western blots as described in Supplementary Methods. Results are presented as mean ± s.d. from three independent experiments. The dashed line indicates values from uninfected Huh7.5.1 cells set at 100%. Statistics: *, *p*-value < 0.05, Mann-Whitney test. Right: representative Western blot analysis of OGT and actin. (C) *OGT* expression and viral load in liver tissue from 22 HCV-infected patients and 6 patients not infected with HCV described in[55]. Spearman correlation: rho = 0.06004019, p-value = 0.77.

(D-E) OGT expression in liver tissue from 22 HCV-infected patients and 6 patients not infected with HCV according to fibrosis (D) or activity (E) scores described in[55]. Wilcoxon test: F1 vs F0 p-value = 0,38; F2 vs F0 p-value = 0,18; F3 vs F0 p-value = 0,43; F4 vs F0 p-value = 0,17; A1 vs A0 p-value = 0,28; A2 vs A0 p-value = 0,23; A3 vs A0 p-value = 0,09. (F) *OGT* expression in tumor (HCC) and non-tumor (Ctrl) liver tissue from 39 HCV-infected patients, 83 HBV-infected, 80 patients with alcoholic liver disease (ALD) and 13 patients with non-alcoholic liver disease (NAFLD) as described in Supplementary Methods. *, *p*-value < 0.05, Wilcoxon test.

Table 1. Computational analysis of miR-501-3p and miR-619-3p targets and pathway enrichment.

miRNA ID	Target gene symbol	***Pathway*** **or network**
miR-501-3p	*MEF2A*; *PPP3CA*; *PPP3CC*	*Calcium signaling*
	HMGCS1	*Cholesterol biosynthesis*
	AFF4; *CHMP1B*; *CUX1*; *DCLK1*; *LMX1A*; *PTBP2*; *RBMS1*; *RC3H1*; *SCN2A*; *SEC63*; *ZFHX4*	Inflammatory response, dermatological diseases and conditions, inflammatory disease
	CDK6; *CSDE1*; *GLI2*; *HOXD10*; *LSM5*; *MEF2A*; *MYCN*; *OGT*; *PPP2R2C*; *PPP2R5E*; *SEMA3C*; *TFDP2*	Cellular development, nervous system development and function; organ morphology
	CIT; *COL10A1*; *FNBP1L*; *GAN*; *HERC1*; *KPNA4*; *NONO*; *SHPRH*; *STRN*; *TARDBP*; *UBE2H*; *USP37*	Cell death and survival; cellular compromise; free radical scavenging
	ATXN1; *CBLL1*; *CEBPA*; *DCC*; *PEX5L*; *RCC2*; *RNF144A*; *ZC3H12C*	Cell morphology, cellular assembly and organization; cellular function and maintenance
miR-619-3p	*RUNX1T1*; *SMAD3*	*Adipocyte biogenesis*
	FOXG1; *GPBP1*; *MID1*; *MKL2*; *MSI1*; *PCBP2*; *WDFY3*	Cell cycle; organismal injury and abnormalities; cancer
	ACVR2B; *DCX*; *ESRRG*; *MAPK9*; *OGT*; *PCBP1*; *PDE3B*; *SMAD3*; *SMARCC1*; *TGFB3*; *PAPOLA*	Carbohydrate metabolism, energy production; small molecule biochemistry
	RUNX1T1; *SHANK2*; *SLC35D1*	Gene expression, lipid metabolism, small molecule biochemistry

Supplementary Information

A functional microRNA screen uncovers O-linked N-acetylglucosamine transferase as a host factor modulating hepatitis C virus morphogenesis

Katharina Herzog[1,2*], Simonetta Bandiera[1,2*], Sophie Pernot[1,2], Catherine Fauvelle[1,2], Frank Jühling[1,2], Amélie Weiss[2,3,4,5], Anne Bull[6], Sarah C. Durand[1,2], Béatrice Chane-Woon-Ming[2,7], Sébastien Pfeffer[2,7], Marion Mercey[8], Hervé Lerat[8], Jean-Christophe Meunier[6], Wolfgang Raffelsberger[2,3,4,5], Laurent Brino[2,3,4,5], Thomas F. Baumert[1,2,9,#], Mirjam B. Zeisel[1,2,10,#]

[1]Inserm, U1110, Institut de Recherche sur les Maladies Virales et Hépatiques, Strasbourg, France; [2]Université de Strasbourg, Strasbourg, France; [3]Institut de Génétique et de Biologie Moléculaire et Cellulaire, Illkirch, France ; [4]CNRS, UMR7104, Illkirch, France ; [5]Inserm, U1258, Illkirch, France ; [6]Inserm U1259, Faculté de Médecine, Université François Rabelais and CHRU de Tours, Tours, France ; [7]Architecture et Réactivité de l'ARN – UPR 9002, Institut de Biologie Moléculaire et Cellulaire du CNRS, Strasbourg, France; [8]Institute for Advanced Biosciences, Centre de Recherche UGA - Inserm U1209 - CNRS UMR 5309, Grenoble, France, [9]Institut Hospitalo-Universitaire, Pôle Hépato-digestif, Hôpitaux Universitaires de Strasbourg, Strasbourg, France; [10]Inserm, U1052, CNRS UMR 5286, Centre Léon Bérard (CLB), Cancer Research Center of Lyon (CRCL), Université de Lyon (UCBL), Lyon, France

*Authors contributed equally to this work

Supplementary Material and methods

Cells and cell culture conditions. The source and culture conditions of Huh7.5.1 cells have been described[1]. HeLa cells were purchased from ATCC and cultured in Dulbecco´s modified Eagle medium (Gibco® DMEM GlutaMAX™, ThermoFisher Scientific) containing 1% sodium pyruvate as described for Huh7.5.1 cells[1].

Viruses and infectivity assays. Cell culture-derived recombinant cell culture-derived hepatitis C virus (HCVcc) Jc1 (genotype 2a/2a chimera), H77R2a (genotype 1a/2a chimera engineered for *Renilla* luciferase expression), Con1R2a (genotype 1b/2b chimera engineered for *Renilla* luciferase expression), and JcR2a (genotype 2a/2a chimera engineered for *Renilla* luciferase expression) were generated in Huh7.5.1 cells as described[1, 2, 3, 4]. HCVcc infectivity was determined by calculating the 50% tissue culture infectious dose (TCID50) using anti-NS5A antibody as described[5, 6] or by assessing luciferase activity. HCVcc were used at 10^5-10^6 TCID50/mL throughout the study. HCV RNA was purified using a QIAmp viral RNA minikit (Qiagen) and analyzed by one-step RT-qPCR using a Sensi Fast NO ROX kit (Bioline) according to the manufacturer's instructions. Standard curves were performed using 10-fold dilution series of HCV RNA.

Purification of HCVcc particles using sucrose cushion or iodixanol density gradient. HCVcc (JcR2a) were concentrated 10-fold using a Vivaspin column (GE Healthcare). For sucrose cushion purification, HCVcc were purified by overlaying 3.5 mL of culture media on 1.5 mL of 20% sucrose, and by ultracentrifuging samples for 4h at 40,000 rpm on a SW-55 rotor (Beckman Coulter). Purified HCVcc were resuspended in 30 µL of PBS for analysis via immunocapture and electron microscopy. Density distributions of infectious HCVcc were determined by overlaying 0.5 mL culture media on a 5 mL, 4%-40% iodixanol step gradient, and ultracentrifuging samples for 16h at 40,000 rpm on a SW-55 rotor (Beckman Coulter): 625 µl fractions were carefully harvested from the top of each tube, and density was determined by weighing. Infectivity of each fraction was quantified by TCID50 using anti-NS5A antibody as described[5, 6], while HCV RNA of fractions was purified and analyzed as described above. ApoB and ApoE concentrations of fractions were determined by enzyme-linked immunosorbent assay (Human Apolipoprotein B or E ELISA^{PRO} kit, Mabtech) undiluted or in a 1:50 dilution, respectively, according to the manufacturer's instructions (Mabtech).

miRNA mimics and siRNAs. Non-targeting control miRNA, miR-501-3p mimic, miR-619-3p mimic, antagomiR-122, antagomiR-501-3p, non-targeting control antagomiR, non-targeting control siRNA, siRNAs targeting *OGT, CD81* or *apoliporotein E* (*ApoE*) and a library of 28 custom ON-TARGETplus smart pool siRNAs were purchased from Dharmacon (GE Healthcare).

miRNA expression analysis. Total RNA (100 ng) was purified from control or HCV-infected Huh7.5.1 cells using Tri reagent® (Thermo Scientific) and Direct-zol™ RNA purification kit (Zymo Research). Total RNA was first polyadenylated and reverse transcribed using a miScript II RT system (Qiagen) according to the manufacturer's instructions. The obtained cDNA was subjected to RT-qPCR using miScript SYBR Green kit (Qiagen). Primers were the mature miRNA sequence for the forward primer (Thermo Scientific) and the universal miScript primer (Qiagen) for the reverse primer. Data were analyzed by the ΔΔCt method using small nucleolar RNA, C/D box 61 (SNORD61) as an endogenous reference and the non-infected samples as a calibrator[7].

Antibodies. Rabbit anti-OGT antibodies DM-17 and AL24 were purchased from Sigma or kindly provided by Dr. G. W. Hart and Dr. S. Hardivillé (Johns Hopkins University School of Medicine, Baltimore, MD)[8], respectively. Mouse anti-β-actin antibody was purchased from Abcam and mouse, rabbit or sheep HRP-conjugated secondary antibodies (A9044, A0545 and A3415, respectively) were purchased from Sigma. Sheep anti-NS5A serum for determination of TCID50 was a kind gift from M. Harris[9]. Human anti-E2 (AR3A) antibody[10] for electron microscopy analysis was kindly provided by Mansun Law (SCRIPPS, California, USA).

Western blotting. OGT and actin protein expression in human cells was assessed by Western blot as described[8] with some modifications. Briefly, cells were lysed in lysis buffer no. 6 (R&D Systems) according to the manufacturer's instructions. Equal amounts of protein

(40 µg) were size-separated through a Mini PROTEAN® TGX Stain-Free™ gel electrophoresis (Bio-Rad) and transferred to PVDF membranes (Bio-Rad). Immunoblots were performed using rabbit anti-OGT (1:2000) and mouse anti-β-actin (1:1000) antibodies[8, 11]. Antigen-antibody complexes were detected by incubating the membrane with the appropriate HRP-conjugated secondary antibodies (1:5000; 1:10,000) and imaged by enhanced chemiluminescence with a ChemiDoc MP imager (Bio-Rad). Quantification of protein expression was performed using ImageLab™ 5.2.1 software (BioRad). For analysis of OGT and GAPDH expression in liver tissue from HCV transgenic (FL-N/35) or wild-type mice[12], crude protein extracts were prepared by homogenization of frozen mouse livers (50–100 µg) in tissue lysis buffer from the Ambion PARIS RNA (Thermo Scientific) and protein isolation kit, supplemented with protease inhibitors (cOmpleteTM EDTA-free protease inhibitor mixture, Sigma-Aldrich) and phosphatase inhibitors (PhosSTOPTM, Sigma-Aldrich), using a tissue homogenizer (MP Fast Prep24, MP Biomedicals, Santa Ana, CA) and MP Lysing Matrix A tubes. Proteins were quantified using the BCA assay (Thermo Fisher Scientific). Western blotting was performed as described above.

Immunocapture and electron microscopy analysis of viral particles. Sucrose-cushion purified or iodixanol gradient fractionated HCVcc (JcR2a) produced in cells transfected with a non-targeting siRNA control or a pool of siRNA against OGT were transferred via anti-E2 antibody AR3A on electron microscopy (EM) grids through immunocapture (IC) as described[13]. Particles were stained with uranyl acetate dihydrate and observed in a JEOL 1230 electron microscope. Series of electron micrographs were acquired at random from IC EM grids. The images were then analyzed with Image-J software, to determine the particle size distribution.

Gene expression analysis in patient-derived liver tissue. For OGT expression analysis in patient's samples, raw data were retrieved from the Gene Expression Omnibus (GSE84346) and re-analyzed by quality-trimming (cutadapt) and mapping (HISAT2) to human genome

assembly hg19. Reads mapping to Gencode v.19 genes were counted using htseq-count and normalized applying DESeq2. Activity and fibrosis scores as well as viral load were taken from the supplemental data published in[14]. To analyze OGT expression in liver tissue of chronic hepatitis B or C patients, FPKM values and clinical data were retrieved from The Cancer Genome Atlas (TCGA, https://www.cancer.gov/about-nci/organization/ccg/research/structural-genomics/tcga). This data set includes samples from 39 HCV-infected patients, 83 hepatitis B virus (HBV)-infected, 80 patients with alcoholic liver disease (ALD) and 13 patients with non-alcoholic fatty liver disease (NAFLD).

Supplementary References

1 Zhong J, Gastaminza P, Cheng G*, et al.* Robust hepatitis C virus infection in vitro. Proc Natl Acad Sci U S A 2005;**102**:9294-9.

2 Reiss S, Rebhan I, Backes P*, et al.* Recruitment and activation of a lipid kinase by hepatitis C virus NS5A is essential for integrity of the membranous replication compartment. Cell Host Microbe 2011;**9**:32-45.

3 Da Costa D, Turek M, Felmlee DJ*, et al.* Reconstitution of the entire hepatitis C virus life cycle in non-hepatic cells. J Virol 2012;**86**:11919-25.

4 Fauvelle C, Felmlee DJ, Crouchet E*, et al.* Apolipoprotein E Mediates Evasion From Hepatitis C Virus Neutralizing Antibodies. Gastroenterology 2016;**150**:206-17 e4.

5 Lindenbach BD, Evans MJ, Syder AJ*, et al.* Complete replication of hepatitis C virus in cell culture. Science 2005;**309**:623-6.

6 Bandiera S, Pernot S, El Saghire H*, et al.* Hepatitis C Virus-Induced Upregulation of MicroRNA miR-146a-5p in Hepatocytes Promotes Viral Infection and Deregulates Metabolic Pathways Associated with Liver Disease Pathogenesis. J Virol 2016;**90**:6387-400.

7 Schmittgen TD, Livak KJ. Analyzing real-time PCR data by the comparative C(T) method. Nat Protoc 2008;**3**:1101-8.

8 Iyer SP, Akimoto Y, Hart GW. Identification and cloning of a novel family of coiled-coil domain proteins that interact with O-GlcNAc transferase. J Biol Chem 2003;**278**:5399-409.

9 Macdonald A, Crowder K, Street A*, et al.* The hepatitis C virus non-structural NS5A protein inhibits activating protein-1 function by perturbing ras-ERK pathway signaling. J Biol Chem 2003;**278**:17775-84.

10 Giang E, Dorner M, Prentoe JC*, et al.* Human broadly neutralizing antibodies to the envelope glycoprotein complex of hepatitis C virus. Proc Natl Acad Sci U S A 2012;**109**:6205-10.

11 Verrier ER, Colpitts CC, Bach C*, et al.* A targeted functional RNA interference screen uncovers glypican 5 as an entry factor for hepatitis B and D viruses. Hepatology 2016;**63**:35-48.

12 Lerat H, Honda M, Beard MR*, et al.* Steatosis and liver cancer in transgenic mice expressing the structural and nonstructural proteins of hepatitis C virus. Gastroenterology 2002;**122**:352-65.

13 Piver E, Boyer A, Gaillard J*, et al.* Ultrastructural organisation of HCV from the bloodstream of infected patients revealed by electron microscopy after specific immunocapture. Gut 2017;**66**:1487-95.

14 Boldanova T, Suslov A, Heim MH*, et al.* Transcriptional response to hepatitis C virus infection and interferon-alpha treatment in the human liver. EMBO Mol Med 2017;**9**:816-34.

Supplementary figure legends

Figure S1. (A) Effect of miR-501-3p inhibition on HCV infectivity. Huh7.5.1 cells were transfected with control antagomiR (Ctrl), antagomiR-122 as loss-of-function control to perturb HCV replication and antagomiR-501-3p, prior to infection with HCVcc (JcR2a) according to the two-step protocol depicted in Fig. 1A. After 48h, supernatants were transferred onto naive Huh7.5.1 cells. After 72h, Renilla Luciferase activity of infected Huh7.5.1 cells was determined. Data are expressed as mean percentage as compared to Ctrl ± s.d. Results are from four independent experiments in quadruplicate. The dashed line indicates values from vehicle-treated cells set at 100%. Statistics: *, *p*-value < 0.05, Mann-Whitney test. (B) miR-501-3p expression upon HCV infection. Huh7.5.1 cells were infected with HCVcc (JcR2a).

After 72h, RNA was purified and miR-501-3p expression analyzed by RT-qPCR. Percentage of miR-501-3p expression relative to uninfected Huh7.5.1 cells (Ctrl). Results are presented as mean ± s.d. from three independent experiments in duplicate. The dashed line indicates values from uninfected Huh7.5.1 cells set at 100%. Statistics: *, *p*-value < 0.05, Mann-Whitney test.

Supplementary Table 1. A genome-wide miRNA mimic screen identifies cellular miRNAs modulating HCV infection. Log2(FC), lfdr and effect on HCV infection in part 1 and part 2 of the screen are shown for the individual miRNAs of the miRNA mimic library. In red: proviral effect, in blue: antiviral effect. FC: fold change, lfdr: local false discovery rate